

# Ciz1 as a biomarker and drug target in Glioblastoma multiforme

Olivia Iwanowytsch

Health &  
Medicine

Lancaster  
University



Department of Biomedical and Life Sciences  
Faculty of Health and Medicine  
Lancaster University

Thesis for degree of MSc by Research 2021

## **Declaration**

I declare that everything written in this thesis is my own work and not the work of anybody else. This work has not been previously submitted in the same form for the award of a higher degree or qualification elsewhere.

## Abstract

Glioblastoma (GBM) is the most prevalent primary brain tumour in adults with an extremely poor prognosis. The aggressive and infiltrative nature of these tumours renders them resistant to conventional therapies, posing a huge challenge in terms of treatment. As such, there is an unmet need for the development of more robust biomarkers to improve diagnostic and therapeutic strategies for high-grade gliomas.

CIZ1 is a nuclear matrix associated-protein involved in various biological processes such as X chromosome localisation and inactivation, epigenetic maintenance and initiation of DNA replication. CIZ1 has been implicated in a number of common cancers including breast, prostate and lung. This work will focus on the role of CIZ1 in the initiation of DNA replication and the manipulation of CIZ1 in attempt to reduce growth and proliferation of primary GBM cell lines and unrelated tumour types *in vitro*. The role of CIZ1 as a diagnostic biomarker in GBM will also be assessed via immunohistochemistry (IHC) analysis using a cohort of patient-derived tissue sections.

GBM cell lines require CIZ1 for efficient proliferation; chemical inhibition of CIZ1 with CDK and DDK inhibitors reduced CIZ1 protein levels and proliferative rates in U87-MG and BTNW914 cells. Whilst CIZ1 protein was not depleted, CIZ1 mRNA levels and cell proliferation reduced, S-phase progression also slowed. IHC analysis of FFPE patient-derived tissue sections revealed aberrant subcellular localisation of CIZ1. The mislocalisation of CIZ1 from the nucleus to the cytoplasm can differentiate between normal and tumour cells, implicating CIZ1 as a histopathological biomarker in GBM. Overexpression of CIZ1 was observed where the tumour intersection was visible, although further investigation using an expanded cohort of patient samples is required. Taken together these results support the use of CIZ1 as a biomarker and drug target in GBM; therapeutic approaches to reduce CIZ1 levels could be of clinical significance in the reduction of tumour growth.

## Abbreviations

AKT1	Serine-threonine protein kinase
APC/C	Anaphase promoting complex/cyclosome
APNG	Alkylpurine-DNA-N-glycosylase
ATP	Adenosine triphosphate
BBB	Blood-brain barrier
BER	Base excision repair
BSA	Bovine serum albumin
CDC6	Cell division cycle 6
CDKN2A	Cyclin-dependant kinase inhibitor 2A
CDK	Cyclin-dependant kinase
CDKi	Cyclin-dependant kinase inhibitor
Cdt1	Chromatin licensing and DNA Replication Factor 1
Ciz1	Cip-1 interacting zinc finger protein
CNBr	Cyanogen bromide
CNS	Central nervous system
CRC	Colorectal carcinoma
CRISPR-Cas9	Clustered regularly interspaced short palindromic repeats – CRISPR associated proteins
CSF	Cerebrospinal fluid
CTCs	Circulating tumour cells
CtDNA	Circulating tumour DNA
CVT	CVT-313
DAPI	4',6-Diamidino-2-Phenylindole
DDK	Dbf4-dependant kinase
DDKi	Dbf4-dependant kinase inhibitor
DMEM	Dulbecco's Modified Eagle Medium
DYNLL1	Dynein light chain 1
DTT	Dithiothreitol
EdU	Ethynyl deoxyuridine
EGFR	Epidermal growth factor receptor
ER	Estrogen receptor
ER-a	Estrogen receptor-alpha
EVs	Extracellular vesicles
FA	Fanconi anaemia
FBS	Foetal bovine serum
FDA	Food and Drug Administration
GBC	Gall bladder carcinoma
GBM	Glioblastoma
GFAP	Glial fibrillary acidic protein
GST	Glutathione S-transferase
HBS	HEPES buffered saline
HCC	Hepatocellular carcinoma
HDM2	Human double minute 2 protein
HRP	Horseradish peroxidase
IDH1	Isocitrate dehydrogenase 1

IHC	Immunohistochemistry
LIF	Leukaemia inhibitory factor
LMS	Leptomeningeal spread
MCM2-7	Minichromosome maintenance proteins 2-7
MDM2	Mouse double minute 2 homolog
MEFs	Mouse embryonic fibroblasts
MGMT	O <sup>6</sup> -methylguanine-DNA methyltransferase
MH3	Matrin 3-homologous domain 3
MMR	Mismatch repair
MRI	Magnetic resonance imaging
MTKIs	Multitargeted tyrosine kinase inhibitors
MTOR	Mammalian target of rapamycin
NF1	Neurofibromatosis type 1
NM	Nuclear matrix
NSCLC	Non-small cell lung carcinoma
ORC	Origin replication complex
OS	Overall survival
PBS	Phosphate buffered saline
PCNA	Proliferation cell nuclear antigen
PCR	Polymerase chain reaction
PD	Palbociclib (PD0332991) Isethionate
PDGF	Platelet-derived growth factor
PDGFRA	Platelet-derived growth factor receptor alpha
PFS	Progression-free survival
PHA	PHA-767491 dihydrochloride
PI3K	Phosphatidylinositol 3-kinase
PKC	Protein kinase C
Pre-RC	Pre-replication complex
PSA	Prostate-specific antigen
PTEN	Phosphatase and tensin homolog
PVDF	Polyvinylidene Difluoride
RAS	Rat sarcoma
RB1	Retinoblastoma protein 1
Ros	Roscovitine
RTK	Receptor tyrosine kinase
SCLC	Small cell lung carcinoma
SDS	Sodium Dodecyl Sulfate
SDS-PAGE	Sodium Dodecyl Sulfate Polyacrylamide Gel Electrophoresis
SiRNA	Short-interfering ribonucleic acid
ShRNA	Short hairpin ribonucleic acid
TBS	Tris Buffered Saline
TCGA	The Cancer Genome Atlas
TKIs	Tyrosine kinase inhibitors
TKR	Tyrosine kinase receptor
TMZ	Temozolomide
TP53	Tumour protein p53
TTFs	Tumour-treating fields

UPS	Ubiquitin-proteasome system
VEGF	Vascular endothelial growth factor
VEGF-A	Vascular endothelial growth factor A
WHO	World Health Organisation
XL	XL-413 hydrochloride
YAP	Yes-associated protein

# Contents

<b>Abstract .....</b>	<b>3</b>
<b>Abbreviations.....</b>	<b>4</b>
<b>Acknowledgements.....</b>	<b>11</b>
<b>Chapter 1: Introduction .....</b>	<b>12</b>
<b>1.1 Introduction.....</b>	<b>12</b>
<b>1.2 Glioblastoma Multiforme .....</b>	<b>12</b>
1.2.1 Epidemiology and Etiology .....	12
1.2.2 Genetic and Molecular pathogenesis.....	13
1.2.3. Molecular classification of GBM.....	14
1.2.4 Clinical symptoms and Diagnosis .....	20
1.2.5 Current treatments .....	21
<b>1.3 Discovery and characterisation of p21Cip1-interacting zinc finger protein 1 (Ciz1) ..</b>	<b>27</b>
<b>1.4 The role of CIZ1 in regulation of the cell cycle .....</b>	<b>29</b>
1.4.1 Initiation of DNA replication .....	30
1.4.2 Role of Ciz1 in DNA replication.....	31
<b>1.5 Role of CIZ1 in tumourigenesis.....</b>	<b>34</b>
1.5.1 Overexpression of CIZ1 and its role in tumourigenesis.....	34
1.5.2 Dysregulation of oncogenic transcriptional programs by CIZ1 .....	36
1.5.3 Alternative CIZ1 splicing as a driver or marker of tumourigenesis.....	37
<b>1.6 Potential for CIZ1 as a diagnostic and prognostic biomarker in cancer .....</b>	<b>38</b>
<b>1.7 Aims .....</b>	<b>38</b>
<b>Chapter 2: Materials and Methods.....</b>	<b>40</b>
<b>2.1 Cell culture .....</b>	<b>40</b>
<b>2.2 Primary GBM cells .....</b>	<b>40</b>
<b>2.3 Sodium Dodecyl Sulfate Polyacrylamide Gel Electrophoresis (SDS-PAGE).....</b>	<b>41</b>
<b>2.4 Western blotting .....</b>	<b>41</b>
2.4.1 Transferring protein to a Polyvinylidene Difluoride (PVDF) membrane .....	41
2.4.2 Probing membranes .....	42
<b>2.5 Preparation of immunopurified anti-CIZ1 antibody.....</b>	<b>43</b>
2.5.1 CIZ1-N471 expression.....	43
2.5.2 CIZ1-N471 purification .....	44
2.5.3. Covalent coupling of Ciz1-N471 to resin .....	45
2.5.4 Affinity purification of Ciz1-N471 Antibody .....	46
<b>2.6 Small molecule CDK/DDK inhibitor treatments .....</b>	<b>47</b>
<b>2.7 PrestoBlue™ Cell Viability Assay.....</b>	<b>49</b>
<b>2.8 Transfection of BTNW914 cells with siRNA .....</b>	<b>50</b>
<b>2.9 RNA extraction and qRT-PCR .....</b>	<b>51</b>
<b>2.10 Cell cycle analysis by flow cytometry .....</b>	<b>51</b>
<b>2.11 Apoptosis assays.....</b>	<b>52</b>
<b>2.12 Immunofluorescence .....</b>	<b>52</b>

2.13 Determining proportion of S-phase cells by EdU Fluorescence microscopy.....	53
2.14 Statistical analysis.....	53
2.15 Immunohistochemistry analysis of FFPE tissue sections.....	53
2.15.1 Antigen retrieval.....	54
2.15.2 Immunostaining .....	54
2.15.3 Validation of CIZ1-N471 antibody .....	55
<b>Chapter 3: Effect of CDK and DDK small molecule inhibitors on CIZ1 expression.....</b>	<b>56</b>
3.1 Introduction .....	56
3.2 CDK and DDK inhibition reduces CIZ1 levels and proliferation in an unrelated tumour type .....	58
3.3 Effects of CDK and DDK inhibition on proliferation in SW620, PC3 and SW480 cancer cell lines .....	63
3.4 Chapter discussion.....	68
3.4.1 CDK/DDK inhibition reduced CIZ1 levels in an unrelated tumour type.....	68
3.4.2 Dose-dependent effects of CDK/DDK inhibition on proliferation .....	68
<b>Chapter 4: Evaluation of small molecule kinase inhibitors to reduce CIZ1 levels in GBM.....</b>	<b>71</b>
4.1 Analysis of CDK and DDK inhibition in established GBM cell line U87-MG .....	72
4.2 Primary GBM cells retain markers of glial origin.....	77
4.3 Analysis of CDK and DDK inhibition in primary GBM BTNW914 cell line .....	79
4.4 CIZ1 depletion in BTNW914 primary GBM cells .....	83
4.5 Chapter discussion.....	86
4.5.1 CDK and DDK inhibition reduces CIZ1 levels and proliferation <i>in vitro</i> .....	86
4.5.2 Effects of CIZ1 depletion on proliferation and cell cycle profile in primary GBM cells .....	91
<b>Chapter 5: Evaluation of CIZ1 as a biomarker in GBM.....</b>	<b>93</b>
5.1 Aims .....	95
5.2 Validation of the CIZ1-N471 antibody .....	95
5.3 Optimisation of immunopurified anti-CIZ1 antibody concentration for IHC analysis of patient GBM tissue sections .....	96
5.4 IHC analysis of patient-derived FFPE GBM tissue sections .....	98
5.4.1 Organisation of cells in the brain .....	100
5.4.2 Imaging of 'normal' regions identified CIZ1 staining in specific cell types .....	101
5.4.3 CIZ1 staining patterns in normal tissue vs tumour tissue .....	102
5.4.4 Cancer morphology in GBM tissue .....	104
5.4.5 Abnormalities in vasculature of tumour tissue .....	106
5.4.6 Migration and invasion.....	111
5.5 Chapter discussion.....	114
5.5.1 Validity of CIZ1 as a biomarker in GBM .....	114
<b>Chapter 6: General discussion.....</b>	<b>117</b>
6.1 Future perspectives .....	119
<b>Chapter 7: References .....</b>	<b>121</b>

# Figures and Tables

## Figures

Figure 1.1: Schematic of TKR activation and the downstream signalling pathways involved in the pathogenesis of GBM.....	19
Figure 1.2: Structure of human CIZ1 protein.....	27
Figure 1.3: The role of CIZ1 in the initiation of DNA replication.....	32
Figure 2.1: Schematic of anti-CIZ1 antibody production.....	46
Figure 3.1: Model for CIZ1 accumulation in cancer: Opposing regulation of CIZ1 by CDKs and the UPS.....	57
Figure 3.2: Treatment of A549 cells with CDK and DDK inhibitors.....	59
Figure 3.3: Cell death profile of A549 cells after CDK/DDK inhibition.....	61
Figure 3.4: Recovery of CIZ1 with proteasomal inhibitor MG132 after kinase inhibition.....	63
Figure 3.5: Cell proliferation analysis after CDKi and DDKi treatment in SW620 cells...64	
Figure 3.6: Cell proliferation analysis after CDKi and DDKi treatment in PC3 cells.....	65
Figure 3.7: Cell proliferation analysis after CDKi and DDKi treatment in SW480 cells...66	
Figure 3.8: Titration of PHA-767491 induces a dose-response effect in PC3 cells.....	67
Figure 4.1: Treatment of U87-MG cells with CDK and DDK inhibitors.....	73
Figure 4.2: Recovery of CIZ1 with proteasomal inhibitor MG132 after kinase inhibition.....	75
Figure 4.3: Cell death profile of U87-MG cells after CDK/DDK inhibition.....	76
Figure 4.4: Optimisation of GFAP antibody for immunofluorescence in BTNW914 cells.....	78
Figure 4.5: Treatment of BTNW914 cells with CDK and DDK inhibitors.....	80
Figure 4.6: Recovery of CIZ1 with proteasomal inhibitor MG132 after kinase inhibition.....	81
Figure 4.7: Cell death profile of BTNW914 cells after CDK/DDK inhibition.....	82
Figure 4.8: Analysis of BTNW914 cells following CIZ1 depletion.....	84
Figure 5.1: Confirmation of antibody specificity using western blotting.....	96
Figure 5.2: Optimisation of immunopurified anti-CIZ1 antibody for IHC.....	97
Figure 5.3: IHC analysis of 12 patient-derived FFPE tissue sections from primary GBM patients.....	99
Figure 5.4: Neuron structure within the brain cortex.....	100
Figure 5.5: CIZ1 staining patterns in specific cell types of normal brain tissue.....	102
Figure 5.6: Differential CIZ1 staining between healthy and tumour tissue.....	103
Figure 5.7: CIZ1 staining in the nuclear compartments of tumour cells.....	104
Figure 5.8: Heterogeneity within the tumour microenvironment.....	106
Figure 5.9: Vasculature and endothelial cell staining in normal tissue.....	107
Figure 5.10: Vascularisation and staining of endothelial cells.....	108

Figure 5.11: Morphology of vasculature in tumour tissue.....	110
Figure 5.12: Infiltrating edge of tumour.....	112
Figure 5.13: Migration and invasion of tumour cells along the brain surface.....	113

## Tables

Table 1.1: CIZ1 contributes to tumorigenesis in various cancers.....	34
Table 2.1: List of antibodies used in this study.....	42
Table 2.2: Components and their concentrations required to make up autoinduction media.....	44
Table: 2.3 Small molecule inhibitors used for <i>in vitro</i> kinase inhibition studies.....	48
Table 5.1: List of tissue samples used in IHC analysis.....	98

## Acknowledgements

Firstly, I'd like to thank my supervisor Dr Nikki Copeland for his continuous support and guidance throughout this project, the knowledge I have gained is invaluable. I'd like to thank Professor Timothy Dawson and Katherine Ashton at Royal Preston Hospital for their assistance with the BTNW patient samples and expertise in histopathology. I'd also like to thank Freya Ferguson for her encouragement and willingness to help and James Tollitt for his teaching of practical techniques and answering my many stupid questions.

# Chapter 1: Introduction

## 1.1 Introduction

Glioblastoma multiforme (GBM) is the most prevalent malignant primary brain tumour in adults. GBM is classified as a grade IV astrocytoma with a median patient survival of 12-15 months (Davis, 2016). The aggressive nature of these tumours poses a huge challenge in terms of treatment. Surgical resection followed by chemotherapy has remained the standard of care for decades emphasising the need for increased understanding of the initiation and progression of these tumours to allow for the development of novel and effective therapeutics.

Cip1-interacting zinc-finger protein 1 (CIZ1) has been implicated to have a role in tumorigenesis in a number of cancers but its role in GBM is yet to be determined. This project aims to investigate if CIZ1, a nuclear matrix-associated DNA replication initiation factor that is a putative diagnostic biomarker in lung cancer (Higgins et al., 2012; Coverley et al., 2017) and a prognostic biomarker in colorectal carcinoma (Wang et al., 2014), is associated with GBM. The expression of CIZ1 in FFPE tissue sections will be investigated and the potential to reduce CIZ1 levels with repurposing of cyclin-dependant kinase (CDK) family inhibitors will be assessed. This literature review will provide an overview of GBM, its pathogenesis and identify the current molecular biomarkers that are used for diagnosis and patient stratification.

## 1.2 Glioblastoma Multiforme

### 1.2.1 Epidemiology and Etiology

In Europe and North America, there are 2-3 GBM diagnoses per 100,000 adults each year, with a higher incidence in men compared to women (1.26:1). In infants, GBM occurs in approximately 1.1-3.6 per 100,000 infants, again with a higher incidence in males (3.3:1) (Ostrom et al., 2015). Whilst there is no morphological difference

between GBM in adults and children, glioma in children has a higher proliferation activity according to the Ki-67 proliferation index (Urbańska et al., 2014).

The etiology of GBM is yet to be elucidated, with only two factors shown to decisively increase the risk of glioma development; exposure to high doses of ionising radiation and inheriting mutant genes associated with rare familial syndromes. Allergic conditions, asthma and high serum levels of IgE are associated with a reduced glioma risk. Asthma-related germline polymorphisms have confirmed this association in GBM (Schwartzbaum et al., 2006).

The development of GBM is spontaneous in most cases, with the familial form constituting only 5% of cases and having a different genetic background to spontaneous GBM. The presence of genetic diseases including tuberous sclerosis, neurofibromatosis type 1 (NF1) and Turcot syndrome can lead to the development of GBM. Some of the genetic abnormalities include loss of genetic material within chromosome 10q, amplification of epidermal growth factor receptor (EGFR) and AKT3 and mutations in Phosphatase and tensin homolog (PTEN), tumour protein p53 (TP53) and NF1 genes (Verhaak et al., 2010). Mutations in TP53, EGFR and AKT can promote deregulation of the G1/S checkpoint and are associated with the presence of numerous genetic abnormalities in glioma cells as well as GBM development. There is a high risk of GBM development in postmenopausal women indicating the involvement of sex hormones in glioma development (Carrano et al., 2021). An increased BMI is also shown to increase risk of GBM incidence (Urbańska et al., 2014).

### 1.2.2 Genetic and Molecular pathogenesis

GBM is often reported in two different clinical forms, primary and secondary GBM. Primary GBM is the most common form, representing 95% of all GBM cases. Primary GBM typically arises de novo within 3-6 months in older patients. Secondary GBM arises from previously existing lower grade astrocytomas in younger patients. There are some molecular differences observed between the subtypes, although the same

pathways tend to be affected and therefore response to current treatments in both clinical forms is similar (Alifieris and Trafalis, 2015).

Most cases of primary GBM have amplified, mutated EGFR referred to as EGFRvIII. Secondary GBM typically has increased signalling via the platelet-derived growth factor receptor alpha (PDGFRA) receptor. Both of these mutations lead to increased activity of the tyrosine kinase receptor (TKR) and subsequent activation of rat sarcoma (RAS) and phosphatidylinositol 3-kinase (PI3K) signalling pathways (Wang et al., 2015). Primary GBM cases often have amplification of the mouse double minute 2 homolog (MDM2) gene, a ubiquitin ligase that targets p53 for proteasomal degradation, along with PTEN mutations and homozygous deletions of cyclin-dependant kinase inhibitor 2A (CDKN2A) (Esemen et al., 2022). Secondary GBM cases frequently contain TP53 mutations, isocitrate dehydrogenase 1 (IDH1) mutations and MET amplification. Progression from low grade glioma to high grade gliomas is related to the inactivation of the retinoblastoma protein 1 (RB1) gene and upregulation of human double minute 2 (HDM2) activity. These genetic and molecular alterations lead to abnormal regulation of the cell cycle and growth factor mediated signalling pathways resulting in a subsequent increase in proliferation, inhibition of apoptosis, invasion and angiogenesis (Cloughesy et al., 2014).

### 1.2.3. Molecular classification of GBM

Due to the recent insight into the genetic heterogeneity of GBM, The Cancer Genome Atlas (TCGA) have created four different molecular subclasses of GBM which include classical, mesenchymal, proneural and neural types. These molecular subclasses have been categorised based on specific gene expression profiles and alterations of EGFR, NF1 and PDGFRA/IDH1 respectively.

#### 1.2.3.1 Classical GBM

Classical GBM is characterised by high-level EGFR amplification, loss of chromosome 10 and astrocytic cell-like gene expression patterns. Amplification of the *EGFR* gene is seen in 40% of GBM cases with half of these cases also having a mutation in the

EGFRvIII encoding gene. EGFRvIII is frequently observed in human cancers, this mutated gene is constitutively active and promotes tumour growth, potentially being linked to a poor clinical outcome. EGFRvIII contains an intragene rearrangement with in frame deletions of exons 2-7 which encode part of the extracellular domain of the protein (Aldape et al., 2015). Studies have demonstrated that ectopic expression of EGFRvIII in glioma cell lines results in constitutive autophosphorylation and activation of Shc-Grb2-Ras and PI3K pathways (Keller and Schmidt, 2017). EGFRvIII expression also induces tumourigenicity, cell proliferation and blocks apoptosis via modulation of Bcl-X<sub>L</sub> gene expression. These tumourigenic effects are not observed when wild-type EGFR is overexpressed. EGFRvIII is known to drive cell proliferation but its expression is defined to a fraction of GBM cells. Studies have demonstrated that cells expressing EGFRvIII promote their own proliferation but also the proliferation of neighbouring cells expressing wild-type EGFR implying a paracrine signalling mechanism driven by EGFRvIII-positive cells (Nishikawa et al., 2004). Human glioma tissue, cell lines and stem cells expressing EGFRvIII also expressed cytokines IL-6 and leukaemia inhibitory factor (LIF). Expression of these proteins results in activation of the cytokine co-receptor gp130 inducing the expression of wild-type *EGFR* in neighbouring cells (Inda et al., 2010). Intratumoural heterogeneity may be essential for EGFRvIII function in GBM. Aberrations in *EGFR* are present in other cancers such as non-small cell lung carcinoma (NSCLC) however these are different to those found in GBM. Focal *EGFR* amplification is present at high rates in gliomas (>20 copies) and mutations producing EGFRvIII and missense mutations occur within the extracellular domain as appose to the intracellular domain in non-gliomas. Previous studies have demonstrated the clinical relevance of the EGFRvIII mutation therefore making it an attractive therapeutic target (Keller and Schmidt, 2017). Deletion of exons 2-7 in EGFRvIII produces a novel peptide sequence which acts as an immunogenic tumour-specific target and provides the framework for a peptide-based vaccination. The vaccine rindopepimut was developed for the treatment of newly diagnosed GBM patients. Rindopepimut consists of the EGFRvIII peptide sequence conjugated to keyhole limpet hemocyanin and showed promising progression-free and overall survival (OS) rates in single-arm phase II trials; immune responses specific to EGFRvIII were elicited with minimal adverse effects (Schuster et al., 2015). However, in phase III trials,

Rindopepimut was discontinued as the vaccine was showing no significant benefits to patient OS (Malkki, 2016).

#### 1.2.3.2 Mesenchymal GBM

Mesenchymal GBM predominantly contains deletions in the NF1 gene and the majority of patient samples have lower NF1 expression. Large-scale sequencing analysis by TCGA demonstrated that 15% of glioma samples have inactivated NF1 by genetic loss or mutation (Verhaak et al., 2010). Increased proteasomal degradation of NF1 as a result of protein kinase C (PKC) hyperactivation can also cause NF1 inactivation (Chandrika et al., 2016). Neurofibromin 1 is the protein product of the *NF1* gene and acts as a tumour suppressor by downregulating *RAS* and mammalian target of rapamycin (mTOR) signalling pathways in astrocytomas. Studies with NF1 null murine astrocytes demonstrated that loss of NF1 increased proliferation and migration of cells as a result of mTOR hyperactivation due to increased Ras signalling. Stat3 is another downstream target of NF1 regulated by mTORC1 and Rac1; its increased activity results in increased cyclin D1 expression (Banerjee et al., 2011). Homozygous loss of NF1 in astrocytes of mouse models was not sufficient to induce tumour formation however caused an increase in cell growth. Genetic depletion of NF1 in glial cells in combination with germline *TP53* mutation resulted in astrocytoma development *in vivo* (Zhu et al., 2005) and further progression to GBM upon *PTEN* deletion (Kwon et al., 2008), these same effects are also observed in neural stem and progenitor cells using the same combination of genetic alterations (Alcantara Llaguno et al., 2009).

The majority of GBM cases possess activation of the PI3K-AKT-mTOR and RAS-MAPK signalling pathways which are associated with mesenchymal and proneural subtypes of GBM. Aberrations in these pathways include mutations in genes encoding the catalytic (PIK3CA) and regulatory (PIK3R1) domains of PI3K resulting in activation of PI3K. Also, deletions or silencing mutations in PTEN, the main negative regulator of the PI3K-AKT pathway are present in 30% of GBM cases (Aldape et al., 2015). Furthermore, epigenetic and mi-RNA based repression of PTEN has been observed (Huse et al., 2009). *PTEN* is the most commonly deleted gene in the RTK pathway in GBM, with

complete loss of its locus on chromosome 10q. *PTEN* is a tumour suppressor gene which inhibits PI3K signalling such as RB1 and neurofibromin 1, a negative regulator of RAS signalling. AKT is also a downstream target of the PI3K pathway. *PTEN* dephosphorylates phosphatidylinositol 3,4,5 triphosphate which is required for AKT activation (Kwon et al., 2008). In addition, reduced *PTEN* expression is associated with poor prognosis in GBM (Phillips et al., 2006) and knockout of *PTEN* in postnatal mouse brains resulted in higher grade astrocytoma formation in mouse models (Wei et al., 2006).

#### 1.2.3.3 Proneural GBM

The proneural subtype is characterised by focal amplification of *PDGFRA* and point mutations in *IDH1*. Proneural GBM also contains the highest proportion of *TP53* mutations compared to the other subtypes and has an oligodendrocytic cell expression profile. The proneural subtype can be subdivided into glioma CpG (G-CIMP)-positive and -negative subgroups based on the DNA methylation patterns which is directly linked to the mutational status of *IDH1/2*.

*PDGFRA* amplification is found in 15% of all GBM cases, mainly observed in the proneural subtype. Of these tumours with *PDGFRA* amplification, 40% contain an intragenic deletion which consists of an in-frame deletion of 243 base pairs within exons 8 and 9 of the extracellular domain (*PDGFRA*<sup>Δ8,9</sup>) (Aldape et al., 2015). In frame gene fusions of *KDR/VEGFR-2* in the extracellular domain and *PDGFRA* in the intracellular domain have also been observed, the subsequent mutant proteins are constitutively active and have transforming abilities making them an attractive target for *PDGFRA* inhibition (Cancer Genome Atlas Research, 2008). *PDGFRA* signaling is activated by upregulation of platelet-derived growth factor (PDGF) ligands A-D in 30% of glioma tumours. Expression of *PDGFRB* is limited to proliferating endothelial cells in GBM (Cantanhede and de Oliveira, 2017). As with EGFR and EGFRvIII, PDGF and *PDGF* amplification appear to promote aggressive glioma growth (Phillips et al., 2013). In mouse models, cells within the subventricular zone of the lateral ventricle transduced with a retrovirus expressing PDGF developed tumours which resembled GBM; large with a diffuse nature. Infected and uninfected *PDGFRA*-positive cells had significantly

increased proliferative rates indicating that *PDGF* expression promotes tumourigenesis by both paracrine and autocrine signaling mechanisms. Cells distinct from the transformed cells within the tumour environment eventually developed into tumour cells suggesting a novel model for tumourigenesis which differs from the accepted model of linear gliomagenesis (Fomchenko et al., 2011). *PDGFRA* amplification is frequently observed in both paediatric and high-grade astrocytomas and was found to increase with glioma grade, with GBMs having higher levels of *PDGFRA* amplification than lower-grade anaplastic astrocytomas. *PDGFRA* amplification in IDH1 mutant GBM patients was associated with a poor prognosis in adults but not children. IDH1 mutants are uncommon in *de novo* GBM however are enriched in the proneural subtype as with *PDGFRA* amplification with nearly half of these tumours being positive for *PDGFRA* amplification (Phillips et al., 2013).

#### 1.2.3.4 Neural GBM

The neural subtype is identified by the expression of neuron markers, including *NEFL*, *SYT1* and *SLC12A5*. This subtype is associated with a normal brain tissue gene expression profile with astrocytic and oligodendrocytic cell markers. Diagnosis of neural GBM can be made by observing morphology using a light microscope with very few normal cells visible on pathology slides. Although these subtypes consists of mutations and alterations in DNA copy number, there are no distinctive mutations found in neural GBM (Verhaak et al., 2010).

Primary and secondary GBM can be indistinguishable histologically but have differing genetic and epigenetic profiles. The majority of GBM cases with *IDH1* mutations have a proneural gene expression pattern however only 30% of these proneural subtypes have *IDH1* mutations. Therefore, for a molecular diagnosis, *IDH1* mutation is more definitive of secondary GBM, with secondary GBM being more genetically homogenous in relation to *IDH1* mutation. The heterogeneity of the different GBM subtypes results in different treatment efficacy among patients and so there is a requirement for development of novel personalised therapies to target specific alterations at the molecular level (Alifieris and Trafalis, 2015).

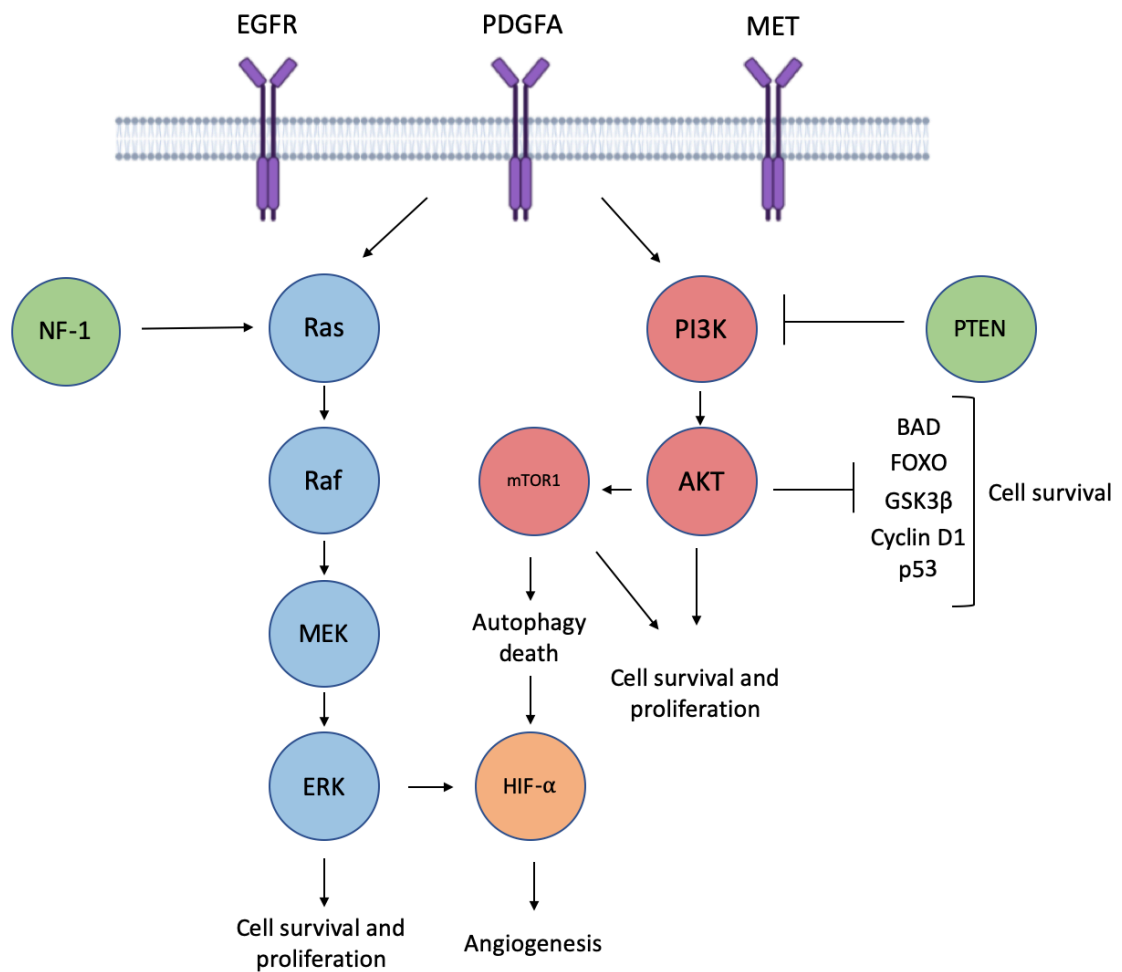


**Figure 1.1 Schematic of TKR activation and the downstream signalling pathways involved in the pathogenesis of GBM.** TKR activation occurs through the binding of a growth factor to the transactivation domain of its receptor leading to receptor dimerisation and subsequent activation of major downstream signalling pathways Ras/ERK and PI3K/AKT. Activation of these signalling pathways results in a number of biological effects including cell survival, proliferation, induction of angiogenesis and inhibition of apoptosis. EGFR – epithelial growth factor receptor, PDGFA – platelet derived growth factor receptor, MET – mesenchymal-epithelial transition factor, NF-1 – neurofibromin 1, PTEN – phosphatase tensin homolog, PI3K – phosphoinositide-3-kinase, MEK – MAPK extracellular signalling-related kinase, ERK – extracellular regulated kinase, mTOR – mammalian target of rapamycin 1, HIF-1 $\alpha$  - hypoxia-inducible factor-1 $\alpha$ , BAD – Bcl-2-associated death promoter, FOXO – forkhead box O, GSK3 $\beta$  – glycogen synthase kinase-3 beta.

#### 1.2.4 Clinical symptoms and Diagnosis

Due to the nature of symptoms associated with GBM, including headaches, ataxia and dizziness, glioma is often initially misdiagnosed as an infection, circulatory disease or immunological disease. The occurrence of seizures in patients not previously diagnosed with epilepsy can also be an indication for a potential GBM diagnosis (Walter et al., 2019). Magnetic resonance imaging (MRI) is the primary diagnostic tool used in GBM, with a tumour diameter of approximately 4 cm at diagnosis. For a definitive GBM diagnosis, histopathological examination of the resected tumour is required, this can be by surgical resection or a fine needle aspiration biopsy where resection is not feasible (Schultz et al., 2005). The World Health Organisation (WHO) sets out criteria for morphological diagnosis of GBM. Tumours of the central nervous system (CNS) are classified based on morphology, grade of malignancy (I-IV), proliferative index, responsiveness to treatment and survival rate. Gliomas are the most common tumours of the CNS and include astrocytomas, oligodendrogliomas and ependymomas. Malignant gliomas can be subdivided into grade III/IV tumours such as anaplastic astrocytoma, anaplastic oligodendroglioma, and anaplastic ependymomas and grade IV tumours including GBM (Alifieris and Trafalis, 2015).

GBM is classified as a grade IV tumour which represents the most malignant tumours. GBM has a mean diagnosis age of 64 and a mean OS of 6-12 months (Alifieris and Trafalis, 2015). Confirmation of primary diagnosis requires IHC analysis to confirm the presence of glial fibrillary acidic protein (GFAP), an intermediate filament protein of mature astrocytes. GFAP is a marker specific to astrocytes in both normal and pathological states and is thought to play a role in astrocyte maturation. Loss of *GFAP* expression is associated with increased malignancy of astrocytic tumours and increased proliferative rates of glioma cells compared to *GFAP* positive cells in GBM. Thus, loss of *GFAP* expression indicates undifferentiated states of tumour cells but does not provide an explanation for tumour progression. Furthermore, the S100 acid protein in glial cells is also a specific marker for CNS tumours but cannot be used for differential diagnosis (Urbańska et al., 2014).

### 1.2.5 Current treatments

Treatment of GBM should ultimately result in tumour regression and increased survival in a disease-free state. GBM is a highly proliferative tumour and infiltrates surrounding tissues, rendering resection and radiotherapy as insufficient treatment options (Davis, 2016). The blood-brain barrier (BBB) poses a challenge to treatment due to strict maintenance of its functional and structural integrity; transport systems such as efflux machinery can restrict the entry of drugs to the brain. Also, tumour cells located within hypoxic areas are resistant to radiotherapy (Khosla, 2016). The current standard of care for GBM is maximal safe resection of the tumour followed by chemotherapy and radiotherapy. The best results are achieved when radiotherapy is given after surgery at a dosage of 5000-6000 cGy (Urbańska et al., 2014). Current efforts are focused on understanding the molecular pathogenesis of gliomas as resistance to treatment is posing difficulties to the current standard of care. Glioma stem cells have an involvement in resistance to radiotherapy via activation of DNA-damage response pathways. They are also involved in resistance to standard chemotherapy via O<sup>6</sup>-methylguanine-DNA methyltransferase (MGMT) and inhibition of apoptosis. These efforts are also in place to discover methods to penetrate the BBB providing a mechanism of entry for a wider range of therapeutics (Alifieris and Trafalis, 2015).

The three main treatments currently approved for GBM are radiotherapy, temozolomide (TMZ) and tumour-treating fields (TTFs). TMZ is included in the standard chemotherapeutic treatment for glioma and has the highest average survival rates in patients compared to other chemotherapies. The lipophilic nature of TMZ means it is able to penetrate the BBB allowing for oral administration. Survival rates are further increased when TMZ is administered in combination with radiotherapy (Khosla, 2016). TMZ is a DNA alkylating agent able to induce cell cycle arrest at the G<sub>2</sub>/M transition leading to subsequent apoptosis. TMZ acts by modifying DNA or RNA via the addition of methyl groups at N<sup>7</sup> and O<sup>6</sup> sites on guanine and O<sup>3</sup> on adenine. Methylation of O<sup>6</sup> on guanine results in insertion of a thymidine base instead of cytosine opposite the methylguanine upon DNA replication which can lead to cell death. These methylated bases can remain modified or be fixed by DNA mismatch

repair (MMR). Alternatively, modified bases can be removed by base excision repair (BER) by a DNA glycosylase such as alkylpurine-DNA-N-glycosylase (APNG) or dealkylated by a demethylating enzyme such as MGMT. When MMR proteins are expressed in GBM cells, they are vulnerable to TMZ whereas expression of MGMT, APNG and BER proteins confers resistance to TMZ (Lee, 2016). Blockage of the NHERF-1 synthesis pathway in glioma cells increases sensitivity to the cytotoxicity of TMZ and to the induction of apoptosis in tumour cells.

#### 1.2.5.1 Tumour-treating fields (TTFs)

TTFs are the most recent development in GBM therapeutics to receive approval from the Food and Drug Administration (FDA). TTFs work by delivering alternating electrical fields to tumour cells via cutaneous transducer arrays, exerting biophysical force on intracellular charged and polarisable molecules known as dipoles. The optimal conditions for TTF delivery are at low-intensity (1-3 V/cm) and intermediate-frequency (100-300 kHz) which disrupts a range of essential biological processes within the cell ultimately leading to cell death. TTFs disrupt DNA repair mechanisms by downregulating the expression of BRCA and Fanconi anaemia (FA) pathway genes which are associated with increased DNA replication stress and double-strand break formation. TTFs also promote antitumour immunity by stimulating macrophages to secrete reactive oxygen species, nitrous oxide and proinflammatory cytokines IL-1 $\beta$ , TNF- $\alpha$  and IL-6. Furthermore, dendritic cell recruitment and maturation and accumulation of CD4+ and CD8+ T cells encourages immunogenic cell death (Rominiyi et al., 2021). The development of the TTF delivery device Optune (Novocure™) was first approved by the FDA in 2011 for treatment of recurrent GBM as a monotherapy. It was intended for use as an alternative to standard GBM treatment once surgical and radiation options had been exhausted. In a randomized clinical trial of Optune versus standard chemotherapy, both treatment groups had equal OS rates however the group receiving Optune experienced fewer side effects making it an attractive therapeutic for GBM (Stupp et al., 2012). In 2015, Optune received further approval for use alongside TMZ in newly diagnosed GBM patients following surgical resection. In a study assessing the efficacy of Optune in combination with TMZ versus Optune

alone, combination therapy significantly increased progression free survival and OS (Stupp et al., 2015).

#### 1.2.5.2 The use and development of targeted therapies in GBM

GBM is a highly vascularised cancer, with high vascularisation and vascular proliferation as key diagnostic indicators. Vascular endothelial growth factor (VEGF) promotes the growth of endothelial cells located within blood vessels and regulates normal and pathologic blood vessel growth. In cancer, VEGF is mainly produced by tumour cells but also by the tumour-associated stroma. In GBM, vascular endothelial growth factor A (VEGF-A) is overexpressed, and its levels are 30-fold higher than those in lower-grade astrocytomas and are associated with a poor prognosis. Inactivation of VEGF-A inhibits angiogenesis and tumourigenesis demonstrating the importance of VEGF-A involvement in the pathogenesis of GBM (Kim et al., 2018).

Anti-angiogenic therapy was developed to block the VEGF-dependant pathway. The human IgG1 monoclonal antibody Bevacizumab was engineered to selectively bind VEGF-A with high affinity and neutralise its activity by blocking interaction with VEGF receptor tyrosine kinases VEGFR1 and VEGFR2 on the surface of endothelial cells (Garcia et al., 2020). Bevacizumab has numerous biological effects including direct inhibition of tumour-directed angiogenesis, direct effects on VEGF receptor expression in GBM cells and indirect effects including the disruption of the glioma stem cell niche (Kim et al., 2018).

Bevacizumab was first approved by the FDA in 2009 for the treatment of recurrent GBM in patients who had poor response to prior treatment. The approval of Bevacizumab was based on two main phase II clinical trials without the need for a randomised phase III trial. In one of the phase II trials NCI 06-C-0064E, patients were administered Bevacizumab followed by addition of irinotecan to the next dose of Bevacizumab. The progression-free survival (PFS) after 6 months was significantly greater than historical controls with a mean OS of 31 weeks (Kreisl et al., 2009).

In newly diagnosed GBM patients administered with Bevacizumab, reduced microvascular proliferation and microvessel density was observed. Analysis of resected human GBM tumours revealed reduced or depleted VEGF-A expression and downregulation of VEGF receptors (Tamura et al., 2016). In two randomised, double-blind, placebo-controlled phase III clinical trials assessing the effects of Bevacizumab in newly diagnosed GBM patients there was a significant or near-significant increase in PFS in the group administered with Bevacizumab in combination with radiation with concurrent and adjuvant TMZ compared to the placebo group (Chinot et al., 2014; Fu et al., 2016). However, in a study using hypofractionated radiotherapy in combination with TMZ or TMZ plus bevacizumab in elderly patients over 75 years old, there was no significant difference in the mean OS and PMS between the two treatment groups (Ohno et al., 2019).

#### 1.2.5.3 The use and development of small molecule kinase inhibitors for GBM treatment

Small molecule kinase inhibitors have been produced for the targeted inhibition of different kinase families that have an involvement in tumour initiation and progression. EGFR tyrosine kinase inhibitors (TKIs) are small molecule competitive inhibitors which bind to the ATP-binding site on the tyrosine kinase domain of the receptor, inhibiting the catalytic activity of the kinase. The EGFR TKI gefitinib showed event-free survival of 13.2% after six months in a phase II trial of recurrent GBM (Rich et al., 2004). Erlotinib was shown to be more effective against malignant gliomas than gefitinib, with higher *EGFR* expression levels associated with a better therapeutic response (Haas-Kogan et al., 2005). The literature demonstrates that EGFR clearly has an important role in the pathogenesis of high-grade gliomas however clinical trials with EGFR inhibitors have failed to show significant results. This could be attributed to the acquisition of new resistance mutations or failure to cross the BBB effectively (Alifieris and Trafalis, 2015).

Multitargeted tyrosine kinase inhibitors (MTKIs) are able to antagonise multiple kinases although they predominantly have inhibitory activity against specific kinases.

The reversible MTKI Vandetanib (ZD6474) is an anti-angiogenic agent which acts against EGFR, VEGFR-2, -3 and RET. In a U87-MG xenograft model, Vandetanib in combination with TMZ reduced tumour volume by 94%, greater than that achieved by either monotherapy (Jo et al., 2012). In phase II clinical trials with recurrent GBM patients, Vandetanib had no significant activity in patients that had received fractionated radiosurgery prior and some patients experienced seizures as an unexpected side effect (Kreisl et al., 2012).

Many cancers exhibit constitutive activation of CDKs and of cell cycle dysregulation such as melanoma (Vijayaraghavan et al., 2018). As a result, CDK4 and 6 are frequently investigated targets for kinase inhibition in cancer. Deletion of the tumour suppressor and negative regulator of CDK4, *P16INK4a* is observed in 38% of cancers (Spring et al., 2016). Gene amplification and germline mutations in CDK4 are common aberrations in melanoma and result in constitutive activity of CDK4, enhancing cell proliferation (Goel et al., 2018). CDK6 is regulated by cyclin D and CDK inhibitor proteins. Overexpression of CDK6 is present in various cancers including medulloblastoma, leukaemia and melanoma and its overexpression associated with chromosomal rearrangements (Cao et al., 2020). Palbociclib Isethionate (PD0332991) is a CDK4/6 inhibitor developed to arrest the cell cycle and restrict growth of proliferating tumour cells (Chen et al., 2018). PD0332991 is particularly effective in tumours lacking p16INK4a or overexpressing cyclin D such as bladder and gastric cancers. Tumours lacking functional RB1 appear to be resistant to PD0332991 treatment (Gopalan et al., 2018). The effectiveness of PD0332991 as a monotherapy has been investigated in many phase I/II clinical trials and has been approved by the FDA for treatment of hormone receptor-positive breast cancers in combination with anti-oestrogen therapies. Clinical trials have revealed PD0332991 to be relatively ineffective at providing single agent anti-cancer activity due to the development of tumour resistance (Serra et al., 2019), emphasising the need for PD0332991 to be administered in combination with other agents in order to be of clinical significance. In GBM, inhibition of CDK4/6 arrests growth of intracranial GBM xenografts (Michaud et al., 2010) and increased OS in mouse models of brainstem glioma (Barton et al., 2013). Combination of CDK4/6 and mTOR inhibitors enhances the effects of

PD0332991 in gliomas by blocking compensatory signalling mechanisms, improving penetration of PD0332991 across the BBB and enhancing cytostatic to cytotoxic conversion (Olmez et al., 2017). Resistance to PD0332991 is mainly mediated by RB1 inactivation however activation of CDK2, cyclin D amplification and loss of p21CIP1 or p27KIP1 may also contribute to tumour adaptation and subsequent resistance (Arnedos et al., 2018). In a more recent study, CDK4 expression was found to be significantly elevated in glioma cells and tissues. Overexpression of CDK4 resulted in increased colony formation and cell proliferation whereas knockdown of CDK4 restricted colony formation and proliferation. The CDK4/6 inhibitor Ademaciclib reduced proliferation and induced apoptosis in glioma cells and increased sensitivity to TMZ. CDK4-mediated phosphorylation of Rb demonstrates a possible oncogenic role of CDK4 in glioma. CDK4/6 inhibition also restricted growth of glioma xenograft models *in vivo*, enhancing p-RB levels, reducing Ki-67 levels and enhancing activation of caspase 3 (Cao et al., 2020). Therefore, CDK4/6 inhibition is an attractive target for glioma treatment and can potentially overcome TMZ resistance.

The use of kinase inhibitors in the treatment of GBM shows promising potential where the inhibitor target is implicated in tumour growth and progression. Due to the heterogeneity within GBM tumours, combination therapies are likely to be most effective at reducing tumour growth. Combination therapies have shown to enhance the effects of small molecule inhibitors or enhance the response to chemotherapeutic agents such as TMZ. Combining small molecule inhibitors which target gene products of different core pathways in GBM is likely to be the way forward in small molecules inhibitor therapies. GBM is a highly proliferative tumour and is heavily reliant on CDK activity for tumour maintenance and progression. As CDKs are key in cell cycle regulation, targeting them offers great potential to reduce tumour growth and the literature surrounding the use of CDKis in cancer therapy justifies the adaption of these inhibitors for the reduction of CIZ1 levels and tumour growth in GBM.

### 1.3 Discovery and characterisation of p21<sup>Cip1</sup>-interacting zinc finger protein 1 (Ciz1)

CIZ1 was first discovered via its interaction with cell-cycle regulator p21<sup>Cip1/Waf1</sup> using the *S. cerevisiae* yeast two-hybrid system. p21<sup>Cip1/Waf1</sup> inhibits cell-cycle progression by binding to and inhibiting cyclin/CDK complexes in G1 phase (Mitsui et al., 1999). CIZ1 was isolated and characterised for a second time in human medulloblastoma (Warder and Keherly, 2003).

CIZ1 is a nuclear protein that has been found to have complex regulatory activity. CIZ1 has been linked to several areas of nucleic acid metabolism including regulation of the initiation phase of DNA replication (Copeland et al., 2010; Coverley et al., 2005), X chromosome localisation and X chromosome inactivation (Ridings-Figueroa et al., 2017; Sunwoo et al., 2017), as well as epigenetic maintenance (Stewart et al., 2019). CIZ1 is associated with Alzheimers, dystonia and cancer. This section will review its role in regulation of the cell cycle, the current evidence supporting a role for CIZ1 as a target in cancer and its current use as a potential diagnostic and prognostic biomarker in specific tumour types.

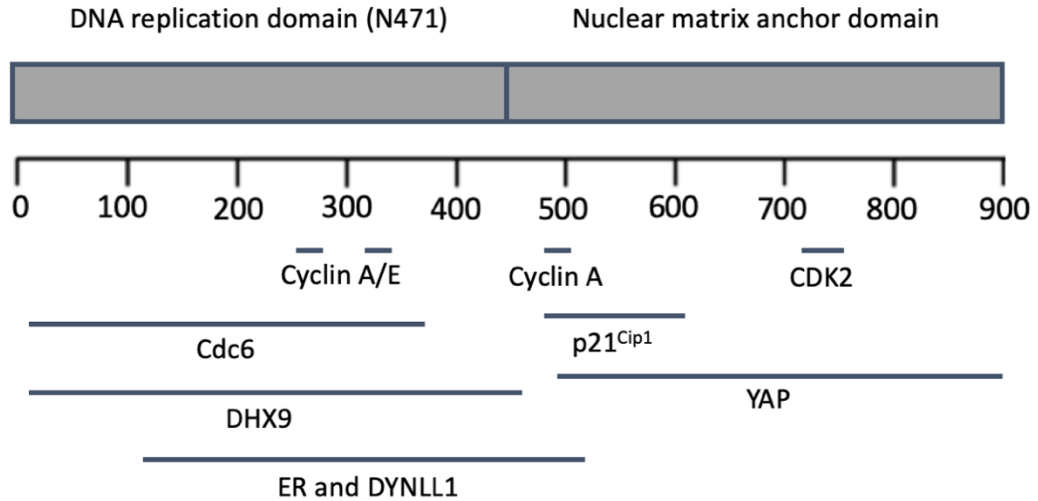


**Figure 1.2 Structure of human CIZ1 protein.** CIZ1 contains an N-terminus DNA replication domain and C-terminus nuclear matrix (NM) anchor domain. Sequences of interaction sites with CIZ1 are labelled: cyclin A and E, CDK2, Cdc6, p21<sup>Cip1</sup>, DHX9, YAP, oestrogen receptor (ER) and dynein light chain (DYNLL1). X-axis denotes amino acid number.

CIZ1 is predicted to be a natively disordered protein, with several functional domains identified. Its N-terminus has polyglutamine repeats and a glutamine-rich region which promotes the initiation of DNA replication via interactions with the pre-RC protein Cdc6 and cyclin A-CDK2. The C-terminus of CIZ1 consists of three zinc-finger motifs and one matrix 3-homologous domain 3 (MH3) which contain nuclear matrix binding domains (Ainscough et al., 2007; Copeland et al., 2010; Pauzaite et al., 2016). CIZ1 binds to p21<sup>Cip1/Waf1</sup> via a region of 150 amino acids containing a zinc-finger motif (Mitsui et al., 1999). Co-expression of CIZ1 and p21<sup>Cip1/Waf1</sup> *in vitro* results in cytoplasmic distribution of p21 in comparison to its localisation within the nucleus when expressed individually. This suggests that CIZ1 is a nuclear protein able to regulate the subcellular localisation of p21 (Mitsui et al., 1999).

## 1.4 The role of CIZ1 in regulation of the cell cycle

The cell cycle must be tightly controlled to ensure precise timing and maintenance of cell division when required. The cell cycle consists of four phases: G1 phase, S-phase, G2 phase and M phase which occur during cell division. The two main events in cell division are DNA replication which occurs in S-phase and cell division which occurs in M phase. These two events are separated by gap phases, G1 and G2 respectively, which allows cells to prepare for these events or arrest the cell cycle if needed (Clark et al., 2019). In G1 phase, cells grow and commit to entering the cell cycle after exposure to extracellular signals. The main events in G1 phase include origin licensing, loading of pre-RC components followed by activation of helicase and DNA polymerases and replisome formation (Parker et al., 2017). In S-phase, the timing of replication origin firing is critical for successful DNA replication. During early S-phase euchromatin is replicated, origin activation is strongly correlated with transcription of early S-phase genes. In the first half of S-phase 75% of genes are replicated, euchromatin is a more loosely packed structure of chromatin allowing transcription machinery to access the DNA more easily. During late S-phase there is replication of heterochromatin at the nuclear and nucleolar periphery (Rhind and Gilbert, 2013). The structures located at the ends of chromosomes, telomeres, are also replicated during S-phase with different replication times being linked to the localisation of chromosomes post replication (Arnoult et al., 2010). In G2 phase, cells ensure the DNA has been replicated accurately and prepare for mitotic division by assembly of the mitotic spindle in response to increasing CDK levels. There is also a checkpoint which blocks entry into M phase if DNA damage is present (Kousholt et al., 2012). In M phase, the sister chromatids of chromosomes are segregated into two separate daughter cells by mitosis which consists of four stages: prophase, metaphase, anaphase and telophase (Clark et al., 2019).

The regulation of DNA replication is strictly regulated by cyclin-CDK complexes to ensure the genome is replicated only once per cycle. Cyclin-CDK activity oscillates

throughout the cell cycle to specify transition thresholds at S-phase and mitosis which denote the G1/S transition and G2/M transition respectively. The oscillating activity of cyclin-CDK complexes temporally separates replication licensing from replication origin firing. In actively dividing cells, pre-replication complex (pre-RC) assembly begins during late mitosis following a drop in CDK activity due to anaphase promoting complex/cyclosome (APC/C) activation, phosphatase activation and cyclin degradation. Replication licensing is regulated by cyclin-CDK activity whereby high CDK activity inhibits licensing during late G1 phase (Sclafani and Holzen, 2007).

#### 1.4.1 Initiation of DNA replication

DNA replication occurs at defined sites within chromosomes, resulting in the aggregation of active replication complexes called replication factories. Initiation of DNA replication is highly spatially and temporally controlled in a process that spans mitosis through to the activation of replication factories in S-phase. This process can be divided into four specific events; origin specification, pre-RC assembly, helicase activation and replisome formation/activation (Parker et al., 2017). Origins are specified at low kinase levels after activation of the anaphase promoting complex that results in degradation of the mitotic kinase cyclin B (Pauzaite et al., 2016). Origin specification begins with the binding of the origin replication complex (ORC) to A-T rich motifs. In G1 phase ORC facilitates the binding of Cdc6, the chromatin licensing and DNA Replication Factor 1 (Cdt1) leading to recruitment of the minichromosome maintenance 2-7 (MCM2-7) complex to putative origins that are collectively called the pre-RC. This complex associates with putative replication origins that are spaced between 50-100 kilobases along the chromosomes (Bleichert et al., 2015). Formation of the pre-RC is CDK activity independent and utilises ATPase activity of Cdc6 and ORC to aid MCM2-7 helicase loading onto DNA. Once the pre-RC is associated with chromatin the DNA is 'licensed' for DNA replication and can be activated by recruitment of additional factors (Evrin et al., 2009). Activation of the replication helicase is achieved through the binding of MCM2-7, Cdc45 and GINS, known as the CMG complex, aided by the activity of cyclin E-CDK2 and Dbf4-dependant kinase (DDK) (Parker et al., 2017). This activates MCM2-7 helicase activity and completes formation

of the DNA replication initiation complex resulting in localised DNA unwinding (Kanke et al., 2012). The replication machinery is then able to load after the opening of the chromatin structure by the replicative helicase complex that includes DNA polymerases  $\alpha$ ,  $\delta$ , and  $\epsilon$ , which associate with proliferation cell nuclear antigen (PCNA), along with accessory factors leads to completion of replisome assembly and initiation of DNA replication (Burgers and Kunkel, 2017).

The process of eukaryotic DNA replication must occur with extreme fidelity and be precisely regulated to ensure chromosomes are replicated only once per cell cycle to maintain integrity of the genome. DNA is copied by semi-conservative replication, whereby the leading strand is synthesised continuously in the same direction as the moving replication fork and the lagging strand is synthesised discontinuously in the opposite direction. There are 3 phases of DNA replication which include initiation, elongation and termination. Initiation involves the formation of replication fork by localised DNA unwinding followed by primer binding (Fragkos et al., 2015). The DNA polymerase  $\alpha$ -primase complex initiates DNA replication on the leading strand and production of Okazaki fragments on the lagging strand. DNA polymerases  $\delta$  and  $\epsilon$  are also required for DNA replication,  $\delta$  is the main polymerase involved in leading-strand synthesis and  $\delta$  and  $\epsilon$  are the main polymerases involved in lagging-strand synthesis (Bhagavan and Ha, 2015, Baris et al., 2022). The replication of the DNA by the replisome is known as elongation. Replication fork arrest occurs when terminator proteins bind Ter sites located within non-transcribed spacers of rDNA, checkpoint proteins are also required for stable fork arrest. These events comprise termination of DNA replication (Mohanty et al., 2006).

#### 1.4.2 Role of Ciz1 in DNA replication

CIZ1 interacts with the pre-RC through cell division cycle 6 (Cdc6) interactions during late G1 phase. CIZ1 binds to cyclin E promoting recruitment of Cdc6 and assembly of the pre-RC. Sequentially, CIZ1 localises cyclin-A-cyclin dependant kinase 2 (Cyclin-A-CDK2) activity to the chromatin and nuclear matrix. During S-phase cyclin A displaces cyclin E from CIZ1 allowing binding of CDK2 onto the pre-RC. Cyclin-A-CDK2 is then

able to induce phosphorylation of CIZ1 at three threonine residues. This prevents CIZ1 interacting with Cdc6 and cyclin-A-CDK2, promoting recruitment of PCNA and activation of the replisome. Mutation of cyclin-binding motifs (Cy motifs) or depletion of CIZ1 via short-interfering RNA (siRNA) prevents recruitment of cyclin A-CDK2 to chromatin and therefore suggests CIZ1 promotes subnuclear localisation of cyclin A-CDK2 at the G1/S transition for successful initiation of DNA replication (Copeland et al., 2010; Copeland et al., 2015). At high CDK levels, CIZ1 becomes phosphorylated at multiple sites resulting in hyperphosphorylation, blocking interactions with cyclin A-CDK2 and preventing localisation to the nuclear matrix therefore preventing the initiation of DNA replication (Copeland et al., 2015).

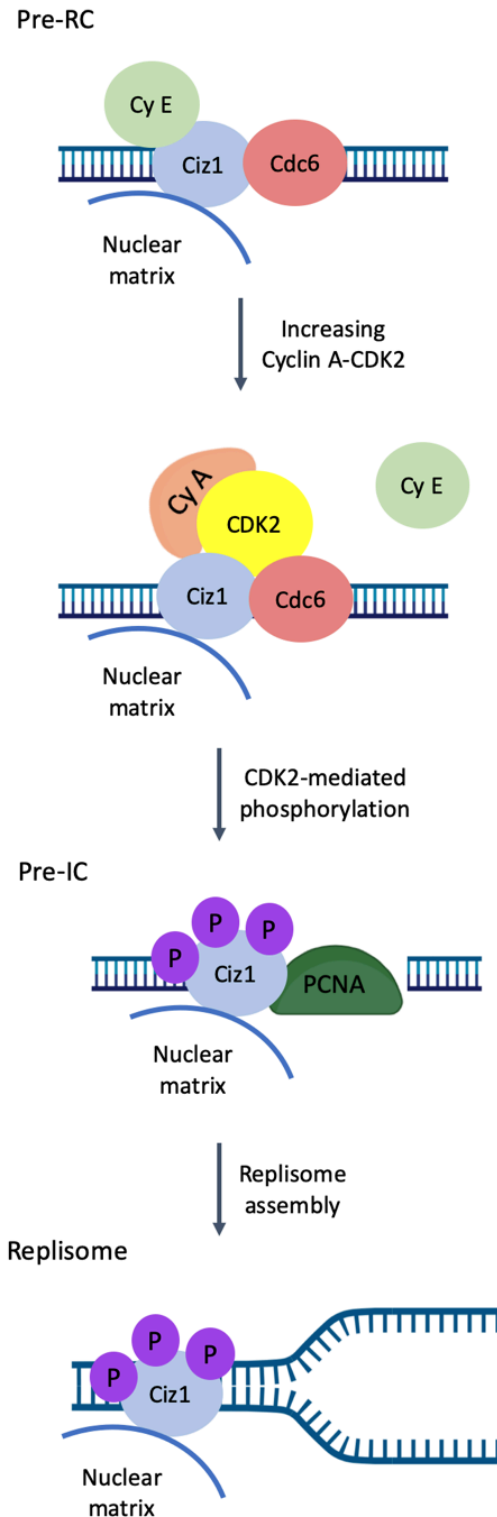


**Figure 1.3 The role of CIZ1 in the initiation of DNA replication.** In early G1 phase, CIZ1 binds CDC6 promoting recruitment to the nuclear matrix and formation of the pre-replication complex. CIZ1 accumulates as cyclin A levels increase at the G1/S transition and cyclin E is displaced by the cyclin A-CDK2 complex leading to phosphorylation of CIZ1 at T293 preventing further interactions with cyclin A-CDK2 and Cdc6. PCNA is recruited resulting in assembly and activation of the replisome. The binding of DNA polymerase  $\alpha$ -primase completes the initiation of DNA replication.

CIZ1 also acts as a kinase sensor able to promote DNA replication and prevent re-replication. CIZ1 promotes the initiation of DNA replication at low kinase levels when in a hypophosphorylated state. This state allows for interactions with cyclin A-CDK2 and delivery to licensed origins. Whereas, hyperphosphorylation of CIZ1 when CDK activity is high, prevents recruitment of cyclin A-CDK2 subsequently blocking activation of origins where it is bound (Copeland et al., 2015).

## 1.5 Role of CIZ1 in tumourigenesis

Aberrant CIZ1 expression, regulation and splicing has been implicated in various cancer types including breast, prostate and lung which are among the most common cancers in the UK and are responsible for the highest cancer-related mortalities. The role of CIZ1 in tumourigenesis is down to three main mechanisms: overexpression, transcriptional regulation and alternative splicing. In addition to the oncogenic roles of CIZ1, tumour suppressor functions of CIZ1 have been observed. CIZ1-deficient mice grew with no obvious developmental defects but were prone to leukaemia development by retroviral insertional mutagenesis. Furthermore, CIZ1-deficient mouse embryonic fibroblasts (MEFs) displayed no defects in cell cycle status, cell growth or DNA damage response however were more sensitive to hydroxyurea-mediated replication stress, suggesting these MEFs have a defective DNA repair process. These MEFs were also susceptible to oncogene-induced transformation. Taken together, these results suggest a potential tumour suppressor role of CIZ1 (Nishibe et al., 2013).

### 1.5.1 Overexpression of CIZ1 and its role in tumourigenesis

CIZ1 contributes to cellular proliferation *in vitro* (Copeland et al., 2010; Copeland et al., 2015) and *in vivo* through induction of tumourigenesis in mouse xenograft models (Higgins et al., 2012), suggesting CIZ1 is associated with tumour initiation and growth. CIZ1 may have oncogenic functions, overexpression of CIZ1 is associated with enhanced tumour growth in prostate cancer (Liu et al., 2015), colorectal (Wang et al., 2014), gall bladder (Zhang et al., 2015) and hepatocellular carcinoma (HCC) (Wu et al.,

2016). In small cell lung and non-small cell lung carcinoma, tumour cells rely on an alternatively spliced transcript of CIZ1 to support S-phase and drive tumour cell proliferation (Higgins et al., 2012). In each case, siRNA-mediated depletion of CIZ1 reduced proliferation *in vitro* and subsequent tumour growth in xenograft models. These findings provide a potential therapeutic opportunity for selective reduction of tumour growth.

**Table 1.1: CIZ1 contributes to tumourigenesis in various cancers.** Table summarises the effects of CIZ1 alterations and short hairpin RNA (shRNA)/siRNA-mediated depletion of CIZ1 on tumour growth.

Type of cancer	CIZ1 Alteration	Therapeutic Intervention	Effects of Intervention
Gall bladder carcinoma (GBC)	Overexpression	siRNA	Reduced proliferation and migration <i>in vitro</i> . Reduced tumour growth in mouse xenograft models (Zhang et al., 2015).
Colorectal carcinoma (CRC)	Overexpression	siRNA	Reduced RKO cell proliferation and colony formation <i>in vitro</i> (Wang et al., 2014).
Breast cancer	Overexpression	siRNA	Reduced cell proliferation, tumourigenesis and anchorage dependant growth (Liu et al., 2016).
Prostate cancer	Overexpression	siRNA	Reduced proliferation and colony formation <i>in vitro</i> . Inhibited tumour formation in mouse xenograft models (Liu et al., 2015).
Hepatocellular carcinoma (HCC)	Overexpression	siRNA	Reduced growth, migration and metastasis of HCC cells <i>in vitro</i> (Wu et al., 2016).
Lung cancer	Alternative splicing	shRNA	Restricted growth of tumour cells both <i>in vitro</i> and in mouse xenograft models (Higgins et al., 2012).

Overexpression of CIZ1 has been implicated in cell proliferation and tumour growth in a number of human cancers. In human prostate carcinoma CIZ1 mRNA and protein expression levels were found to be higher in high-grade prostate cancer than low-grade prostate cancer and normal tissue. Knockout of the *CIZ1* gene in PC-3 cells reduced proliferation, colony formation and S-phase entry *in vitro* (Liu et al., 2015). *CIZ1* knockdown also suppressed expression of genes encoding the serine-threonine protein kinase (AKT1) and prostate-specific antigen (PSA) which are implicated in prostate carcinoma. In mouse xenograft models, *CIZ1* knockdown significantly reduced tumour formation compared to controls. Both *in vitro* and *in vivo* data provide evidence for the role of *CIZ1* in cell proliferation and tumour growth in PC-3 cells however it's important to consider that reduced proliferation could somewhat be due to reduced expression of AKT1 and PSA (Liu et al., 2015). In GBC, expression of *CIZ1* was found to be significantly higher in human GBC tissue compared to adjacent normal tissue. Forced expression of *CIZ1* was used to assess the oncogenic role of *CIZ1* in GBC; overexpression of *CIZ1* in GBC-SD and SGC-996 cell lines promoted anchorage-independent growth. Knockdown of *CIZ1* in SGC-996 and EH-GB2 cells inhibited growth, colony formation and migration of these cell lines. In mouse xenograft models generated using SGC-966 cells, tumour growth was significantly reduced in the knockdown cells compared to the control cells (Zhang et al., 2015). Together these findings demonstrate the role of *CIZ1* in promoting the tumorigenicity of GBC cells.

### 1.5.2 Dysregulation of oncogenic transcriptional programs by *CIZ1*

The precise molecular mechanisms by which *CIZ1* contributes to tumourigenesis are not fully understood. However, studies have shown *CIZ1* to play a role in the signalling pathways involved in tumourigenesis. Aberrant oestrogen expression is the main risk factor for the development of breast cancer. *CIZ1* is able to bind oestrogen receptors increasing the expression of oestrogen downstream target genes, suggesting *CIZ1* may contribute to the initiation and development of breast cancer. *CIZ1* interacts with the oestrogen-induced protein DLC1 resulting in increased CDK2 activity and a subsequent increase in cell proliferation. The oestrogen receptor (ER) in these cells is bound by oestrogen receptor- $\alpha$  (ER- $\alpha$ ) in the cytoplasm resulting in dimerisation of the activated

ER followed by translocation to the nucleus. CIZ1 binds the ER- $\alpha$  via its N-terminus which encourages binding of the ER- $\alpha$  and responding elements to the DNA resulting in transcription of target genes including *CIZ1*. The oestrogen-induced transcription of *CIZ1* upregulates the oestrogen signalling pathway creating a positive feedback loop (Liu et al., 2016).

CIZ1 also interacts with Yes-associated protein (YAP) and regulates its transcriptional activity in HCC cells. YAP/TAZ signalling is involved in cancer progression and is an oncogenic transcription factor in numerous cancers. Enhanced expression of YAP/TAZ and nuclear localisation is associated with poor clinical outcome in breast, prostate, lung and colorectal cancers. Hippo-YAP signalling is dysregulated in HCC and plays a role in tumourigenesis. Previous studies have demonstrated that CIZ1 activates YAP signalling in HCC cells and this promotes growth and migration of these cancer cells (Wu et al., 2016), however the precise mechanisms by which CIZ1 activates YAP signalling were unknown. A continuation study demonstrated the interaction of CIZ1 with GST-YAP1 in a GST pull-down assay via the nuclear matrix anchor domain of CIZ1. Knockdown of *CIZ1* blocked expression of YAP downstream target genes CTGF and Cyr61. Further investigation using a chromatin immunoprecipitation assay assessed the binding of the YAP/TEAD complex to the CTGF promoter and revealed decreased binding of YAP to the CTGF promoter upon CIZ1 knockdown (Lei et al., 2016). These findings demonstrate the role of CIZ1 in regulation of the transcriptional activity of YAP and render CIZ1 as a viable therapeutic target in HCC.

### 1.5.3 Alternative CIZ1 splicing as a driver or marker of tumourigenesis.

Alternative splicing of CIZ1 contributes to tumourigenesis in small cell and non-small cell lung carcinoma (NSCLC) cells. The *CIZ1* b-variant is prevalent in these tumours and is characterised by a missing 24 nucleotides from the 3' end of exon 14, with 98% of patients being classified based on the presence of this variant. In human SBC5 small cell lung carcinoma (SCLC) cells siRNAs targeted against the b-variant delivered via an inducible shRNA vector significantly restrained proliferation in these cells. More importantly, in mouse xenograft models of SCLC derived from human SBC5 cells,

shRNA targeted against the CIZ1 b-variant successfully suppressed this variant without affecting other CIZ1 isoforms and significantly restricted tumour growth (Higgins et al., 2012). These *in vitro* and *in vivo* studies demonstrate the exploitation of this specific variant for the reduction of tumour growth, indicating the CIZ1 b-variant as a driver of proliferation in SCLC and NSCLC.

## 1.6 Potential for CIZ1 as a diagnostic and prognostic biomarker in cancer

The CIZ1 b-variant has also been exploited for use as a biomarker in the detection of early-stage SCLC and NSCLC. Proteins which reside in the nuclear matrix are advantageous for use as biomarkers; they are very stable and are resistant to harsh extraction conditions, they are also likely to be involved in the epigenetic control of gene expression which confers the phenotypic traits of cancer cells. (Higgins et al., 2012). The CIZ1 b-variant can be used to detect early-stage lung cancer via a blood test, in Higgins et al. western blot analysis confirmed the presence of this variant in blood plasma from a cohort of SCLC and NSCLC patients, with the variant undetectable in healthy individuals.

CIZ1 has also been investigated as a prognostic biomarker in CRC. Immunohistochemistry (IHC) analysis of CRC patient-derived tissue sections revealed significantly increased expression of CIZ1 in tumour tissue compared to adjacent normal tissue and this increased CIZ1 expression was correlated with a poor OS (Wang et al., 2014).

## 1.7 Aims

CIZ1 deregulation is known to contribute to tumour growth and development in multiple tumour types, although, the role of CIZ1 in the growth of neurological tumours is yet to be investigated. This work will evaluate the role of CIZ1 in GBM tumorigenesis and the dependence of primary GBM cell lines on CIZ1 for proliferation

and tumour growth. Previous studies have implicated CIZ1 regulation by opposing CDK and ubiquitin E3 ligase activity. This study will assess the utility of targeting kinases controlling CIZ1 expression levels in established and primary cell lines. Small molecule inhibitor and gene knockout studies will evaluate and compare the dependency of established and primary GBM cell lines on CIZ1 for survival.

To evaluate the potential of CIZ1 as a biomarker in GBM, the expression and localisation of CIZ1 in GBM tissue will be investigated. IHC analysis of patient-derived FFPE GBM tissue samples will be performed to compare the expression and localisation of CIZ1 between tumour tissue and relatively healthy tissue.

## Chapter 2: Materials and Methods

### 2.1 Cell culture

SW480 (primary human colorectal carcinoma cell line), SW620 (primary human colorectal carcinoma cell line), PC3 (human prostate adenocarcinoma cell line) and U87-MG (human GBM cell line) cells were cultured in GIBCO's Dulbecco's Modified Eagle Medium (DMEM) (1 g/l glucose with pyruvate and glutaMAX II). A549 (human non-small cell lung cancer cell line) cells were cultured in GIBCO's DMEM with high glucose (4 g/l glucose with pyruvate and glutaMAX II). Primary GBM cells BTNW914 were cultured in HyClone Ham's; F10 Mixture medium with L-glutamine (Cytiva). All media were supplemented with penicillin-streptomycin, glutamine (100X) (GIBCO) and 10% (v/v) foetal bovine serum (FBS) (Labtech). Cells were grown on 15 cm diameter plates with 30 mL media. Cells were incubated at 37°C, 5% CO<sub>2</sub> and passaged routinely to maintain confluency of 30-70%. Cells were passaged by removal of existing media, cells washed in 10 mL Dulbecco's Phosphate Buffered Saline (PBS) (GIBCO). Cells were trypsinised in 1 mL 0.5% trypsin-EDTA (GIBCO) and 9 mL PBS for 2-3 minutes or until all cells had dissociated from the plate. Trypsin was neutralised with an equal volume of media and split appropriately across the desired number of plates and the appropriate volume made up with media.

### 2.2 Primary GBM cells

Primary GBM cells (BTNW914, female GBM patient, aged 67) were provided by the Brain Tumour North West (BTNW) tissue bank at Royal Preston Hospital. Cell stocks were established from human glioblastoma biopsies obtained from the BTNW tissue bank.

## 2.3 Sodium Dodecyl Sulfate Polyacrylamide Gel Electrophoresis (SDS-PAGE)

Cells were washed twice with 1 mL PBS and lysed in 200  $\mu$ L lysis buffer (650  $\mu$ L 4 x loading buffer, 600  $\mu$ L Milli Q water and 200  $\mu$ L DTT). 1 mM PMSF was added to each well and incubated for 1 minute. Cell extracts were collected, vortexed for 20 seconds and samples boiled in a 95 °C heating block for 10 minutes. Samples were allowed to cool before being loaded onto an SDS-PAGE gel or frozen at – 20 °C until required. 5  $\mu$ L of prestained protein ladder and 10  $\mu$ L of each sample were loaded onto a 10% self-cast SDS-PAGE resolving gel with 5% stacking gel. Gels were run in a Mini-PROTEAN Tetra Cell tank (Bio-Rad) between 100 and 200 V for 1 h or until the sample dye reached the bottom of the gel.

## 2.4 Western blotting

2.4.1 Transferring protein to a Polyvinylidene Difluoride (PVDF) membrane  
For western blot analysis, proteins were run on an SDS-PAGE gel and transferred onto an Amersham Hybond P 0.2  $\mu$ m PVDF membrane (GE Healthcare Life Sciences) using a semi dry transfer system. 8 pieces of filter paper and 1 piece of PVDF membrane were cut into 9 x 7 cm pieces for each gel. Filter paper, PVDF membrane and SDS-PAGE gels were soaked in transfer buffer (10% v/v absolute ethanol, 0.75 mM Tris base (Sigma Aldrich), 10  $\mu$ M CAPS (Sigma Aldrich), 0.01% w/v SDS). 4 pieces of filter paper were placed on the base of the transfer plate. PVDF membranes were hydrated in 98% ethanol, soaked in transfer buffer for 5 minutes and placed on top of the filter paper. Gels were detached from the plates by soaking in transfer buffer and placed on top of the membrane. The remaining 4 pieces of filter paper were stacked on top of the gel. Proteins were transferred onto the membrane at 63 mA/gel, 25 V for 90 minutes.

## 2.4.2 Probing membranes

Following transfer, membranes were blocked in 10 mL blocking buffer (10% v/v Tris Buffered Saline (TBS), 1% w/v BSA, 0.1 % Tween-20) for 1 hour on a roller at room temperature. Membranes were then incubated in the appropriate primary antibody concentration (Table 2.1) in 5 mL blocking buffer overnight on a roller at 4 °C. The following day, membranes were washed in blocking buffer for 4 x 5 minutes and incubated in the appropriate secondary antibody concentration (Table 2.1) for 1 hour on a roller at room temperature. Membranes were then washed in wash buffer (10 % v/v TBS, 0.1 % Tween-20) for 4 x 5 minutes. Western blots were developed with the Bio-Rad Chemidoc MP Imaging System using the SuperSignal™ West Pico PLUS Chemiluminescent Substrate (ThermoScientific).

Protein was quantified against the loading control actin using Image Lab Software (Bio-Rad). Signal intensity of the bands on the western blot was converted into relative number and the protein divided by actin to give relative quantity. The control was then normalised to 1 and every sample divided by the relative control number to give protein quantity.

**Table 2.1 List of antibodies used in this study.** Table indicates antibodies used, antibody code, dilution used and source. The Covalabs Ciz1-N471 antibody was used for western blotting experiments only.

Antibody	Code	Dilution	Source
Ciz1-N471	Copeland et al. 2015	1:1000	Covalabs
Actin	A-1978	1:10000	Sigma Aldrich
HRP anti-rabbit secondary	Ab6721	1:5000	Abcam
HRP anti-mouse secondary	62-6520	1:5000	Invitrogen
GFAP	Ab190288	1:800	Abcam
Alexafluor 488 nm goat anti-mouse IgG secondary	A11001	1:2000	Invitrogen

## 2.5 Preparation of immunopurified anti-CIZ1 antibody

### 2.5.1 CIZ1-N471 expression

Competent *E. coli* BL21 (DE3) cells were transformed with the pGEX6p3-N471 plasmid (Copeland et al., 2010) and cultured overnight on LB agar plates with 100 µg/mL ampicillin. Single colonies were used to inoculate a 10 mL LB broth, Ampicillin 100 µg/ml starter culture to inoculate a 75 mL LB, 100 µg/mL ampicillin that was incubated overnight at 200rpm, 37°C. This was used to inoculate 750 mL auto-induction medium (ZY medium, 1 x 5052, 1 x NPS, 1 x trace metals, 1mM MgSO<sub>4</sub>, Ampicillin (100 µg/mL) and incubated for 20 hours with shaking at 200 rpm, 20°C.

**Table 2.2** Components and their concentrations required to make up autoinduction media.

Solution	Component	Concentration
ZY	Tryptone	10 g/l
	Yeast extract	5 g/l
NPS	Ammonium sulfate	0.5 M
	Potassium phosphate	1 M
	Sodium phosphate	1 M
5052	Glycerol	250 g/l
	Glucose	2.78 mM
	$\alpha$ -Lactose	5.84 mM
1000x trace metals	FeCl <sub>3</sub>	50 $\mu$ M
	CaCl <sub>2</sub>	20 $\mu$ M
	MnCl <sub>2</sub>	10 $\mu$ M
	ZnSO <sub>4</sub>	10 $\mu$ M
	CoCl <sub>2</sub>	2 $\mu$ M
	CuCl <sub>2</sub>	2 $\mu$ M
	NiCl <sub>2</sub>	2 $\mu$ M
	Na <sub>2</sub> MoO <sub>4</sub>	2 $\mu$ M
	Na <sub>2</sub> SeO <sub>3</sub>	2 $\mu$ M
	H <sub>3</sub> BO <sub>3</sub>	2 $\mu$ M

### 2.5.2 CIZ1-N471 purification

Bacteria were harvested by centrifugation in the SLC6000 rotor at 4500 rpm for 15 minutes, 4 °C. The bacterial pellet was resuspended in 25 mL resuspension buffer (HEPES buffered saline, HBS; 50 mM HEPES pH 7.8, 135 mM NaCl, 3 mM EDTA), 2 x Roche complete protease inhibitors, 1 mM PMSF, 1 mM DTT at room temperature. The solution was sonicated for 4 x 15 seconds with a 1-minute interval between each sonication in an ice slurry. Sonication was performed at 25 – 30 microns peak to peak

using a probe 2 cm in diameter. The cell lysates were centrifuged in the ss34 rotor at 20,000 rpm, 30 minutes, 4°C. 750 µl Glutathione Sepharose 4B beads (GE Healthcare Life Sciences) were resuspended in 50 mL bead washing buffer (HBS, 1mM DTT) and incubated on a shaker at room temperature for 1 hour. The beads were recovered by centrifugation at 1000rpm for 1 minute, buffer removed with a pipette to avoid disturbance of the beads. The cell lysate was added to the beads and incubated on an end-over-end mixer for 1 hour, 4°C. The unbound lysate was removed by centrifugation at 1000 rpm and aspiration with a serological pipette. Beads were washed 5 times in 10 mL wash buffer (HBS, 1 Roche complete protease inhibitor and 1 mM DTT) and mixed by inversion for 2 minutes and centrifuged at 1000 rpm for 1 minute.

For removal of the GST tag, beads were washed 3 times in 10 mL 3C cleavage buffer (50 mM Tris HCl pH 7.0, 150 mM NaCl, 2 mM DTT), transferred to a 1.5 mL Eppendorf leaving 200 µL head space to prevent precipitation of CIZ1-N471 due to mechanical damage. The GST tag was cleaved using 10 µL of the 3C precision protease and the protein digested on an end-over-end mixer overnight at 4°C. To remove CIZ1-N471, the beads were removed by 6s pulse centrifugation, protein aspirated with a pipette and excess beads removed by a second centrifugation step. Protein concentration was determined using a BCA assay (Pierce™ BCA Protein Assay Kit, Thermo Fisher Scientific), estimating a protein concentration of 1 mg/mL. Protein purity was assessed via SDS-PAGE and Coomassie blue staining. The protein and the beads were snap frozen in liquid nitrogen.

### 2.5.3. Covalent coupling of Ciz1-N471 to resin

CIZ1-N471 was dialysed in sodium phosphate buffer containing 0.5 M NaCl pH 6.8. The cyanogen bromide (CNBr) activated resin was washed and swelled in 1 mM cold HCl for 30 minutes. 100 mg of cyanogen bromide resin was used per 1 mg of CIZ1-N471 purified. The resin was washed with 5-10 column volumes of distilled water in a 0.4 mL spin column. The resin was then washed with PBS coupling buffer and immediately transferred to the solution of CIZ1-N471 in coupling buffer. The protein was mixed

with the gel for 2 h at room temperature on an end-over-end mixer and unreacted ligand was washed away using coupling buffer. Unreacted groups were blocked with 0.2 M glycine pH 8.0 on an end-over-end mixer for 16 hours, 4°C. The beads were washed extensively (10 column volumes) to remove the blocking solution, first with coupling buffer pH 8.5 then with 0.1 M acetate buffer pH 4.0 containing 0.5 M NaCl. This wash cycle was repeated 5 times.

#### 2.5.4 Affinity purification of Ciz1-N471 Antibody

The column was equilibrated with 0.5 mL binding/wash buffer (TBS) for 10 minutes. 1 mL of rabbit serum raised against CIZ1-N471 (Covalabs, Copeland et al., 2015) was centrifuged at 4000 rpm for 10 minutes, 4°C to remove aggregates and debris. The serum was diluted 1:1 in binding/wash buffer and 0.5 mL was applied to the column. The serum was mixed with the beads on an end-over-end mixer for 1 hour, 4°C. The beads were centrifuged to remove unbound protein and the flow through was collected. The column was washed with 5 x 0.5 mL TBS and the absorbance at 280 nm checked to ensure low absorbance prior to elution. The antibody was eluted with 5 x 300  $\mu$ L 100 mM glycine pH 2.5 and the fractions collected in separate tubes containing 30  $\mu$ L 1 M Tris pH 8.0. The tubes were mixed gently to neutralise. The absorbance of the fractions were measured to identify the immunoglobulin containing fractions, the protein concentration of each fraction was determined at A280 nm using the extinction coefficient ( $\epsilon_{\text{percent}} = 14$ ) and the concentrated fractions were pooled. The remaining serum was reapplied to the column and the process repeated.

To evaluate protein purity, protein samples were run on an SDS-PAGE gel and Coomassie blue staining allowed visualisation of protein bands (Figure 2.1 B) The results revealed a strong band at 60 kDa which corresponds to the purified CIZ1-N471. There is likely co-purification of N471 with human HSP-70 which has been observed in previous studies (Copeland et al., 2015).

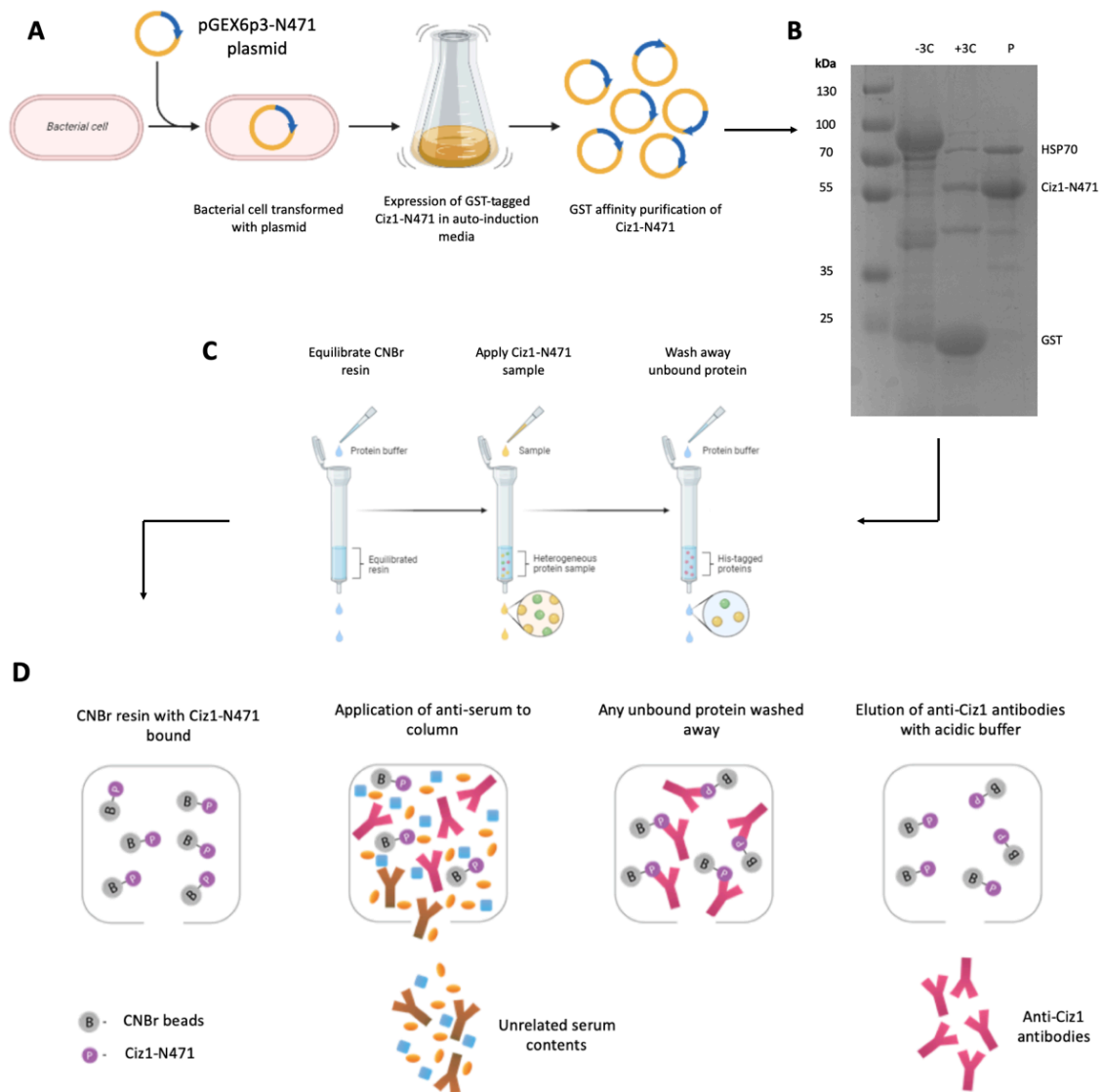


**Figure 2.1 Schematic of anti-CIZ1 antibody production.** A) Transformation of competent *Escherichia coli* Rosetta (DE3) cells with pGEX6p3-N471 plasmid. Induction of E-CIZ1-GST expression in auto-induction media followed by GST affinity purification of CIZ1-N471. B) Coomassie blue stained SDS-PAGE gel showing GST-tagged CIZ1-N471 bound to glutathione sepharose beads (-3C), GST fragment after 3C cleavage with 3C precision protease (+3C) and CIZ1-N471 protein fragment after 3C cleavage (P). C) Immobilisation of CIZ1-N471 onto a CNBr resin. D) Application of serum immunised against CIZ1 to immobilise anti-CIZ1 antibodies. Elution of anti-CIZ1 antibodies with an acidic buffer.

## 2.6 Small molecule CDK/DDK inhibitor treatments

Adherent cells were removed from the plate as described in section 2.1. Detached cells were transferred to a falcon tube and centrifuged at 500 rpm for 5 minutes. Cells were

resuspended in 1 mL of media and cell counts were performed using 10  $\mu$ L of the cell suspension on the Neubauer improved haemocytometer. Cell counts were taken from four 1 mm x 1 mm x 0.1 mm grids (volume = 0.1  $\mu$ L) and averaged. Cells were seeded on a 96-well plate at 6000 cells/mL (BTNW914) or 12500 cells/mL (A549, SW620, PC3, SW480, U87-MG). Asynchronous populations of cells at 50-70% confluency were treated with CDK/DDK inhibitors for 6 or 24 hours at the indicated concentrations (Table 2.3) prior to harvesting and wells mixed with a serological pipette to ensure even distribution of the small molecule kinase inhibitor across the well.

**Table 2.3 Small molecule inhibitors used for *in vitro* kinase inhibition studies.** Table indicates inhibitors used, their main targets, IC50 values, concentration and source.

Drug	Target	IC50 cell-free assays	Concentration	Source
Palbociclib (PD0332991) Isethionate. Hereafter referred to as PD.	CDK4 CDK6	11 nM 16 nM	10 µM	Sigma Aldrich
PHA-767491 dihydrochloride. (PHA)	Cdc7	10 nM	10 µM	Sigma Aldrich
CVT-313 (CVT)	CDK2	0.5 µM	10 µM	Santa Cruz Biotechnology
CDK2-IN-73 (CDK2-IN-4)	CDK2	44 nM	10 µM	Selleckchem
Ro-3306	CDK1	20 nM	10 µM	Selleckchem
XL-413 hydrochloride (XL)	Cdc7	3.4 nM	10 µM	Selleckchem
Roscovitine (Ros)	CDK2	0.7 µM	30 µM	Selleckchem
MG132	Proteasomal inhibitor	1.2 µM	10 µM	Sigma Aldrich

## 2.7 PrestoBlue™ Cell Viability Assay

Adherent cells were detached from the plate and counted as described in section 2.6. Cell number optimisation was performed using a cell stock of 200,000 cells/ml and

serially diluting the cells across a 96-well plate. Plates were incubated for 24 hours at 37 °C, 5% CO<sub>2</sub>. 10 µL 10X PrestoBlue™ Cell Viability Reagent (Invitrogen) was added to 90 µL of cells/media, plates were incubated at 37 °C, 5% CO<sub>2</sub> for 1 hour and the fluorescence excitation read at 560 nm and the emission read at 610 nm using a 96-well plate reader (Tecan Infinite® M200 PRO). Background fluorescence was corrected for and the cell number was plotted against the relative fluorescence units to determine the cell number which allows for 3 cell doublings within a linear range. After determining cell number, cells were seeded on a 96-well plate at 6000 cells/mL (BTNW914) or 12500 cells/mL (A549, SW620, PC3, SW480, U87-MG).

Cells were treated with CDK/DDK inhibitors for up to 96 hours as described in section 2.6 and PrestoBlue™ assays carried out as indicated above. Triplicate repeats for each inhibitor concentration were averaged and the data standardised to day 0. The percentage viability was calculated by standardising the data to the highest value so that it is represented as of 100% of the control population. Graphs were plotted at time vs the % viability with error bars representing the mean ± SD. For analysis of inhibitor titration studies, OriginPro 2019b was used to produce dose-response curves and generate IC50 values using the equation  $y = A1 + (A2-A1)/(1 + 10^{((\text{LOG}x0-x)*p)})$ .

## 2.8 Transfection of BTNW914 cells with siRNA

Transfection of BTNW914 cells was performed using the Nucleofector™ 2b system (Lonza). Anti-Ciz1 siRNA molecules directed against two regions of mouse CIZ1 that are present in all identified CIZ1 splice variants were transcribed *in vitro* using the Ambion Silencer kit. Cells were transfected with anti-CIZ1 siRNA (s24488) (Ambion) in Basic Nucleofector™. Solution for Mammalian Glial Cells according to the Amaxa™ Basic Nucleofector™ Kit for Primary Mammalian Glial Cells (Lonza protocol) using the Nucleofector™ programme T-020. A control sample containing no siRNA was used as a positive control for CIZ1 and a negative control for siRNA knockout. Cells were harvested 24 hours after transfection for analysis. For qRT-PCR, RNA was extracted,

cell cycle analyses were performed by flow cytometry analysis and CIZ1 protein levels determined 24, 48 and 72 post-transfection. PrestoBlue™ was used to compare cell proliferation rates.

## 2.9 RNA extraction and qRT-PCR

Total RNA was extracted and purified according to the Invitrogen PureLink™ RNA mini kit (ThermoFisher) instruction manual and the RNA quantified using a Nanodrop (ThermoScientific). Transcript levels were quantified with the EXPRESS One-Step Superscript™ qRT-PCR Kit (Invitrogen) and a total of 0.1 µg RNA was used for template. TaqMan primers for CIZ1 (Hs00967155) and GAPDH (Hs02758991) were used for quantitation using the FX96 Touch™ Real-Time PCR Detection System (BIO-Rad). CIZ1 transcript abundance is shown relative to the GAPDH.

## 2.10 Cell cycle analysis by flow cytometry

Cells were labelled with 10 µM EdU for 1 hour prior to harvest. Cells were harvested by trypsinisation, quenched in an equal volume of media and centrifuged at 500 x *g*, 5 minutes. The media was discarded, cells washed 3 times in 0.5 mL PBS, 1 % w/v BSA, followed by centrifuging at 500 x *g*, 5 minutes after each wash. Cells were then fixed in 100 µl 4 % PFA for 15 minutes at room temperature and harvested by centrifugation as described. Cells were washed 3 times in 0.5 mL PBS, 1 % w/v BSA, followed by centrifuging at 500 x *g*, 5 minutes after each wash and the pellets frozen at -20 °C. Cells were permeabilised with 500 µl PBS, 0.5% Triton X-100 for 20 minutes. Cells were washed 3 times in 0.5 mL PBS, 1 % w/v BSA, followed by centrifuging at 500 x *g*, 5 minutes after each wash and harvested. Cells were resuspended in 100 µl Click IT EdU cell proliferation assay cocktail (152 µl 1 x reaction mix, 8 µl CuSO<sub>4</sub>, 0.48 µl Alexa Fluor 488/566, 40 µl additives) for 30 minutes protected from light. Cells were washed 3 times in 0.5 mL PBS, 1 % w/v BSA, followed by centrifuging at 500 x *g*, 5 minutes after each wash and stained with either 100 µg/mL propidium iodide (PI) in 0.1 % Triton X-100 in PBS or 100 µg/mL Hoechst 33342 (Thermo Scientific). Data was collected for

10,000 cells using the Beckman Coulter CytoFLEX and channels for FITC (525/40) and PE (585/42) with gating consistent across all samples.

## 2.11 Apoptosis assays

Cells were treated with DMSO and CDK/DDK inhibitors added as described in Table 2.3 at 1:1000 except for PD0332991 which was added at 1:500 for 24 hours. Media was removed from the cells and transferred to a falcon tube. Cells were trypsinised and neutralised in the appropriate tube containing media. Cells were spun down at 500 g for 5 minutes and the supernatant discarded. Cells were washed in 1 mL cold PBS and spun down as previous. Cells were resuspended in 1 mL media and stained with 100 µg/mL PI and 100 µg/mL YO-PRO-1, inverting tubes to mix. Cells were incubated on ice for 30 minutes. Data was collected for 10,000 cells using the Beckman Coulter CytoFLEX and channels for FITC (525/40) and PE (585/42) with gating consistent across all samples and the appropriate compensation applied. Compensation was performed using control cell samples stained with PI only and YO-PRO-1 only, an unstained permeabilised cell control was also used. Using these samples, a compensation matrix was generated which was applied to the data.

## 2.12 Immunofluorescence

One million cells were seeded on 10 cm cell culture plates containing glass coverslips and the plates incubated overnight at 37°C, 5% CO<sub>2</sub>. The following day, the coverslips were removed and transferred to a 24-well plate. The coverslips were washed 3 x in PBS for 1 minute on ice followed by fixation in 4 % PFA for 20 minutes at room temperature. Coverslips were washed 3 x in PBS for 1 minute on ice and permeabilised with 0.1 % Triton X-100 in PBS for 20 minutes on ice. Coverslips were incubated in antibody buffer (PBS, 0.1 % w/v Triton X-100, 0.02 % SDS, 1 % w/v BSA) for 5 minutes on ice followed by 2 x washes in antibody buffer. Antibody optimisation was performed using a range of antibody concentrations from 1:50 to 1:1600. The GFAP primary antibody (Table 2.1) was subsequently added at the optimal concentration of

1:800 and incubated in a humidified chamber for 1 hour, 37°C. Coverslips were transferred back into the 24-well plate, washed 3 x in antibody buffer and 3 x in PBS. The secondary antibody was then added at 1:2000 (goat anti-mouse HRP conjugate Alexa Fluor 488, Table 2.1) and incubated in a humidified chamber in the dark for 1 hour, 37°C. Coverslips were removed and washed 3 x in antibody buffer and 3 x in PBS. Coverslips were dipped into Milli-Q water to remove excess buffer and mounted onto microscope slides face down in VectaShield plus DAPI to stain DNA. Coverslips were imaged the same day using a Zeiss LED illuminated microscope.

### 2.13 Determining proportion of S-phase cells by EdU Fluorescence microscopy

Cells were pulse labelled with 10  $\mu$ M EdU for 30 minutes and fluorescently labelled according to the Click-IT EdU imaging kit (Alexa Fluor 488) protocol (Invitrogen) according to manufacturer's instructions. Cells were counterstained with DAPI (Vector Laboratories) and EdU was visualised by fluorescence microscopy using a Zeiss LED illuminated microscope. The number of EdU positive nuclei were counted out of 100 DAPI labelled nuclei and the percentage of cells in S-phase was determined.

### 2.14 Statistical analysis

Statistical analysis of the results was performed by a one-way ANOVA post-hoc Tukey test using IBM SPSS Statistics 24. A p-value of  $\leq 0.05$  was indicated by \* in the graphs,  $\leq 0.01$  as \*\* and  $\leq 0.005$  as \*\*\*. Graphs where statistical analysis was performed contain three experimental repeats showing the mean  $\pm$  standard deviation (SD).

### 2.15 Immunohistochemistry analysis of FFPE tissue sections

Provided by BTNW, formalin-fixed paraffin-embedded (FFPE) tissue biopsies were sectioned at 4  $\mu$ M thick and single-labelled immunohistochemistry was performed. 20

patient samples were provided and had been prepared up to the point of paraffin removal.

#### 2.15.1 Antigen retrieval

In preparation for immunostaining, sections were heated in a 60°C oven for 1 hour to melt the paraffin wax. Sections were dewaxed in two changes of xylene and rehydrated in a descending series of alcohol concentrations. Sections were boiled in a pressure cooker in 1.5 L 0.01 M citric acid buffer pH 6.0 (0.02 M Citric Acid, 0.05 M NaOH) in a 900 W microwave on high power. Sections were rinsed in warm water, gradually cooling water for 10-15 minutes.

#### 2.15.2 Immunostaining

Immunostaining was performed using the VECTASTAIN® Elite ABC-HRP Kit (Peroxidase, Universal, VECTORLABS). Sections were washed in Tris buffer pH 7.4 (0.05 M Trizma base, 0.079 M sodium chloride, 1% w/v BSA, 500 ml distilled water) and treated with Dako hydrogen peroxide blocking reagent for 5 minutes to block endogenous peroxidase activity. Sections were washed with Tris buffer and incubated with normal blocking serum for 20 minutes.

Sections were incubated with primary antibody solutions at 4°C overnight and an optimal antibody concentration of 1:800 was determined and used in subsequent immunostaining. The following day, slides were washed as previous and incubated with VECTASTAIN® Biotinylated Universal Antibody for 30 minutes. Sections were washed and incubated with VECTASTAIN® Elite ABC reagent for 30 minutes. Sections were washed and incubated in DAB solution (DAB Substrate Kit, Peroxidase (HRP), (VECTORLABS) for 2-10 minutes. Sections were washed in running water for 5 minutes, counterstained in haematoxylin and washed until blue in hot water. Sections were dehydrated in an ascending series of alcohol concentrations, cleared in xylene and mounted onto coverslips using VectaMount® Permanent Mounting Medium. Sections were imaged using a brightfield microscope (Nikon).

### 2.15.3 Validation of CIZ1-N471 antibody

The specificity of the CIZ1-N471 antibody was determined using western blotting. U87-MG cells were harvested and samples prepared for western blotting, blots were probed using the immunopurified anti-CIZ1 antibody and imaged. Following validation of the antibody via western blotting, optimisation of the antibody for IHC was performed by testing antibody concentrations ranging from 1:200 – 1:3200. Sections were imaged and the specificity of CIZ1 staining within the same region of patient sample BTNW2760 was evaluated.

# Chapter 3: Effect of CDK and DDK small molecule inhibitors on CIZ1 expression

## 3.1 Introduction

Several studies have suggested that CIZ1 overexpression is required for tumour growth (Liu et al., 2015; Wang et al., 2014; Zhang et al., 2015). Although the precise mechanisms by which CIZ1 promotes this growth are poorly understood, the importance of CIZ1 overexpression in tumourigenesis has been demonstrated as siRNA-mediated CIZ1 depletion reduces proliferation and migration *in vitro* and tumour growth in mouse xenograft models of lung, prostate, colorectal and gall bladder cancer (Higgins et al., 2012; Liu et al., 2015; Wang et al., 2014; Zhang et al., 2015). These observations suggest CIZ1 could be a potential therapeutic target in cancerous cell lines that exhibit CIZ1 overexpression.

The rational design of inhibitors typically target active sites or allosteric binding pockets on the target surface. However, there is no structural information for CIZ1, making this approach difficult. Evidence has been building that CIZ1 is regulated post-translationally via CDK mediated phosphorylation and ubiquitin proteasome system (UPS) mediated degradation, a process by which cytosolic proteins are targeted for degradation within eukaryotic cells. Studying the regulatory networks controlling CIZ1 expression may provide insight into the tumourigenic activity of CIZ1 and provide potential targets to modulate CIZ1 expression. The model presented here proposes that CIZ1 is regulated by the opposing action of CDKs and the UPS (Figure 3.1). Rising CDK and DDK activity are essential for accumulation of CIZ1 in early G1 phase and inhibition of CDK2 or DDK activity decreases CIZ1 levels in murine fibroblasts. CIZ1 levels are regulated by opposing UPS mediated degradation resulting in CIZ1 degradation later in the cell cycle. Inhibition of CIZ1 translation results in reduction of CIZ1 levels which is reversible by proteasomal inhibition (Pauzaite, 2019).

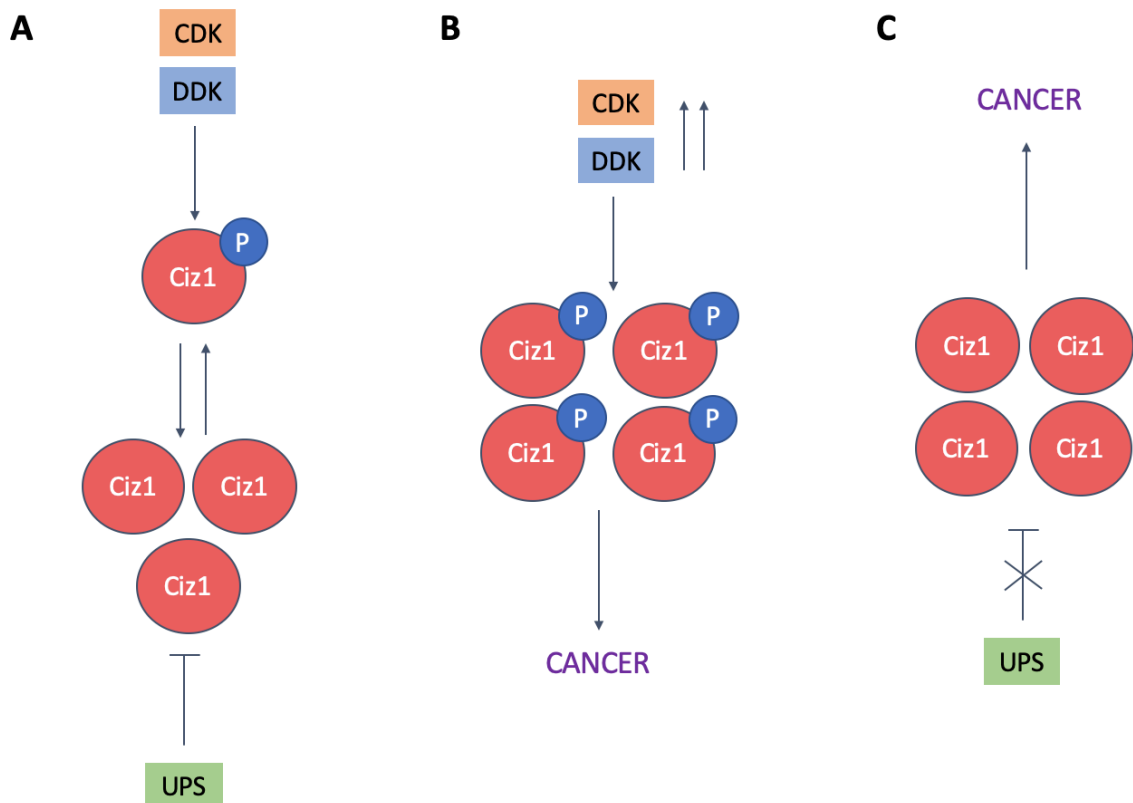


**Figure 3.1 Model for CIZ1 accumulation in cancer: Opposing regulation of CIZ1 by CDKs and the UPS. A)** In normal cells, CIZ1 levels are regulated by CDK/DDK phosphorylation stabilising CIZ1 and protecting it from UPS mediated degradation. This leads to accumulation of CIZ1 in G1 phase and degradation later in the cell cycle, ensuring strict regulation of CIZ1 levels. **B)** In cancer cells, deregulation of the cell cycle can promote increased CDK/DDK activity, resulting in hyper-phosphorylation of CIZ1. This effect would be predicted to increase CIZ1 levels within the cell. **C)** Mutations in the UPS and deregulation of UPS signalling results in CIZ1 over-accumulation leading to cancer.

This data suggests that deregulation of CDK activity or disruption to UPS activity leads to the overexpression of CIZ1. The use of genetic strategies to reduce CIZ1 levels showed that certain cancer cell lines may rely on increased CIZ1 expression for enhanced tumour growth. Therefore, strategies that reduce CIZ1 levels may provide a potential therapeutic opportunity. Furthermore, targeting the components involved in CIZ1 regulation may provide a strategy to block the DNA replication function of CIZ1 and reduce tumour growth. Recent work has demonstrated reductions in CIZ1 levels upon treatment with CDK and DDK inhibitors (Pauzaite, 2019) and so using this approach we will determine whether CIZ1 levels can be reduced in various cell lines.

The development of kinase inhibitors for use as anti-cancer therapies was initially criticised due to toxicity, off-target effects and development of acquired resistance. The design of kinase inhibitors is challenging, 99% of the inhibitors developed target the ATP-binding site which is highly conserved across the 518 kinases in the human kinome (Duong-Ly and Peterson, 2013). Due to the structural conservation across the human kinome, these inhibitors often exhibit a lack of specificity and selectivity. However, with advancing technology, determination of the precise mechanisms by which these inhibitors interact with their kinase targets is allowing for the development of inhibitors with increased selectivity and specificity (Breen and Soellner, 2015).

### 3.2 CDK and DDK inhibition reduces CIZ1 levels and proliferation in an unrelated tumour type

The use of CDK and DDK inhibitors to reduce CIZ1 levels has previously been investigated in several normal and cancer cell lines providing evidence that CIZ1 is required for growth in certain cancerous cell types (Pauzaite, 2019). Here, the initial investigation used the human non-small cell lung cancer cell line (A549) for proof of principle to determine the effect on CIZ1 protein levels upon CDK/DDK inhibition. A549 cells were treated with CDK4/6 (PD0332991), DDK (PHA-767491), CDK1 (Ro-3306) and CDK2 inhibitors (CVT-313 and CDK2-IN-73) for 24 hours. CIZ1 protein levels were analysed by western blotting and blots probed for CIZ1 and actin (Figure 3.2 A). Cell proliferation and apoptosis assays were also carried out to determine the dependency of this cell line on CIZ1 for tumour growth and survival (Figure 3.2 C, Figure 3.3).

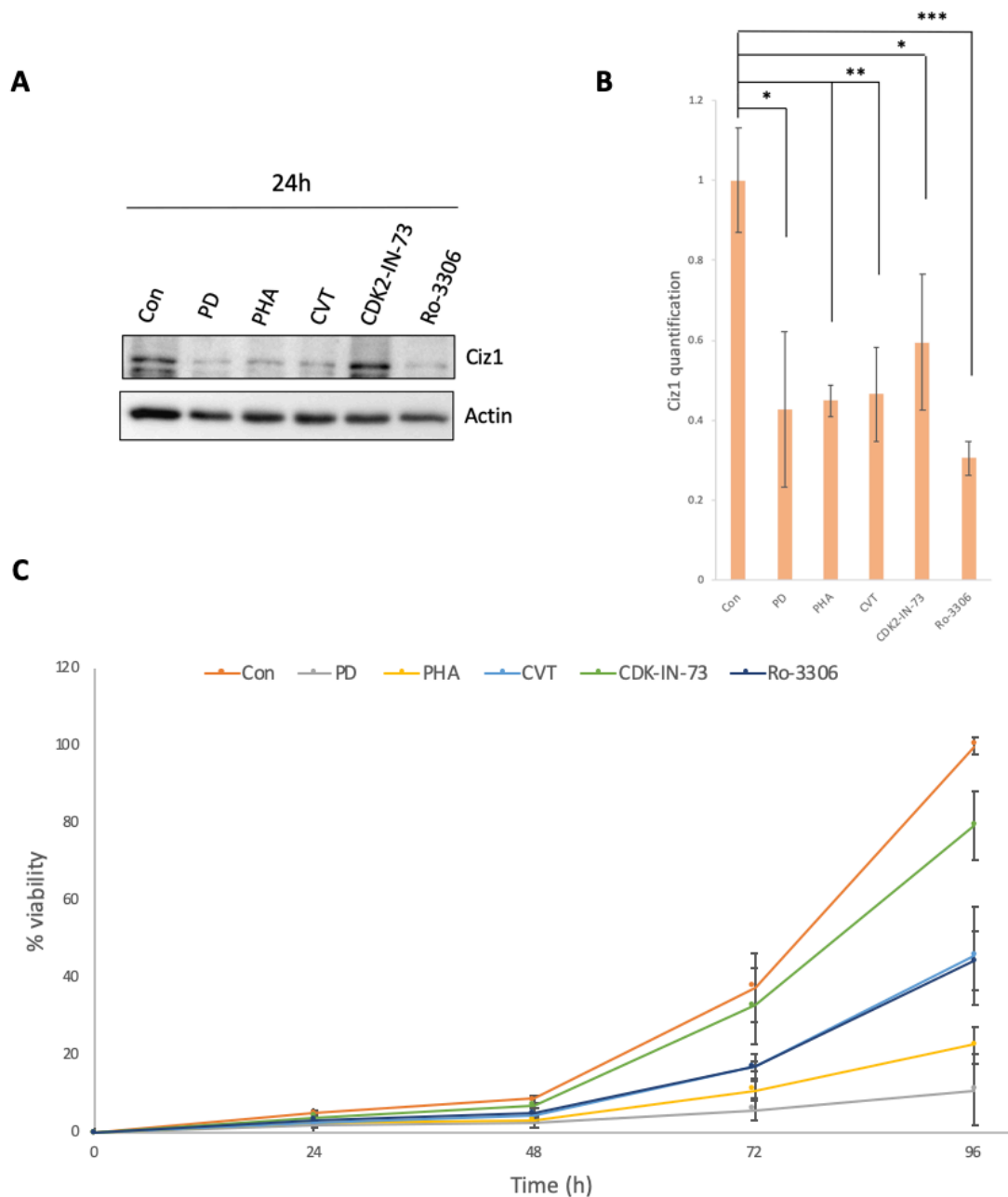


**Figure 3.2 Treatment of A549 cells with CDK and DDK inhibitors. A)** Cells were treated with PD0332991 (PD), PHA-767491 (PHA), CVT-313 (CVT), CDK2-IN-73 and Ro-3306 for 24 hours. Cells were harvested, and western blots probed for CIZ1 and actin. **B)** Quantitation of CIZ1 protein in relation to actin, presented as the mean  $\pm$  SD (n=3). Significance was measured by a one-way ANOVA post-hoc Tukey \* $p \leq 0.05$ . **C)** PrestoBlue™ assays were also performed every 24 hours for 96 hours and graphs plotted, presented as the mean  $\pm$  SD (n=2).

All inhibitors significantly reduced CIZ1 protein levels by >40 % with Ro-3306 being the most potent reducing protein levels by approximately 70% (Figure 3.2 A, B). This reduction in protein levels was associated with a reduction in proliferation over a 96-

hour period with PD0332991, PHA-767491 and Ro-3306 reducing proliferation most prominently as reflected in the protein analysis (Figure 4.1 C). PD0332991 reduced proliferation by 91% and PHA-767491 reduced proliferation by 79%, suggesting a 96-hour treatment period is more effective at reducing cell growth than a 72-hour treatment. CDK2-IN-73 demonstrated poor efficacy reducing proliferation by only 21%.

Further to the effects of CDK and DDK inhibition on protein levels and cell proliferation, the effects of these small molecules on cell death was assessed. A549 cells were treated with CDK and DDK inhibitors 24 hours. Live/dead cell staining was performed, and apoptotic status analysed by flow cytometry. Treatment of cells with the CDK2 inhibitor CVT-313 resulted in the highest rates of apoptosis and cell death, with a 27% increase compared to the control population (Figure 3.3). This suggests CVT-313 has the greatest cytotoxic effect in this cell line as reductions in CIZ1 levels observed with the other inhibitors did not correlate with increased rates of apoptosis or cell death.

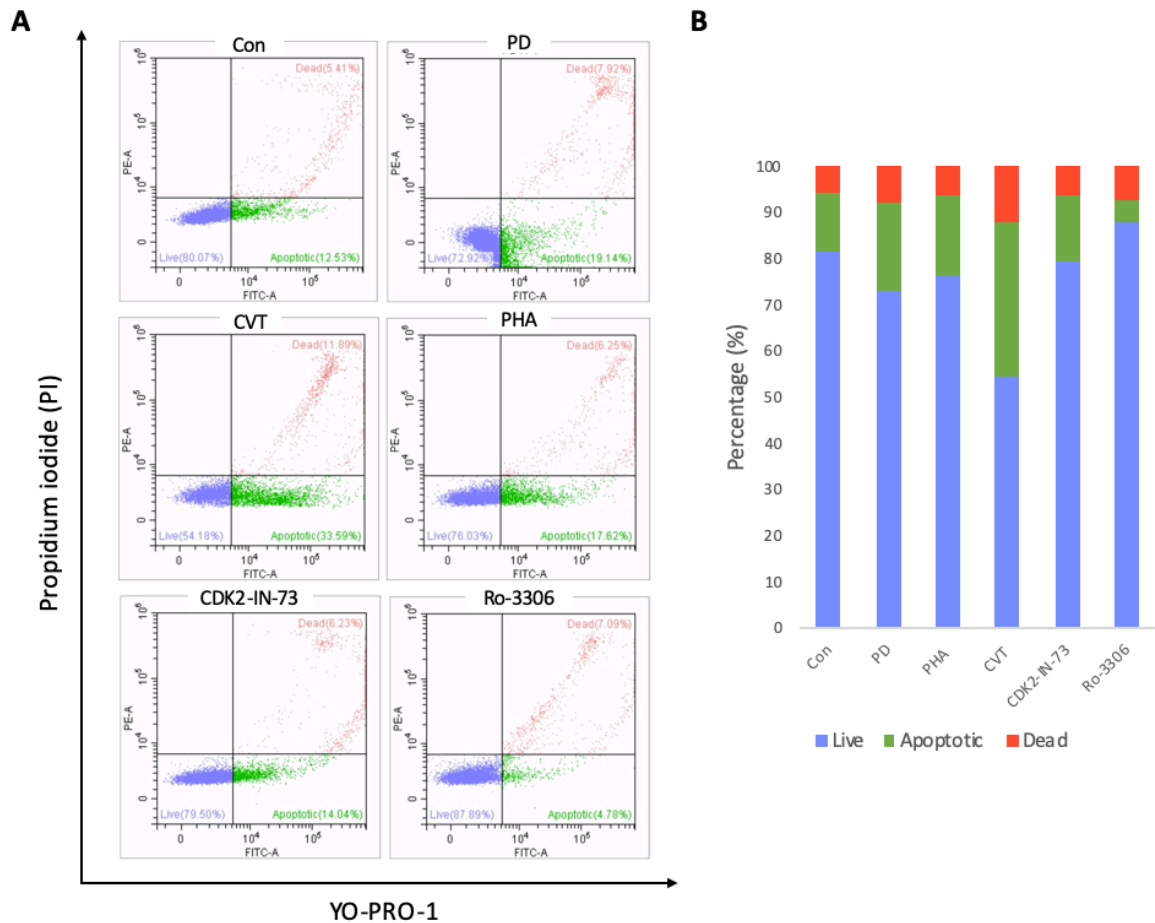


**Figure 3.3 Cell death profile of A549 cells after CDK/DDK inhibition. A)** Cells were treated with 10  $\mu$ M PD0332991 (PD), PHA-767491 (PHA), CVT-313 (CVT), CDK2-IN-73 and Ro-3306 for 24 hours. Cells were stained with YO-PRO-1 and PI and analysed by flow cytometry using channels for FITC (525/40) and PE (585/42). Quadrants represent live cells (bottom left), apoptotic (bottom right) and necrotic/dead (top right). **B)** Cumulative histogram representing the proportion of live, apoptotic and dead cells, (n=1).

As demonstrated previously, CIZ1 levels can be efficiently reduced by CDK and DDK inhibition suggesting a block in cell cycle progression or potentially active degradation of CIZ1 by the UPS. To determine if CIZ1 abundance is regulated by the proteasome in this cell line, cells were treated with the CDK or DDK inhibitor alone or in combination with the proteasomal inhibitor MG132. Only PHA-767491 successfully reduced CIZ1 levels and these were recovered upon addition of MG132 (Figure 3.4 B), suggesting UPS mediated degradation of CIZ1, however further experiments are required to determine any statistical significance. Treatment with PD0332991 and Ro-3306 in combination with MG132 appeared to reduce CIZ1 levels further to treatment with

the inhibitor alone (Figure 3.4 A, E). Proteasomal inhibition had no effect on CIZ1 levels after treatment with CDK2-IN-73 (Figure 3.4 D).

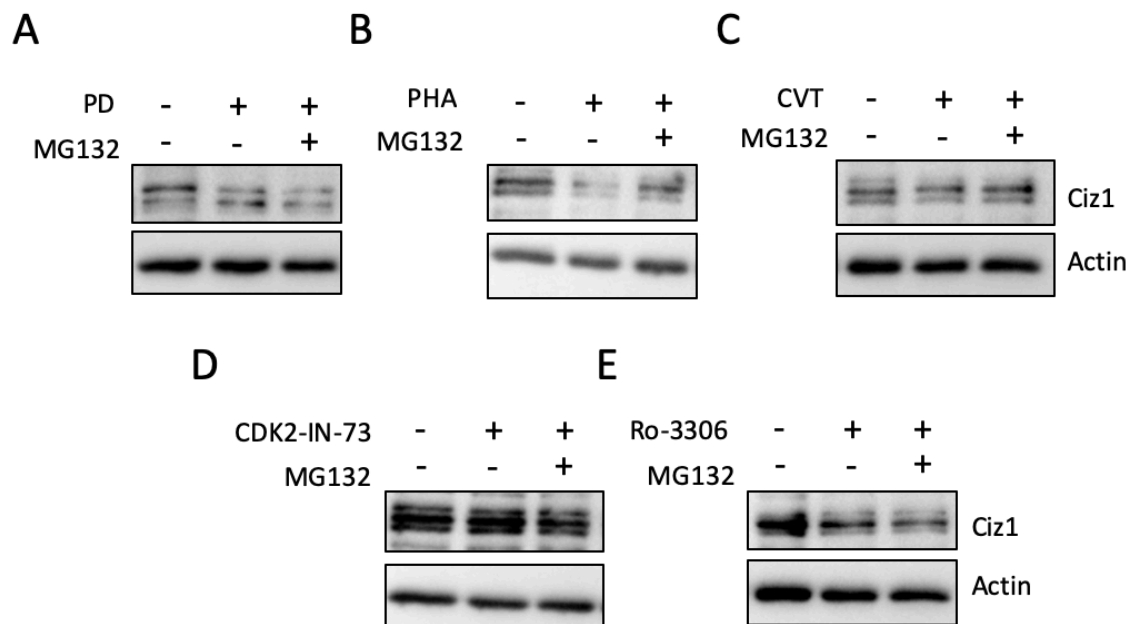


**Figure 3.4 Recovery of CIZ1 with proteasomal inhibitor MG132 after kinase inhibition.** A549 cells were treated with 10  $\mu$ M of PD0332991 (PD), PHA-767491 (PHA), CVT-313 (CVT), CDK2-IN-73 and Ro-3306 for 24 hours  $\pm$  10  $\mu$ M MG132 from 20 to 24 hours. Western blots were probed for CIZ1 and Actin (n=2).

### 3.3 Effects of CDK and DDK inhibition on proliferation in SW620, PC3 and SW480 cancer cell lines

Previous work has demonstrated the effects of CDK and DDK inhibition in the Rb positive cancer cell lines SW620, PC3 and SW480 (Pauzaite 2019). Expanding on this, cell viability studies were carried out in these cell lines to determine if CIZ1 is required for effective proliferation. Cells were treated with CDK2 inhibitors CVT-313 and Roscovitine and DDK inhibitors PHA-767491 and XL-413, the effects on proliferation were analysed using PrestoBlue™ assays over 96 hours.

CDK and DDK inhibitors were titrated between 1 - 10  $\mu\text{M}$  and results demonstrated both CDK2 inhibitor CVT-313 and DDK inhibitor PHA-767491 reduced proliferation in all cell lines, with a concentration of 10  $\mu\text{M}$  resulting in maximal effects (Figure 3.5, 3.6, 3.7). This demonstrates the likely dependence of these cell lines on CDK2 and DDK activity for cell cycle progression and proliferation. The CDK2 inhibitor Roscovitine reduced proliferation in SW620 cells however increased proliferation rates in PC3 and SW480 cells suggesting cell line dependant activity. DDK inhibitor XL-413 was ineffective at reducing proliferation in SW620 and SW480 cells, in PC3 cells XL-413 showed some reduction in proliferation but only at the highest concentration of 10  $\mu\text{M}$ .

These results are consistent with flow cytometry data demonstrating reductions in proliferation after treatment with PHA-767491, CVT-313 and Roscovitine. In contrast, these results show no effects of Roscovitine on proliferation in PC3 and SW480 cells which contradicts previous observations. These results also support the poor efficacy of XL-413 at reducing S-phase entry in SW620, PC3 and SW480 cells, with effects more prominent in PC3 cells compared to other cell lines (Pauzaite, 2019).

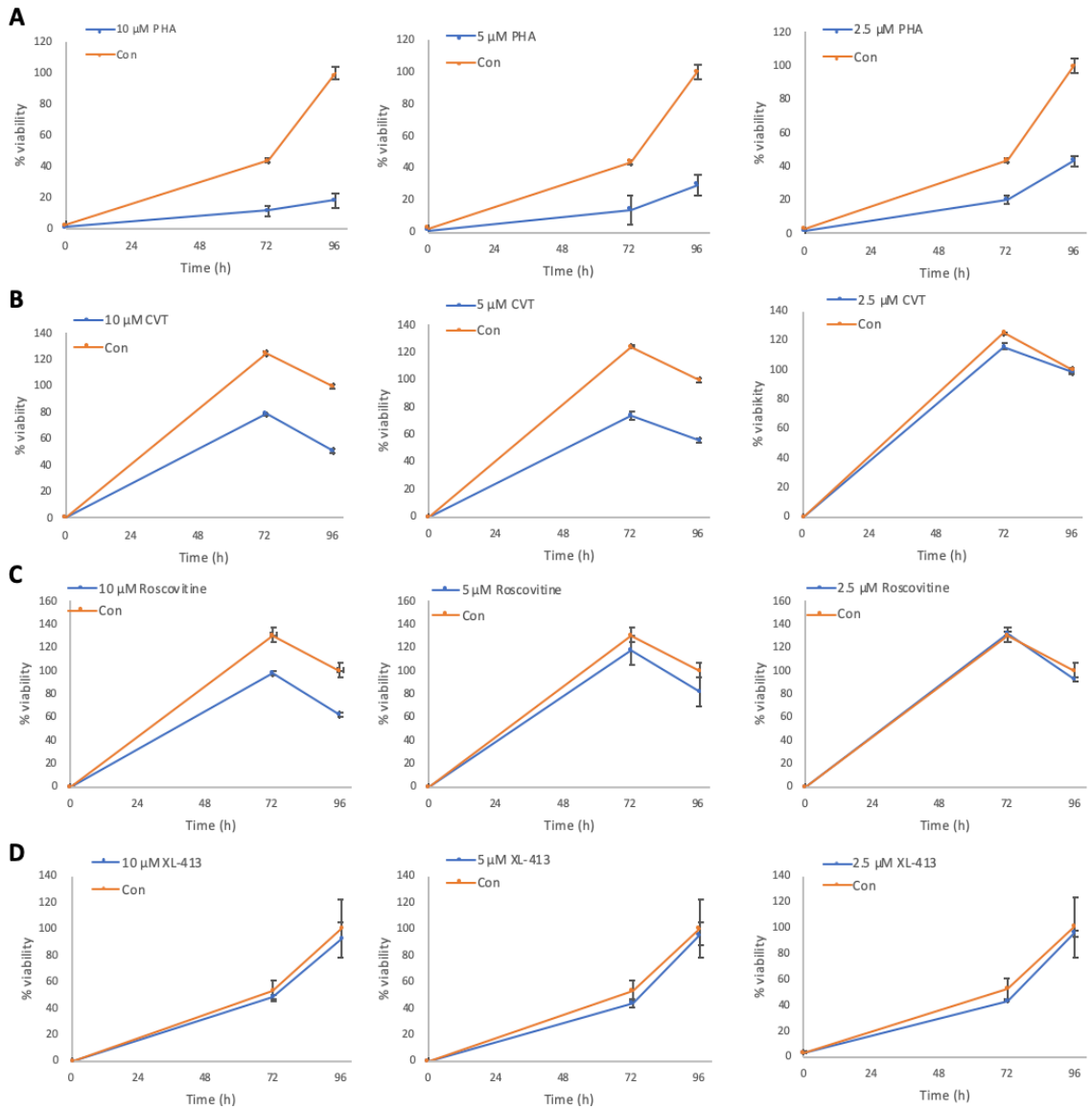


**Figure 3.5 Cell proliferation analysis after CDK and DDK inhibition in SW620 cells.** Cells were treated with (A) PHA-767491 (PHA), (B) CVT-313 (CVT), (C) Roscovitine and (D) XL-413 in triplicate at concentrations ranging from 2.5 μM – 10 μM. PrestoBlue™ cell viability assays were performed at 72 and 96 hours and graphs plotted representing the mean fluorescence for each time point (n=1).

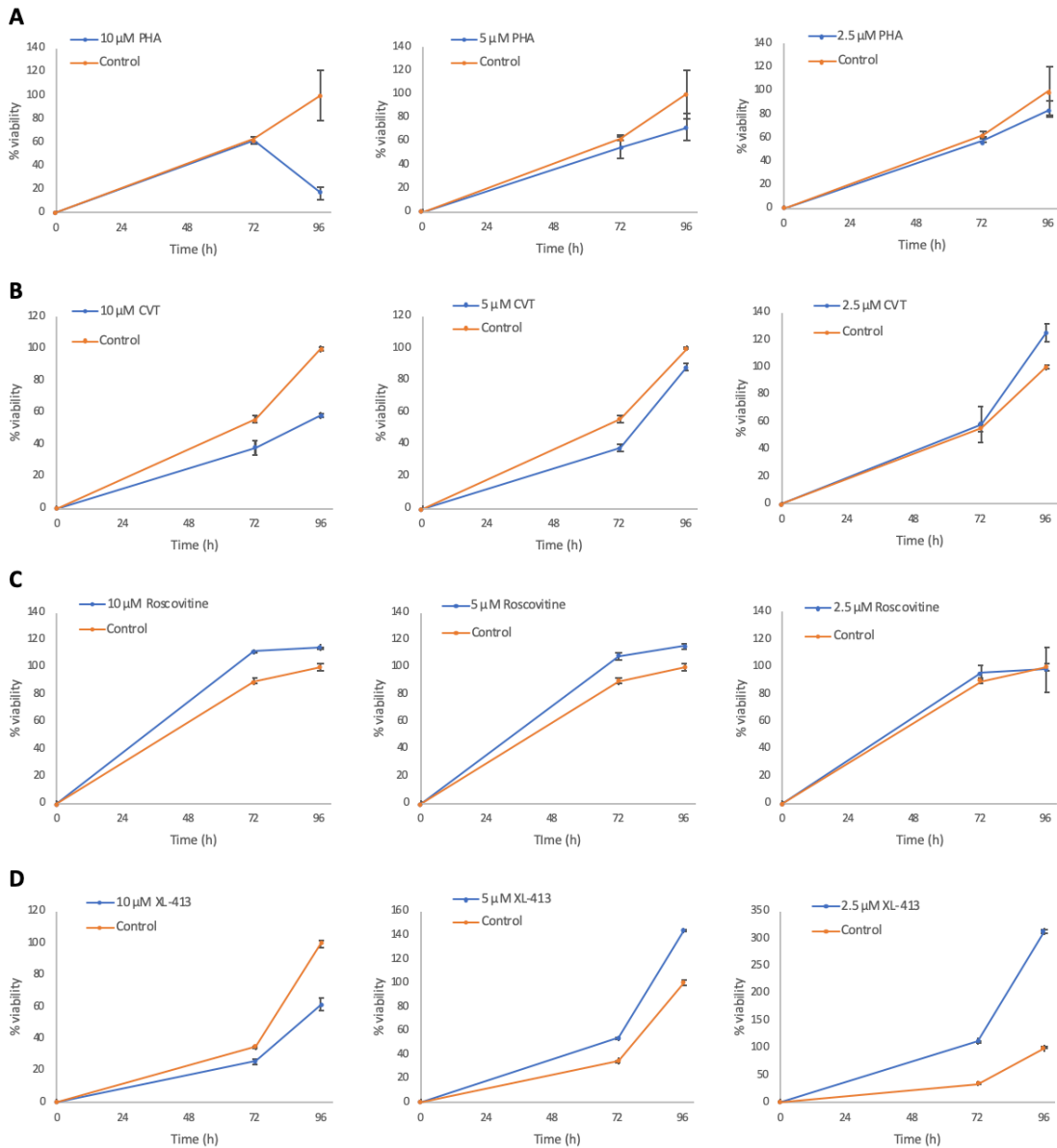


**Figure 3.6 Cell proliferation analysis after CDK and DDK inhibition in PC3 cells.** Cells were treated with A) PHA-767491 (PHA), B) CVT-313 (CVT), C) Roscovitine and D) XL-413 in triplicate at concentrations ranging from 2.5  $\mu$ M – 10  $\mu$ M. PrestoBlue™ cell viability assays were performed at 72 and 96 hours and graphs plotted representing the mean fluorescence for each time point (n=1).

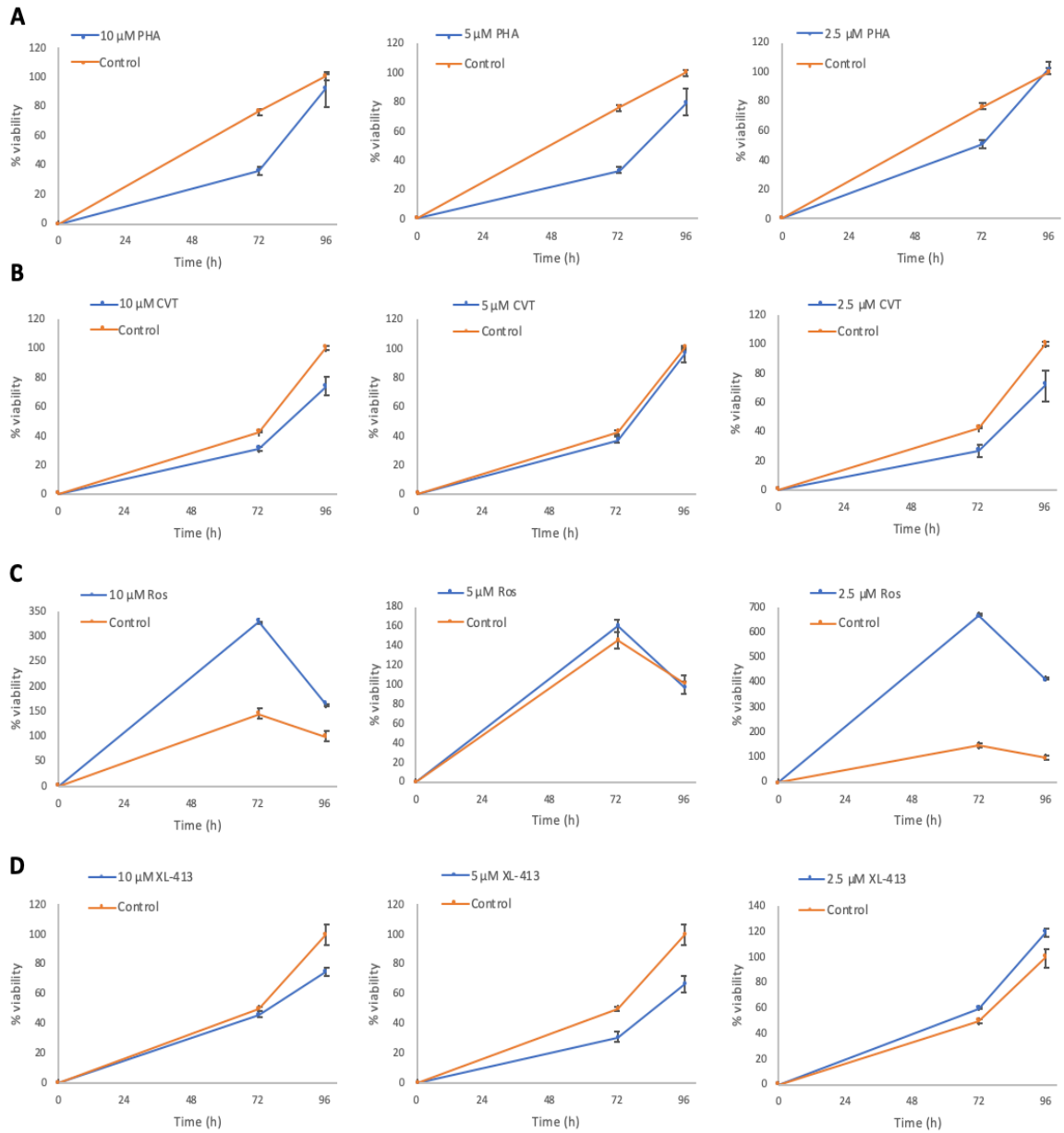


**Figure 3.7 Cell proliferation analysis after CDK and DDK inhibition in SW480 cells.** Cells were treated with A) PHA-767491 (PHA), B) CVT-313 (CVT), C) Roscovitine and D) XL-413 in triplicate at concentrations ranging from 2.5 μM – 10 μM. PrestoBlue™ cell viability assays were performed at 72 and 96 hours and graphs plotted representing the mean fluorescence for each time point (n=1).

To demonstrate the toxicity of these inhibitors *in vitro*, CDK and DDK inhibitors were titrated between 0.1 - 10  $\mu\text{M}$  to investigate whether there is a dose-response effect in these cell lines. Titration of DDK inhibitor PHA-767491 in PC3 cells produced a sigmoidal dose-response curve whereby a relationship is established between inhibitor concentration and proliferation (Figure 3.8). Treatment of PHA-767491 generated a dose-response curve with an IC<sub>50</sub> value of 5.32  $\mu\text{M}$ , the point at which cell viability is reduced by 50%. At the maximal dose of 10  $\mu\text{M}$  cell viability is reduced by approximately 90%. PHA-767491 was the only inhibitor to produce a dose-response effect which was limited to PC3 cells, demonstrating the potency of this inhibitor at reducing proliferation, most likely due to the off-target effects on the CDK2-Rb-E2F transcriptional network.

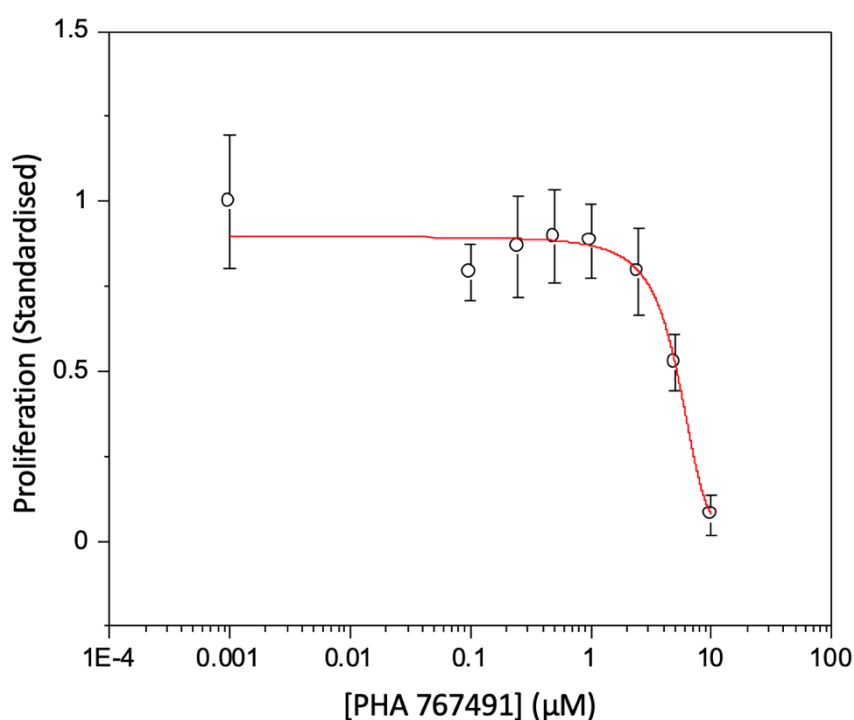


**Figure 3.8 Titration of PHA-767491 induces a dose-response effect in PC3 cells.** PC3 cells were treated with PHA-767491 (0.1 – 10  $\mu\text{M}$ ) for 72 hours. Proliferation was assessed using the PrestoBlue™ assay and values plotted using OriginPro 2019b (IC<sub>50</sub> = 5.32  $\mu\text{M}$ ). Biological triplicates plotted as mean  $\pm$  SD (n=1).

## 3.4 Chapter discussion

3.4.1 CDK/DDK inhibition reduced CIZ1 levels in an unrelated tumour type  
The effects of CDK and DDK inhibition in the NSCLC cell line A549 have not previously been investigated and so this cell line was used as a trial to see if the results were in line with previous work. In contrast to the effects observed in previous cell lines, all inhibitors significantly reduced CIZ1 protein levels demonstrating the sensitivity of this cell line to CDK and DDK inhibition, justifying the use of this cell line as a proof of concept for kinase inhibition studies. Reductions in CIZ1 levels correlated with a subsequent reduction in proliferation suggesting this cell line is reliant on CIZ1 for growth. CIZ1 levels were recovered upon proteasomal inhibition after treatment with PHA-767491 and CVT-313, although, proteasomal inhibition appeared to reduce CIZ1 levels further after treatment with PD0332991 and Ro-3306 and CDK2-IN-73 had no effect. CVT-313 increased rates of cell death and apoptosis by 27% compared to the control population, exhibiting the greatest cytotoxic effect of all inhibitors tested. PD0332991 also increased rates of apoptosis and cell death by 9% suggesting a less prominent cytotoxic activity of this inhibitor in A549 cells. PHA-767491, CDK2-IN-73 and Ro-3306 exhibited minimal cytotoxicity; despite not being able to induce apoptosis and cell death, proliferative rates were still reduced implying cytostatic activity profiles.

### 3.4.2 Dose-dependent effects of CDK/DDK inhibition on proliferation

PHA-767491 and CVT-313 reduced proliferation in SW480, PC3 and SW620 cells, consistent with reductions seen in A549 cells, with effects more prevalent at an inhibitor concentration of 10  $\mu$ M as used in subsequent proliferation assays conducted in this study. The similar potencies observed with DDK inhibitor PHA-767491 and CDK2 inhibitor CVT-313 are likely due to the off-target effects of PHA-767491 on CDK2. The effect of PHA-767491 on CDK2 activity has previously been investigated, PHA-767491 inhibited Rb phosphorylation and therefore reduced E2F mediated transcription of cyclins during G1 phase as seen with CDK2 inhibitors CVT-313 and Roscovitine (Pauzaite, 2019).

PHA-767491 has been shown to consistently reduce CIZ1 levels across a range of cell lines (Chapter 3.2, Chapter 4.1, Chapter 4.3; Pauzaite, 2019), reduce CIZ1 phosphorylation at T293 and reduce cyclin A levels in 3T3 fibroblasts (Pauzaite, 2019). The correlation between CIZ1 and cyclin A levels is potentially related to the reduction in cyclin A-CDK2 activity which is required for accumulation of CIZ1 at the G1/S transition. Transcription of cyclin A is regulated by the Rb-E2F pathway which requires CDK mediated phosphorylation of Rb and therefore suggests that PHA-767491 has dual action against both DDK and CDK2. To support this theory, Rb phosphorylation was measured upon treatment with PHA-767491 and reductions in phosphorylation of Rb at CDK site S811 were observed (Pauzaite, 2019). Collectively, the data demonstrates the dual inhibition of DDK and CDK2 by PHA-767491 which supports previous findings demonstrating the targeting of multiple kinases by PHA-767491 (Erbayraktar et al., 2016).

Interestingly, Cdc7-Dbf4 (DDK) inhibitors PHA-767491 and XL-413 displayed distinct differences in potency across SW620, SW480 and PC3 cells. PHA-767491 inhibits the initiation of DNA replication whereas XL-413 affects replication fork progression but does not affect initiation of DNA replication (Alver et al., 2017). Cdc7 is required to phosphorylate the MCM2-7 helicase promoting the initiation of DNA replication. Cdc7 overexpression is commonly observed in lung, breast and colon cancers (Bonte et al., 2008; Montagnoli et al., 2008) and therefore targeting Cdc7 is an attractive approach for small molecule inhibition. DDK inhibition has been shown to selectively kill cancer cells whilst sparing normal cells and increases apoptosis *in vitro* and in xenograft models (Jin et al., 2018; Natoni et al., 2013).

XL-413 has a higher affinity for DDK than PHA-767491, molecular modelling revealed increased contacts between XL-413 and DDK than PHA-767491 and DDK suggesting increased potency and selectivity of XL-413 towards DDK (Hughes et al., 2012). In contrast to the activity of PHA-767491 and CDK2 inhibitor Roscovitine, XL-413 did not significantly reduce CIZ1 levels, cyclin A levels or Rb phosphorylation in 3T3 cells. The reduction in cyclin A levels observed with PHA-767491 suggests inhibition of CDK2 and

subsequent absence of CIZ1 accumulation. Therefore, it can be concluded that the differential activity of PHA-767491 and XL-413 is down to the varying effects on CDK signalling pathways and Rb phosphorylation at S811. Furthermore, titration of PHA-767491 and XL-413 between 1 – 10  $\mu$ M revealed that PHA-767491 reduced phosphorylation of CIZ1 at T293 and CIZ1 levels at 5 and 10  $\mu$ M, these reductions were not seen with XL-413 treatment (Pauzaite, 2019). Therefore, PHA-767491 may be a potent inhibitor of CDK and DDK, more effective at lower concentrations and XL-413 is a more specific inhibitor with less off-target activity (Koltun et al., 2012).

Proliferation assays revealed Roscovitine to be less potent than CVT-313 and PHA-767491 at reducing proliferation which supports previous findings demonstrating increased inhibition of Rb phosphorylation and subsequent E2F mediated transcription of cyclin E1, E2 and A2 after treatment with CVT-313 and PHA-767491. Previous studies demonstrated that CVT-313 was the only inhibitor able to inhibit transcription of these kinases at 1  $\mu$ M showing it is highly selective towards CDK2 (Pauzaite, 2019). Although PHA-767491, CVT-313 and Roscovitine displayed similar potencies at 10  $\mu$ M, PHA-767491 and CVT-313 were more potent than Roscovitine at the lower concentration of 5  $\mu$ M which is consistent with previous work. These results are also consistent with the reported IC<sub>50</sub> values of CDK2 inhibition (Table 2.3).

## Chapter 4: Evaluation of small molecule kinase inhibitors to reduce CIZ1 levels in GBM

There is no previously published data surrounding the use and development of kinase inhibition to reduce CIZ1 levels in GBM. Having established the effects of kinase inhibition in unrelated cancer cell lines, this approach was trialled in primary and immortalised GBM cells to gain insight into the role of CIZ1 in the growth and survival of GBM. Various CDK inhibitor treatments have been tested in GBM but clinical trials have been unsuccessful due to the limited efficacy of these small molecule inhibitors *in vivo*. The most frequently trialled inhibitor being the CDK4/6 inhibitor PD0332991 (Juric and Murphy, 2020). Inhibition of CDK4 and CDK6 blocks the phosphorylation of Rb protein during early G1 phase leading to cell cycle arrest. This results in downstream suppression of DNA replication and a reduction in tumour cell proliferation. Oral administration of PD0332991 in integrated GBM xenograft models had a successful anti-proliferative effect, which was enhanced when combined with radiotherapy (Cen et al., 2012). Treatment of retinoblastoma protein 1 (Rb1) positive primary GBM cells *in vitro* with radiotherapy in combination with PD0332991 inhibited double-stranded DNA break repair and increased rates of apoptosis (Hashizume et al., 2016). In a phase II trial of PD0332991 involving the treatment of Rb1 positive recurrent GBM patients, PD0332991 monotherapy was not an effective treatment in these patients and therefore clinical trials did not progress any further (Taylor et al., 2018). However, targeting the CDK4/6 pathway in combination with radiotherapy in primary GBM models shows promising potential and requires further investigation.

Previous IHC analysis of GBM sections suggested CIZ1 expression is increased in these tumours (Falkingham, 2020). In this study, the effect of CDK and DDK inhibitors will be investigated, to assess the role of CIZ1 in the proliferation and growth of GBM. This chapter will evaluate the role of CIZ1 in cell cycle regulation either directly via genetic depletion of CIZ1 or indirectly by small molecule inhibition of CIZ1's regulatory kinase network. This work will provide an insight into the potential roles of CIZ1 in cell

proliferation and tumourigenic activity and identify potential therapeutic strategies in various cancer cell lines with a particular focus on high-grade neurological tumours.

#### 4.1 Analysis of CDK and DDK inhibition in established GBM cell line U87-MG

Having established that CDK and DDK inhibition can reduce CIZ1 protein levels, this approach was extended to two GBM cell lines, the widely studied cell line U87-MG and the BTNW primary cell line BTNW914. U87-MG cells were treated with CDK4/6 (PD0332991), DDK (PHA-767491), CDK1 (Ro-3306) and CDK2 inhibitors (CVT-313 and CDK2-IN-73). CIZ1 protein levels were analysed by western blotting at 6 and 24 hours and blots probed for CIZ1 and actin. To determine if these cell lines rely on CIZ1 activity for growth, PrestoBlue™ cell viability assays were also performed to assess the proliferative potential of cells after CDK and DDK inhibition (Figure 4.1).

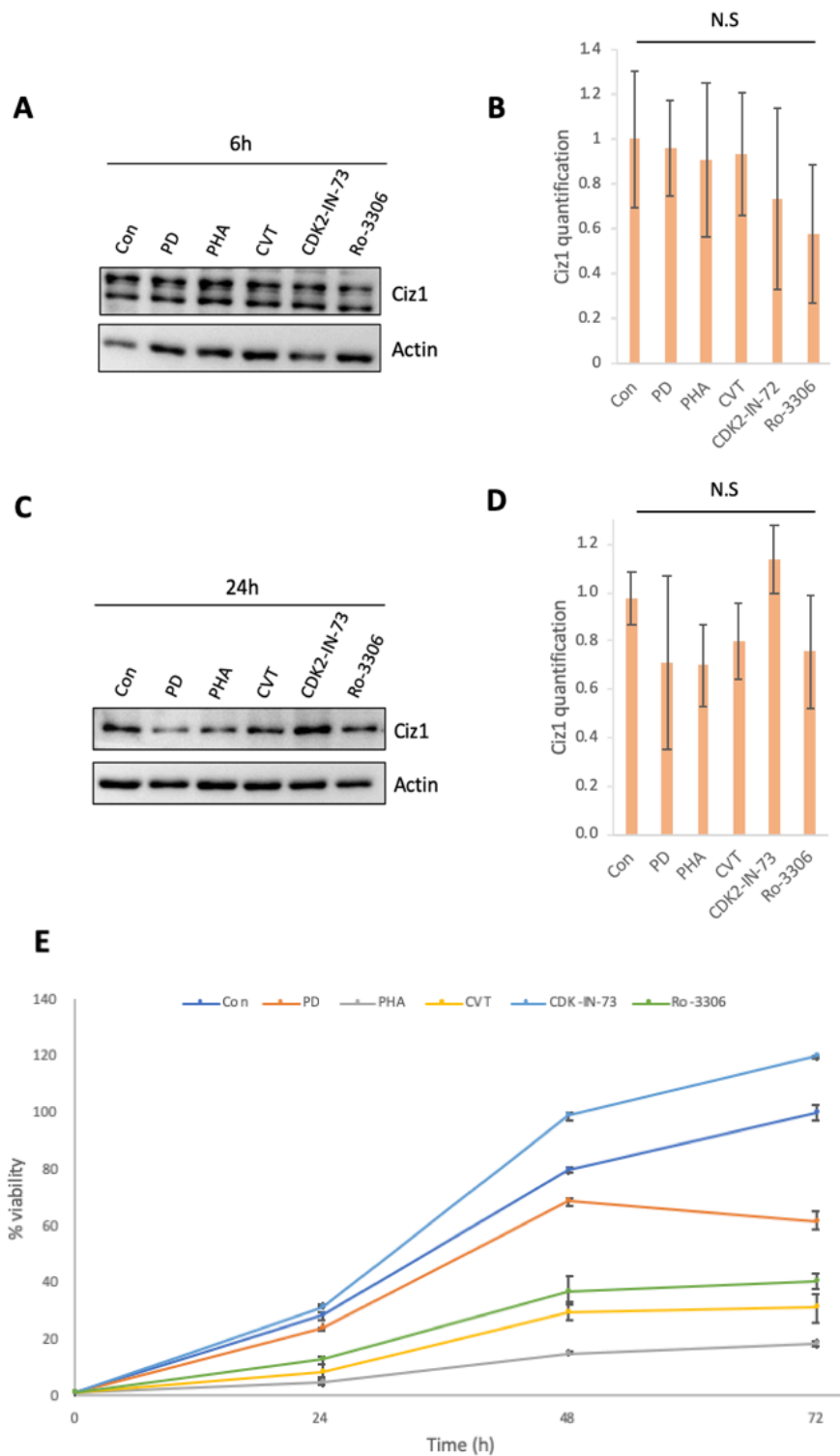


**Figure 4.1 Treatment of U87-MG cells with CDK and DDK inhibitors.** Cells were treated with 10  $\mu$ M PD0332991 (PD), PHA-767491 (PHA), CVT-313 (CVT), CDK2-IN-73 and Ro-3306. Western blots were probed for CIZ1 and actin. **A)** Treatment of cells with CDK or DDK inhibitors for 6 hours. **B)** Quantitation of CIZ1 protein in relation to actin, presented as the mean  $\pm$  SD (n=3) and significance measured by One-Way ANOVA with TUKEY Post-Hoc ( $p < 0.05$ ), non-significant. **C)** As in A but for 24 hours. **D)** As for B, non-significant (n=3). **E)** PrestoBlue™ assays were performed after 0, 24, 48 and 72 hours and presented as the mean  $\pm$  SD (n=2).

Western blot analysis revealed minimal reduction in CIZ1 levels (top band) after treatment with PD0332991, PHA-767491 and CVT-313 for 6 hours. CDK2-IN-73 and Ro-3306 appear to have reduced CIZ1 protein levels after 6 hours, however there were large margins of error (Figure 4.1 A, B). After 24 hours, there is >30% reduction in CIZ1 levels after treatment with PD0332991, PHA-767491, CVT-313 and Ro-3306, however no reduction with CDK2-IN-73 relative to solvent control samples (Figure 4.1 C, D). To further assess the effect of each inhibitor on cellular proliferation, PrestoBlue™ was used to monitor cell growth. This showed PHA-767491, CVT-313 and Ro-3306 to be the most effective at reducing proliferation over a 72-hour period, with each inhibitor reducing growth by 60%. PD0332991 also reduced proliferation relative to controls with a 45% reduction. CDK2-IN-73 showed the weakest effect on growth with only a 15% reduction (Figure 4.1 E). The correlation between CIZ1 reduction and the proliferative rate of cells suggests that CIZ1 levels may be used as a proxy for the efficacy of each inhibitor for tumour growth.

During the cell cycle, oscillating cyclin levels results in varying CDK activity and subsequent differential phosphorylation states of CIZ1. The model for CIZ1 regulation, by the opposing activities of CDKs and the UPS, is cell cycle regulated. During G1 phase when kinase levels are low, CIZ1 is hypo-phosphorylated and initiates DNA replication via binding of CDC6, which promotes recruitment of CIZ1 to the nuclear matrix and formation of the pre-replication complex. In this hypo-phosphorylated state CIZ1 is vulnerable to proteasome-mediated degradation. As kinase levels increase during late G1 phase, cyclin A-CDK2 phosphorylates CIZ1 at T293 which blocks the DNA replication function of CIZ1 and protects it from ubiquitin-mediated degradation (Pauzaite, 2019). To determine if inhibition of CDK and DDK activity promotes proteasome-mediated degradation of CIZ1 in U87-MG cells, the proteasomal inhibitor MG132 was used in combination with CDK and DDK inhibitors and the effects analysed by western blotting (Figure 4.2).

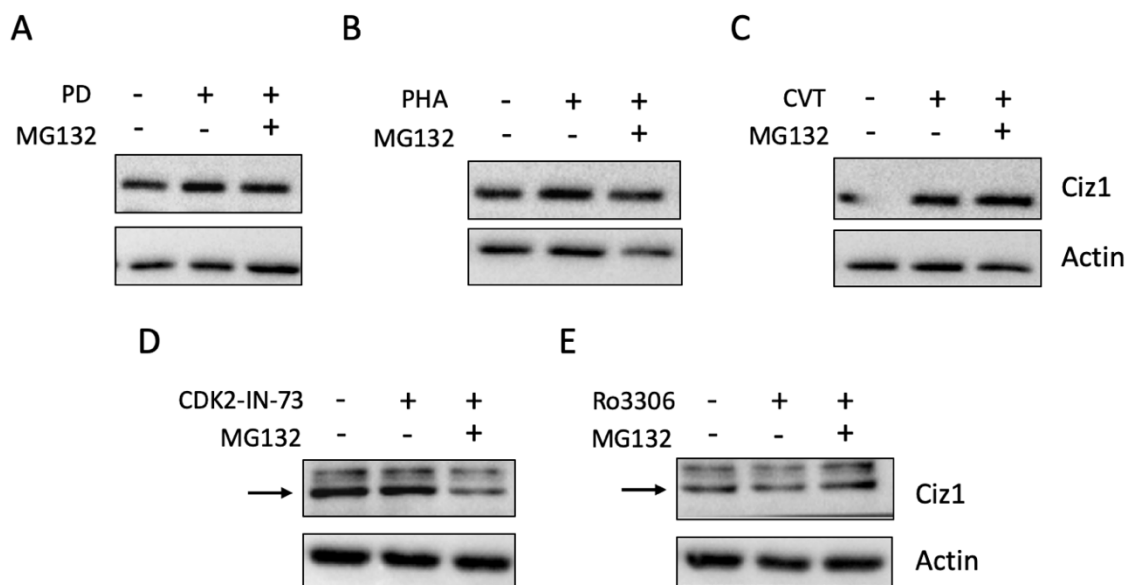


**Figure 4.2 Analysis of CIZ1 protein levels upon proteasomal inhibition post treatment with kinase inhibitors.** U87-MG cells were treated with 10  $\mu$ M of (A) PD0332991 (PD), (B) PHA-767491 (PHA), (C) CVT-313 (CVT), (D) CDK2-IN-73 and E) Ro-3306 for 24 hours  $\pm$  10  $\mu$ M proteasomal inhibitor MG132 from 20 to 24 hours. Western blots were probed for CIZ1 and actin, black arrows indicate CIZ1 band (n=2).

Treatment of U87-MG cells with Ro-3306 resulted in a small reduction in CIZ1 levels and this effect was reversed after addition of MG132. In contrast, treatment with CDK2-IN-73 alone did not appear to reduce CIZ1 levels; however, a reduction can be seen when treated in combination with MG132. As this cell line is relatively insensitive to the effects of CDK and DDK inhibition, we do not see any significant reductions in CIZ1 levels after 24-hour treatment and therefore we cannot accurately assess the recovery of CIZ1 levels by proteasomal inhibition and further experiments would be required to confirm these findings.

CDK and DDK inhibitors can be cytostatic meaning they block cell proliferation or cytotoxic meaning they induce cell death. To determine if inhibition of CDK and DDKs increased cell death in U87-MG cells, cells were treated with CDK and DDK inhibitors for 24 hours. Cells were labelled with PI and the nucleic acid stain YO-PRO<sup>®</sup>-1, apoptotic status was then analysed by flow cytometry (Figure 4.3). PI is a membrane impermeant dye which will label cells undergoing late apoptosis or necrosis and have

loss of membrane integrity. YO-PRO®-1 is permeant to cells undergoing early apoptosis and live cells remain unstained.

Treatment with PHA-767491 and Ro-3306 resulted in the highest rates of cell death, increasing the rates of apoptosis and cell death by 20% and 17% respectively compared to the control population, suggesting a cytotoxic effect of these inhibitors in this cell line. However, treatment with PD0332991, CVT-313 and CDK2-IN-73 showed no major cytotoxic effects when compared to the control population.

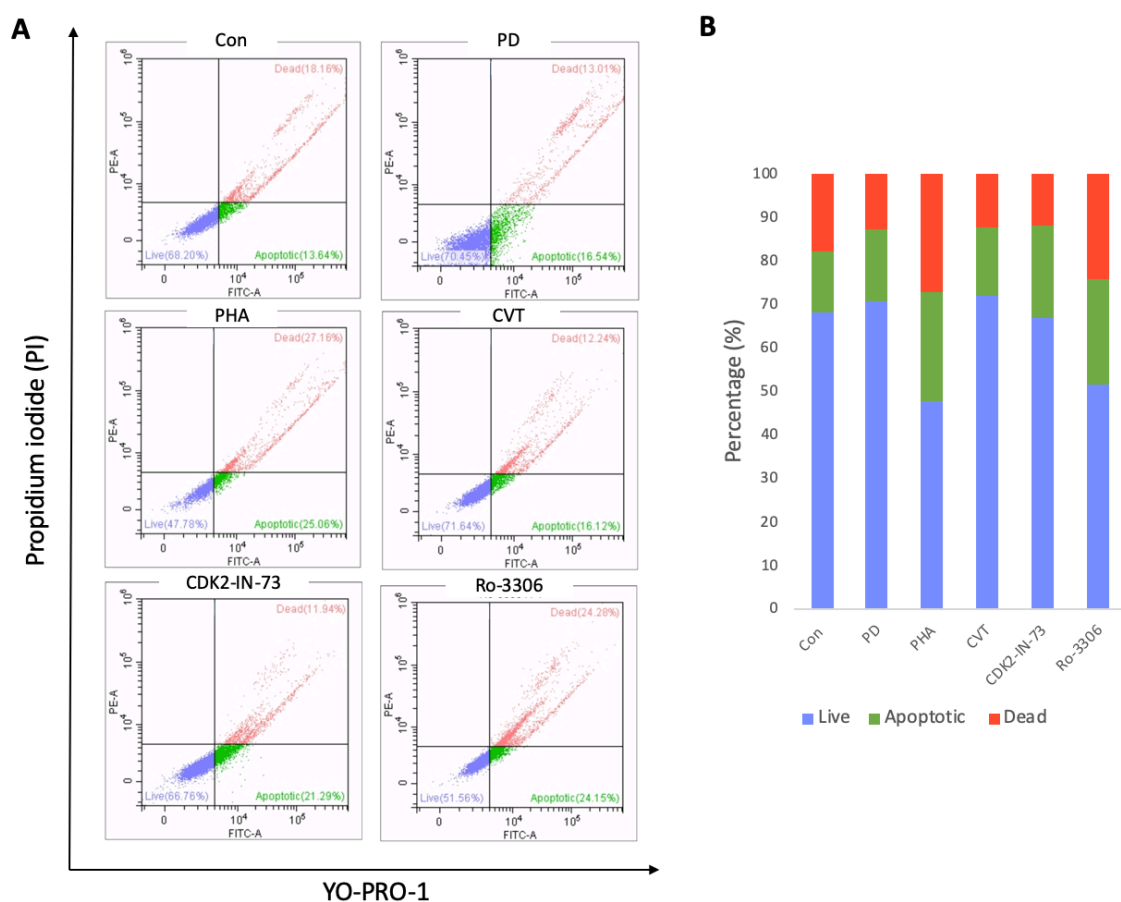


**Figure 4.3 Cell death profile of U87-MG cells after CDK/DDK inhibition. A)** Cells were treated with 10  $\mu$ M PD0332991 (PD), PHA-767491 (PHA), CVT-313 (CVT), CDK2-IN-73 and Ro-3306 for 24 hours. Cells were stained with YO-PRO-1 and PI and analysed by flow cytometry using channels for FITC (525/40) and PE (585/42). Quadrants represent live cells (bottom left), apoptotic (bottom right) and necrotic/dead (top right). **B)** Cumulative histogram representing the proportion of live, apoptotic and dead cells (n=1).

## 4.2 Primary GBM cells retain markers of glial origin

The primary GBM cells, BTNW914, were assessed for expression of glial markers using immunofluorescence. After long-term culture, primary GBM cell lines may lose expression of glial markers, no longer retaining their glial phenotypes. Glial fibrillary acidic protein (GFAP) is a type III intermediate filament protein expressed in various cell types in the CNS including glial cells. GFAP is a highly specific marker for glial cells and its expression is localised to the soma and end feet of cells (Wilhelmsson et al., 2003). Visualisation of the expression and localisation of this protein will allow us to confirm the origin of this cell line and suggest that the data generated is representative of the patient tumour.

GFAP was first identified in the brains of multiple sclerosis patients (Eng et al., 1971) and is now a widely used marker in glial cells. Numerous papers over the past few decades have implicated GFAP in astrocytoma development. GFAP expression is thought to decrease with higher tumour grade, loss of GFAP expression represents an undifferentiated state of glial cells and is associated with more aggressive phenotypes in some GBM tumours (Ahmadipour et al., 2020).

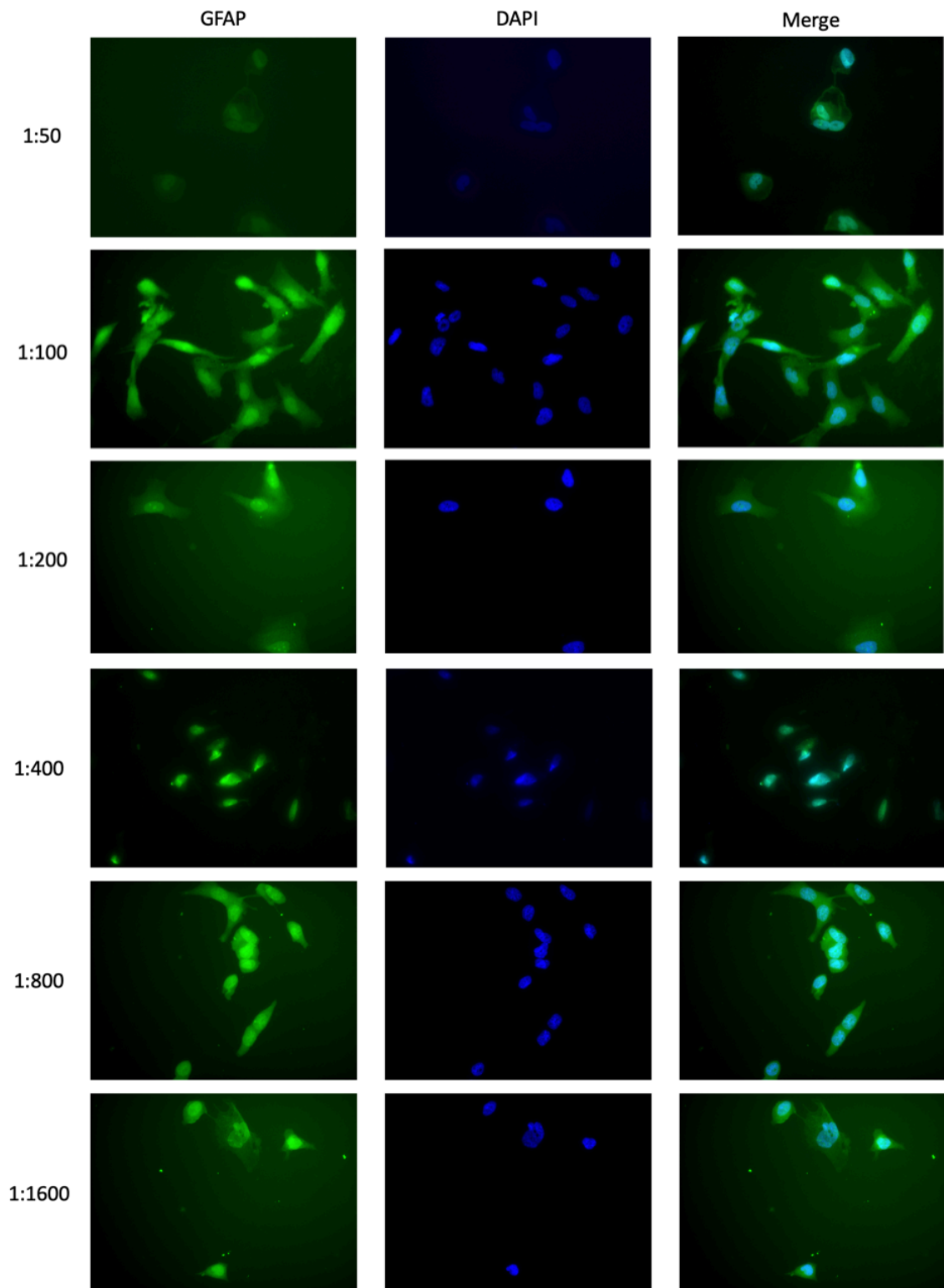


**Figure 4.4 Optimisation of GFAP antibody for immunofluorescence in BTNW914 cells.** Immunofluorescence images of cells treated with GFAP antibody dilutions of 1:50-1:1600. Cells were visualised by fluorescence microscopy using an anti-mouse secondary Alexa Fluor 488 conjugate.

Antibody optimisation revealed an antibody dilution of 1:800 to be optimal for visualisation of GFAP localisation and expression in these glial cells (Figure 4.4). Immunofluorescence examination of these cells demonstrated clear GFAP expression in the cytoplasm of the glial cells confirming that this primary GBM cell line has retained its glial origin during culture. Therefore, the data generated from this cell line can be said to be representative of the patient tumour.

### 4.3 Analysis of CDK and DDK inhibition in primary GBM BTNW914 cell line

The effects of small molecule CDK and DDK inhibitors were assessed and several different outcomes were determined. (i) the effect on CIZ1 levels, (ii) the effect on cellular proliferation and (iii) the effect on cell death and apoptosis. BTNW914 cells were treated with PD0332991, PHA-767491, CVT-313, CDK2-IN-73 and Ro-3306, harvested at 6 and 24 hours and blots probed for CIZ1 and actin (Figure 4.5). 6-hour treatment with CDK and DDK inhibitors resulted in small reductions in CIZ1 levels with CVT-313 being the most potent at reducing CIZ1 protein levels (Figure 4.5 A, B). After 24 hours, CIZ1 levels were reduced by PHA-767491, CVT-313 and Ro-3306 suggesting the cells require prolonged exposure to the inhibitors for effective destabilisation of CIZ1. This may be related to the cell cycle stage, as each inhibitor should specifically target DDK, CDK2 or CDK1 respectively that act at distinct phases of the cell cycle. However, we see an increase in CIZ1 levels after treatment with PD0332991 and CDK2-IN-73 compared to the control (Figure 4.5 C, D). These results suggest that CDK4/6 inhibition does not affect CIZ1 levels in this cell line. However, there are differential effects for CDK2 inhibition with CVT-313 effectively reducing CIZ1 levels, whereas CDK2-IN-73 was ineffective at reducing CIZ1 levels, similar to the U87-MG cell line. Although, none of these findings were of statistical significance. The effect of kinase inhibitors on cellular proliferation was also assessed to determine if this cell line has a requirement of CIZ1 for growth (Figure 4.5 E). The proliferation assays revealed CVT-313 and Ro-3306 to be the most effective at reducing proliferation, with reductions of

45%, which correlates with the reduction in protein levels observed with these inhibitors (Figure 4.5 E).

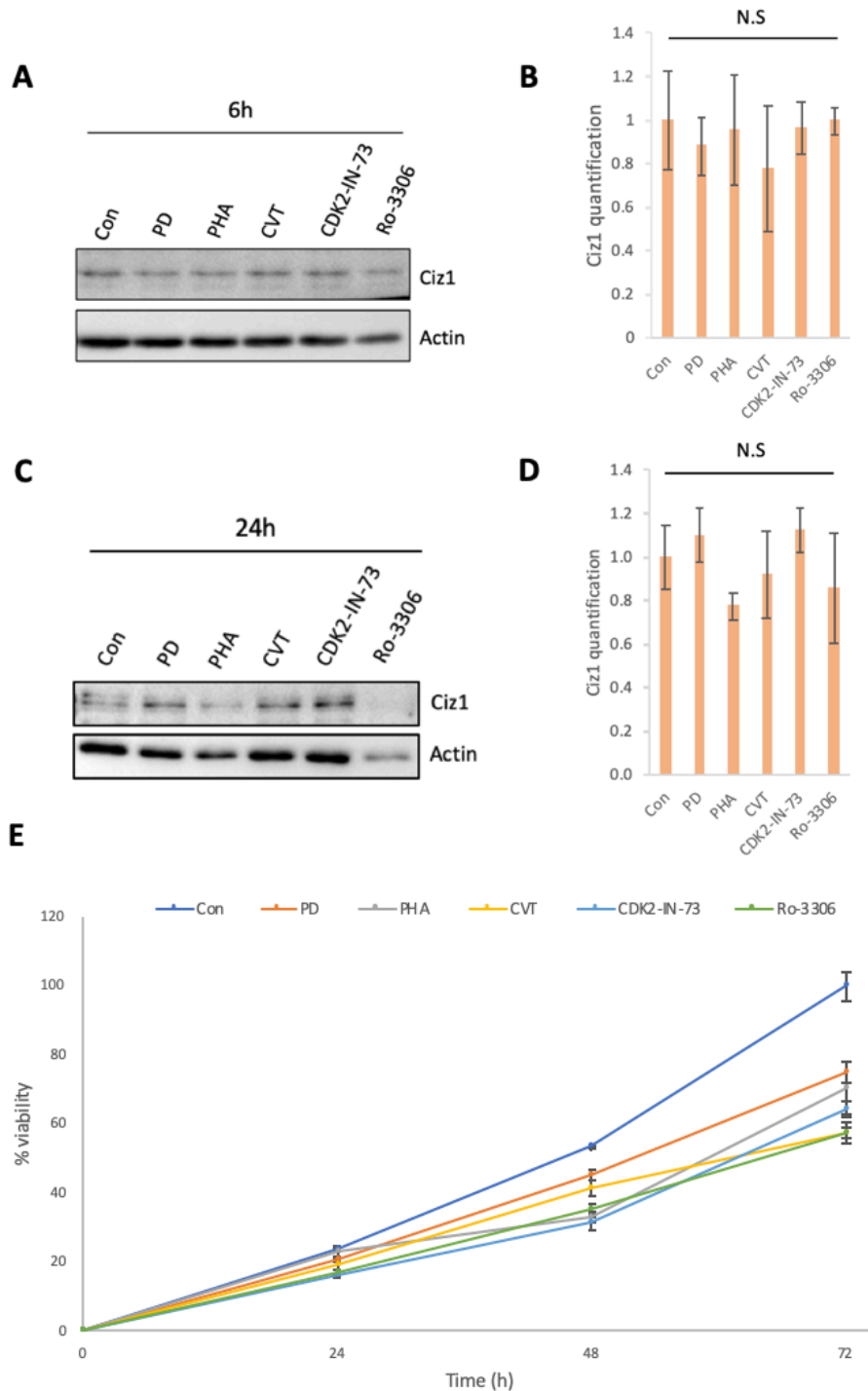


**Figure 4.5 Treatment of BTNW914 cells with CDK and DDK inhibitors.** Cells were treated with 10  $\mu$ M PD0332991 (PD), PHA-767491 (PHA), CVT-313 (CVT), CDK2-IN-73 and Ro-3306. Western blots probed for CIZ1 and actin. **A)** Treatment of cells with CDK/DDK inhibitors for 6 hours. **B)** Quantitation of CIZ1 protein in relation to actin, presented as the mean  $\pm$  SD (n=3) and significance measured by One-Way ANOVA with TUKEY Post-Hoc ( $p < 0.05$ ), non-significant. **C)** As in A but for 24 hours inhibitor treatment. **D)** As for B, non-significant (n=3). **E)** PrestoBlue™ assays were performed after 0, 24, 48 and 72 hours and presented as the mean  $\pm$  SD (n=2).

Next, the role of the proteasome in regulating CIZ1 abundance was also assessed in the primary GBM cell line BTNW914. In contrast to U87-MG cells, western blot analysis revealed a visible recovery of CIZ1 levels after treatment with PHA-767491 and CVT-313. Ro-3306 reduced CIZ1 levels, but this effect was not efficiently reversed by proteasomal inhibition. These results imply that CIZ1 is regulated by the proteasome after inhibition of CDK2 (CVT-313) or DDK (PHA-767491) in primary BTNW914 cell line (Figure 4.6).

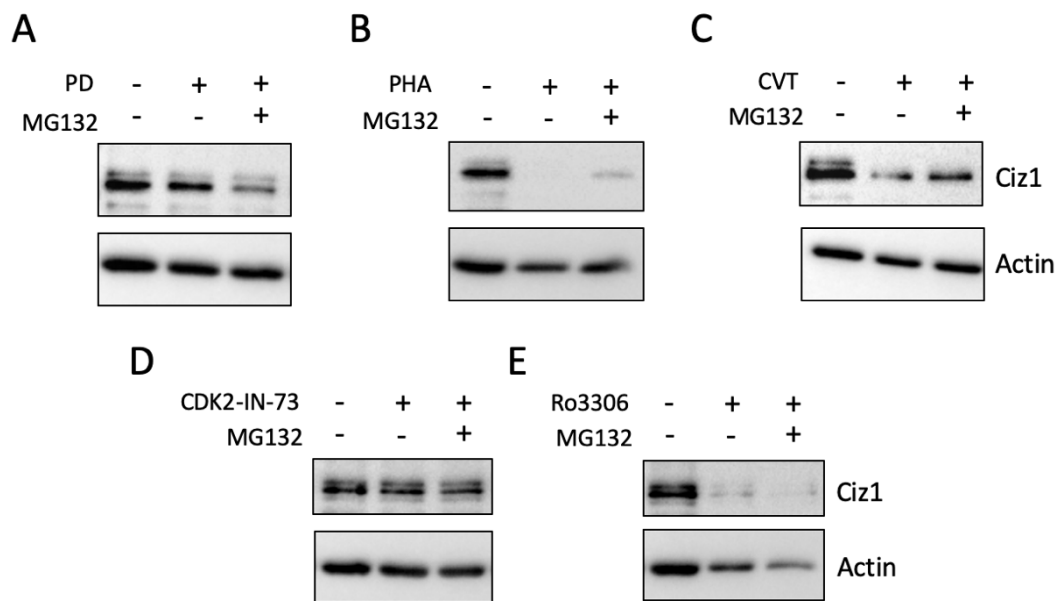


**Figure 4.6 Recovery of CIZ1 with proteasomal inhibitor MG132 after kinase inhibition.** BTNW914 cells were treated with 10  $\mu$ M of A) PD0332991 (PD), B) PHA-767491 (PHA), C) CVT-313 (CVT), D) CDK2-IN-73 and E) Ro-3306 for 24 hours  $\pm$  10  $\mu$ M MG132 from 20 to 24 hours. Western blots were probed for CIZ1 and actin (n=2).

The recovery of CIZ1 levels after proteasomal inhibition for CVT-313 and PHA-767491 is consistent with the working model where CIZ1 is stabilised by kinase mediated phosphorylation (Figure 4.6 B, C). In the absence of CDK2 or DDK activity this destabilises CIZ1 and promotes UPS-mediated degradation. Addition of MG132 after treatment with PD0332991 further reduced CIZ1 levels in comparison to treatment with PD0332991 alone, this could be due to a downstream effect of proteasomal inhibition resulting in activation of alternative degradation pathways.

Finally, to assess the effect of CDK and DDK inhibition on cell survival, BTNW914 cells were treated with CDK and DDK inhibitors as previous and the rates of apoptosis and cell death were determined by flow cytometry (Figure 4.7).

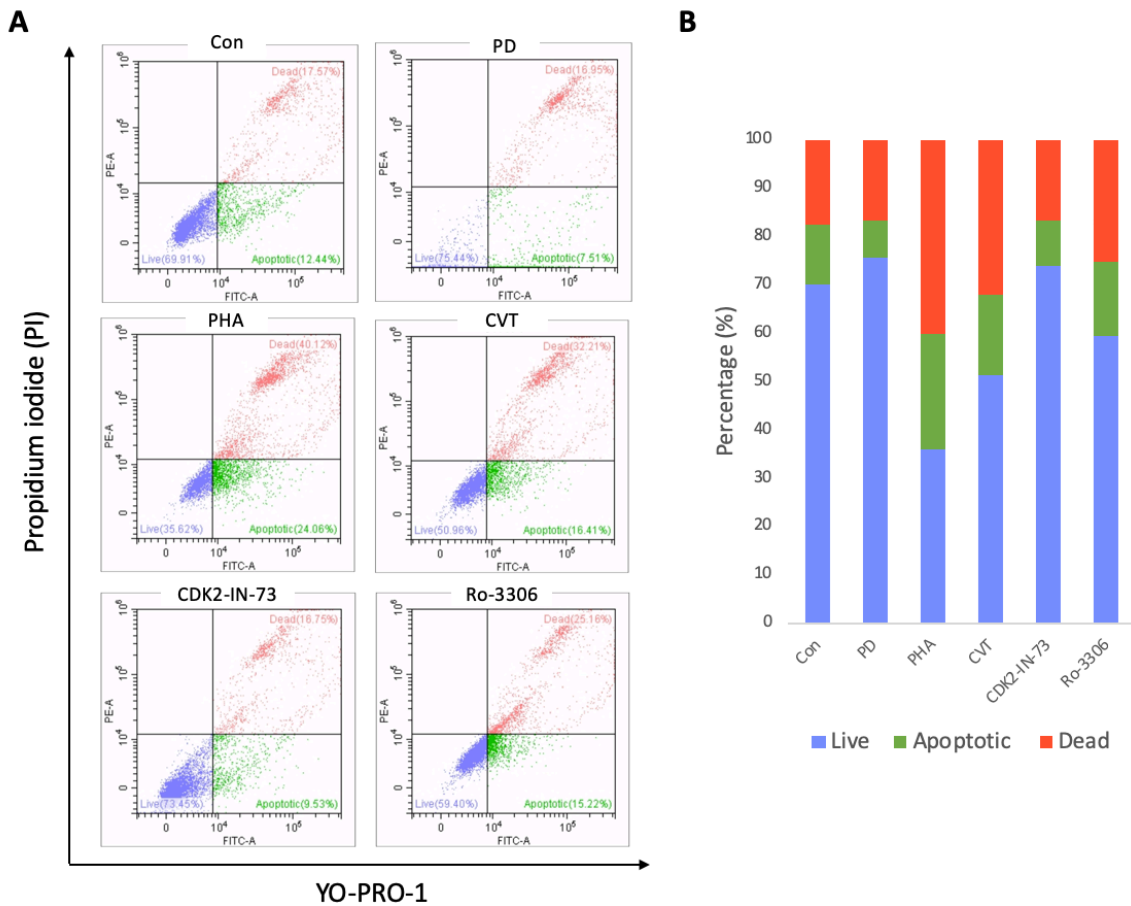


**Figure 4.7 Cell death profile of BTNW914 cells after CDK/DDK inhibition. A)** Cells were treated with 10  $\mu$ M PD0332991 (PD), PHA-767491 (PHA), CVT-313 (CVT), CDK2-IN-73 and Ro-3306 for 24 hours. Cells were stained with YO-PRO-1 and PI and analysed by flow cytometry using channels for FITC (525/40) and PE (585/42). Quadrants represent live cells (bottom left), apoptotic (bottom right) and necrotic/dead (top right). **B)** Cumulative histogram representing the proportion of live, apoptotic and dead cells (n=1).

Treatment with PHA-767491 and CVT-313 increased rates apoptosis and cell death by 34% and 18% respectively compared to the control population, Ro-3306 also increased these rates by 10% (Figure 4.7), consistent with the effects on CIZ1 protein levels and proliferation (Figure 4.5 C, D). These inhibitors were also the most effective at reducing proliferation in the BTNW914 cell line (Figure 4.5 E) suggesting a requirement of CIZ1

for proliferation and survival in this cell line. PD0332991 and CDK2-IN-73 showed little effect on cell death and apoptosis (Figure 4.7).

#### 4.4 CIZ1 depletion in BTNW914 primary GBM cells

The use of siRNA constructs to genetically deplete CIZ1 levels within the cell has been demonstrated in various cancers both *in vitro* and *in vivo*, effectively reducing cell proliferation in CRC (Wang et al., 2014) and tumour growth in mouse xenograft models (Higgins et al., 2012; Liu et al., 2015; Zhang et al., 2015). To determine the dependency of the primary GBM cell line BTNW914 on CIZ1 for growth, CIZ1 was genetically depleted using a small molecule siRNA construct. Using a previously established transfection protocol for BTNW914 cells (Falkingham, 2020), cells were transfected with anti-CIZ1 siRNA and CIZ1 transcript levels, protein levels, cell cycle profile and cell proliferation were monitored (Figure 4.8).

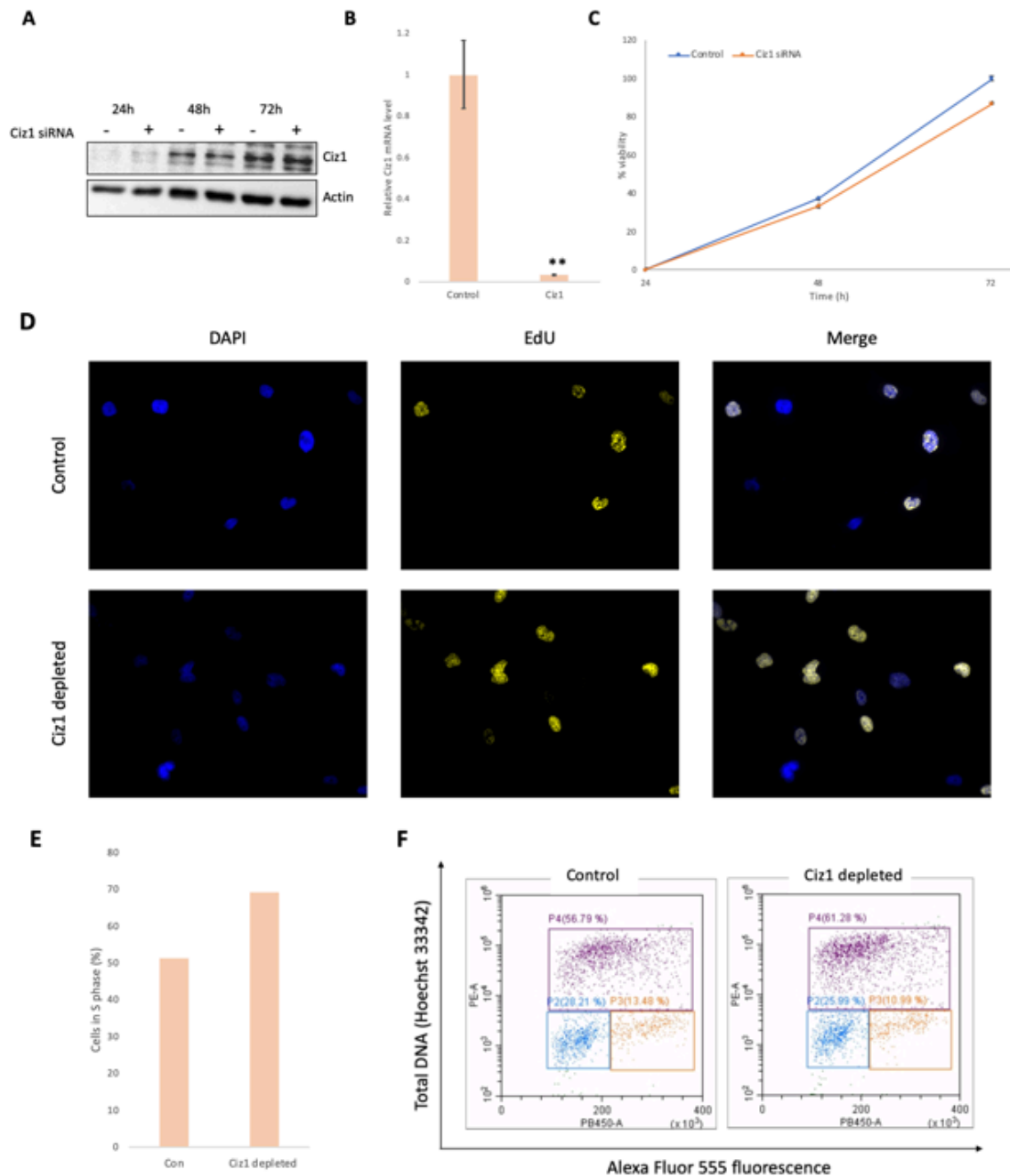


**Figure 4.8 Analysis of BTNW914 cells following CIZ1 depletion.** BTNW914 cells were transfected with anti-CIZ1 siRNA. **(A)** Western blot analysis of CIZ1 protein levels at 24, 48 and 72 hours, blots were probed for CIZ1 and actin. **(B)** RT-qPCR analysis of CIZ1 mRNA levels relative to GAPDH at 24 hours showing mean  $\pm$  SD (n=3), significance measured using a paired one-sample t-test (p=0.0053). **(C)** PrestoBlue™ cell viability assay, 24, 48 and 72 hours post transfection and presented as the mean  $\pm$  SD. **(D)** Immunofluorescence images showing S-phase entry in control and CIZ1 depleted cells at 48 hours. **(E)** Bar chart representing the percentage of S-phase cells by scoring EdU positive cells out of approx. 100 nuclei using immunofluorescence. **(F)** Cell cycle profile analysis by flow cytometry at 24 hours, cells were pulse labelled with EdU 1 hour prior to harvest and stained with Hoechst 33342.

Having successfully depleted CIZ1 mRNA transcripts upon transfection, we would expect to see a reduction in CIZ1 protein levels. However, western blot analysis reveals no reduction in CIZ1 levels at 24, 48 or 72 hours (Figure 4.8 A). After 24 hours CIZ1 levels have dramatically reduced in both the control and transfected populations, the reasons for this being unclear. It's possible that the high rates of cell death after transfection means we are unable to detect small amounts of protein by western blot analysis. Alternatively, cell stress as a result of electroporation may have resulted in a post-translational modification of CIZ1, for example ubiquitination to target CIZ1 for proteasome mediated degradation. There are a number of explanations as to why a reduction in CIZ1 mRNA levels did not translate into a reduction in protein levels. Although the half-life of CIZ1 has not previously been reported in the literature, a high protein stability and therefore longer half-life would explain why there was no reduction in CIZ1 protein levels after 72 hours. Further experiments should be carried out using longer time points and re-transfections every 48 hours to determine if the half-life of CIZ1 preventing any protein reduction at the earlier time points. It is also possible that the siRNA molecules are being degraded before any downstream effects on protein synthesis can be observed. To analyse this, mRNA analysis should be carried out every 24 hours to determine if CIZ1 transcript levels remain depleted over the course of the experiment. Alternatively, the siRNA construct may only target a specific isoform of CIZ1 which is different from the isoform being detected by the primary antibody for western blotting. Multiple siRNA constructs which target all known CIZ1 isoforms should be used in order to determine whether the siRNA construct is the limiting factor in protein knockdown.

Analysis of cell proliferation over a 72-hour period post transfection reveals a small reduction in proliferation in the siRNA transfected cells compared to the control population. The effects of CIZ1 depletion on S-phase entry were analysed by immunofluorescence and flow cytometry. Cells were labelled with EdU and visualised using the Click-IT reaction imaging kit (Alexa Fluor 488) which allowed determination of the number of actively replicating cells using fluorescence microscopy (Figure 4.8 D). EdU positive cells were scored out of 100 nuclei and the percentage of cells in S-phase was calculated. This revealed an increase in S-phase cells in the CIZ1 depleted

population compared to the control (~50% versus ~70%; Figure 4.8 E). Flow cytometry analysis of cells pulse labelled with EdU 1 hour prior to harvest and stained with Hoechst 33342 revealed an increase in the percentage of S-phase cells in the CIZ1 depleted population compared to the control (56% versus 61%; Figure 4.8 F). Both immunofluorescence and flow cytometry analysis revealed an increase in the proportion of cells in the CIZ1 depleted population however this cannot be attributed to CIZ1 as there was no reduction in protein levels. There was no significant change in proliferation rates after CIZ1 depletion (Figure 4.8 C). The data presented is consistent with the effects of CIZ1 depletion in murine fibroblasts (NIH 3T3) where siRNA constructs were ineffective at reducing CIZ1 levels although they were able to reduce cell cycle progression (Copeland et al., 2010).

## 4.5 Chapter discussion

### 4.5.1 CDK and DDK inhibition reduces CIZ1 levels and proliferation *in vitro*

Reduction of CIZ1 protein levels has been demonstrated upon CDK and DDK inhibition *in vitro* (Pauzaite, 2019). The use of CDK and DDK inhibitors to reduce CIZ1 levels is based on the proposed model whereby CIZ1 levels are opposingly regulated by CDKs and the UPS (Figure 3.1). CDK2 and DDK inhibition reduced CIZ1 levels in PC3 and SW480 cells which were then recovered by proteasomal inhibition consistent with the proposed model. A reduction in CIZ1 levels corresponded to a reduction in proliferation suggesting CIZ1 is required for growth in these tumour types (Pauzaite, 2019).

In this work, we are able show that CDK and DDK inhibition reduces CIZ1 levels in numerous cancerous cell lines, with PHA-767491 and CVT-313 being the most potent, producing consistent reductions in protein levels across all cell lines tested. Ro-3306 reduced CIZ1 in both GBM cell lines, although none of these reductions were of statistical significance. Where CIZ1 levels were reduced, cell proliferation was also reduced suggesting a requirement of CIZ1 for growth. Furthermore, cell death assays

revealed PHA-767491 to increase rates of apoptosis consistently across both GBM cell lines suggesting a cytotoxic effect of this inhibitor in these tumours. This is supported by the increase in apoptotic rates observed upon DDK inhibition in other cancer cell lines and xenograft models (Natoni et al., 2013). In HCC cells, PHA-767491 downregulated expression of anti-apoptotic protein myeloid leukemia cell 1 through dual inhibition of Cdc7 and Cdk9. In nude mice HCC xenografts, PHA-767491 increased *in situ* cell apoptosis (Li et al., 2015). In glioblastoma cell lines, U87-MG and U251-MG, PHA-767491 reduced proliferation and induced apoptosis (Erbayraktar et al., 2016). The findings in this study demonstrate CVT-313 increased the rates of apoptosis in BTNW914 but not U87-MG cells suggesting a cytotoxic effect which is specific to tumour subtype. Ro-3306 increased rates apoptosis in U87-MG and BTNW914 cells however, in A549 cells, the reductions in CIZ1 protein levels with Ro-3306 did not result in increased rates of apoptosis or cell death suggesting a vulnerability to CDK1 inhibition in GBM and identifying a potential cell-death inducer.

The CDK1 inhibitor Ro-3306 has off-target effects on cyclin E-CDK2 justifying the reduction in CIZ1 levels across A549, U87-MG and BTNW914 cells. Ro-3306 is an ATP-competitive inhibitor which binds to the ATP binding pocket of CDK1. Previous molecular modelling predicts the binding of Ro-3306 to the ATP-binding pocket of CDK2 as this kinase is most closely related to CDK1 (Kojima et al., 2009). Although, the crystal structure of CDK1 has recently been resolved revealing the ATP binding domains of CDK1 and CDK2 share 86% primary structure homology explaining the off-target activity of this inhibitor. However, Ro-3306 inhibits cyclin B-CDK1 complexes at a 10-fold increase in selectivity relative to cyclin A-CDK2 (Brown et al., 2015).

The inability of the CDK4/6 inhibitor PD0332991 to reduce CIZ1 levels in GBM cell lines could be due to the low activity of CDK4/6 in late G1 phase, discarding a potential role of cyclin D-CDK4/6 activity in promoting CIZ1 accumulation. However, this contradicts findings in chapter 3 where PD0332991 was the only inhibitor to significantly reduce CIZ1 levels in A549 cells (Figure 3.2 A, B) suggesting this cell line is more sensitive to the effects of CDK4/6 inhibition, potentially due its Rb status. CDK4/6 activity is high during early G1 phase and phosphorylates Rb protein, a tumour suppressor protein

which represses gene transcription required for transition from G1 to S-phase. In its unphosphorylated form, Rb binds the transactivation domain of E2F and promoter regions of these genes to form a complex with E2F which subsequently blocks transcription of S-phase genes. In late G1, Rb phosphorylation releases E2F allowing expression of genes for S-phase entry. Therefore, inhibition of Rb phosphorylation means Rb stays bound to E2F and Rb-repressor complex preventing expression of S-phase genes, blocking S-phase entry (Giacinti and Giordano, 2006). This supports the reduction in cell proliferation observed when CIZ1 protein levels remained unchanged. In some cases, treatment with PD0332991 resulted in an increase in CIZ1 levels suggesting a tumour-enhancing effect.

The CDK2 inhibitor CVT-313 reduced CIZ1 protein levels across all cell lines demonstrating a strong binding affinity towards cyclin A-CDK2. Previous work has established CDK2 to be essential for proliferation and therefore renders CDK2 an attractive therapeutic target for reducing tumour growth. In human diploid fibroblasts, neutralisation of CDK2 via microinjection of antibodies directed against CDK2 blocks progression into S-phase. Similar effects were observed in osteosarcoma cells after overexpression of dominant negative mutant CDK2 (Brooks et al., 1997; Sakurikar and Eastman, 2016). CVT-313 acts as a reversible and ATP-competitive inhibitor of cyclin A-CDK2. Recent work has determined the crystal structure of CVT-313 binding to CDK2. CVT-313 binds the ATP-binding pocket of CDK2, interacting directly with Leu83, Asp86 and Asp145 residues, binding is further stabilised by a water-mediated interaction with Asn132 (Talapati et al., 2020). This interaction prevents CDK2-mediated phosphorylation and accumulation of CIZ1, promoting its degradation by the UPS. The experiments carried out in this study support the use of CVT-313 as a potential anti-cancer therapeutic, reducing CIZ1 protein levels and proliferation across a diverse range of cell lines. As previously mentioned, Rb is also a substrate for CDK2 phosphorylation and therefore inhibition of CDK2 will also inhibit the Rb pathway further disrupting S-phase entry. CVT-313 also exerts off-target activity towards CDK1 which may disrupt transition from G2 to M phase further reducing the proliferative rate of cells (Brooks et al., 1997; Sakurikar and Eastman, 2016).

In contrast, ATP-competitive cyclin A-CDK2 inhibitor CDK2-IN-73 was unable to significantly reduce CIZ1 levels across all cell lines tested. CDK2-IN-73 has 2000-fold selectivity over cyclin B-CDK1 making it attractive for studying specific cell cycle components with limited off-target effects. The inability of CDK2-IN-73 to potently inhibit cyclin A-CDK2 contradicts the reduction in CIZ1 levels seen with CVT-313 and requires further investigation.

Across the GBM cell lines, reductions in CIZ1 levels are seen for both PHA-767491 and CVT-313 and these reductions are reversed by MG132 in BTNW914 cells, consistent with the findings in A549 cells. The inconsistencies in CVT-313 activity seen between kinase inhibition alone and in combination with MG132 are likely due to experimental error as CVT-313 was able to effectively reduce proliferation in both U87-MG and BTNW914 cells.

Inconsistencies in inhibitor action across different cell lines may be attributed to a variety of factors. The inhibitor may have limited bioavailability regarding the rate of uptake by the cells *in vitro* and delivery to the intended site of action. In addition, varying gene expression profiles of CIZ1 and the components involved in CIZ1 regulation may alter the effectiveness of the inhibitor at reducing CIZ1 levels. Furthermore, cross-talk between cellular signalling pathways makes it difficult to observe the effects of a specific kinase on CIZ1 accumulation using simple *in vitro* kinase inhibition studies. Depletion of other substrates which may interact with the signalling pathway in question will provide a better understanding of the roles of specific kinases. Future work should focus on the use of these inhibitors in combination with chemotherapeutic agents to determine if depletion of CIZ1 sensitises cells to the activity of these DNA-damaging agents. Despite the absence in significant reductions of CIZ1 protein levels, proliferative rates were reduced by most of the inhibitors suggesting off-target effects on alternative signalling pathways.

This work supports the proposed model of CIZ1 regulation (Figure 3.1) and has extended previous work showing CIZ1 is degraded by UPS after CDK2 and DDK inhibition in PC3 and SW480 cells, further increasing our understanding of the effect

of CDK and DDK inhibitors across different cancer cell types. Although triplicate repeats were obtained for the CDK and DDK inhibition studies carried out, further work is required to validate the reproducibility of these results. Furthermore, investigation into the role of E3 ligases in proteasome-mediated degradation of CIZ1 may provide further opportunities for therapeutic intervention. The role of the proteasome in CIZ1 regulation has been demonstrated by recovery of CIZ1 levels upon proteasomal inhibition and therefore overexpression of the E3 ligases responsible for this degradation may provide another means of reducing CIZ1 levels.

CDK inhibitors were first investigated during the 1990s as pan-CDK inhibitors with the main function to block cell cycle progression and inhibit proliferation. These first-generation inhibitors had poor selectivity and high toxicity resulting in failure in clinical trials. This led to the development of second-generation CDK inhibitors with increased kinase selectivity and fewer adverse effects on somatic cells (Zhang et al., 2021). The majority of these inhibitors have shown promising anti-tumour effects in pre-clinical trials however require further investigation into their safety and efficacy before being approved.

Focusing on the potential use of CDK and DDK inhibitors in GBM treatment, no CDK inhibitors have been approved for use as there are limited findings showing any significant anti-tumour activity. PD0332991 has previously reached phase II trials in adult patients with recurrent Rb-1 positive GBM however failed as an effective monotherapy (Taylor et al., 2018). Different effects were observed in the well-established GBM cell line U87-MG and primary GBM cell line BTNW914 indicating that CDK inhibitor activity may be dependent on the subtype of GBM, emphasising the need to extend this research to include further primary cell lines and compare the effects.

Previous research has clearly demonstrated that selective CDK inhibitors are the way forward for use of CDK inhibitors in cancer therapy and success with the approval of PD0332991 for breast cancer treatment has provided confidence in the development of further CDK inhibitors as potential anti-cancer therapeutics. Although pre-clinical

trials fail due to problems with bioavailability and selectivity of the inhibitors, current research improving mechanisms of drug delivery and developing combination therapies are helping to overcome these current issues.

#### 4.5.2 Effects of CIZ1 depletion on proliferation and cell cycle profile in primary GBM cells

Genetic depletion of CIZ1 via siRNA molecules has been demonstrated in a number of tumour types, successfully reducing cell proliferation and tumour growth. Genetic depletion of cell cycle components which are commonly overexpressed in cancer is a viable means of reducing tumour growth. CIZ1 contributes to tumourigenesis in a number of tumour types due to its overexpression or alternative splicing, siRNA-mediated depletion of CIZ1 in these tumour types successfully reduced proliferation and tumour growth (Higgins et al., 2012; Liu et al., 2015; Wang et al., 2014; Zhang et al., 2015). This justifies our approach of CIZ1 depletion in GBM however in contrast to previous findings, introduction of anti-CIZ1 siRNA did not appear to reduce CIZ1 protein levels despite significant reductions in CIZ1 mRNA levels at 24 hours. In some cases, CIZ1 protein was undetectable in both the control and CIZ1 depleted populations which hasn't previously been observed (Figure 4.8 A). Previous work in which transfection experiments were carried out in mouse embryonic fibroblasts demonstrated that CIZ1 depletion did not affect the cellular pool of CIZ1. This study found differential effects of CIZ1 siRNAs between the soluble and insoluble pools of CIZ1, with the insoluble CIZ1 pool containing p100-CIZ1 and p125-CIZ1 forms being more stable than the soluble pool (Coverley et al., 2005). This may suggest that a specific pool of CIZ1 is resistant to siRNA mediated depletion. Alternatively, failure to deplete the cellular pool of CIZ1 could be due to a post translational modification of CIZ1 under cell stress caused by electroporation. Furthermore, the high rates of cell death post transfection may mean CIZ1 levels are too low to be detected by western blot analysis. The small reduction in proliferation upon CIZ1 depletion (Figure 4.8 C) may be due to low transfection efficiency as these results do not coincide with the reduction in proliferation observed upon CDK2 inhibition in this cell line (Figure 4.5 E)

Measuring transcript levels of a proliferation marker such as Ki67 may provide a better understanding of the role of *CIZ1* in proliferation in this cell line.

The increase in proportion of cells in S-phase demonstrated by both flow cytometry and immunofluorescence suggests depletion of *CIZ1* prolongs progression through S-phase and subsequently slows tumour growth, this could be due to a reduction in DNA synthesis. Importantly, these experiments are only a measure of the proportion of cells in S-phase and do not necessarily provide insight into proliferative potential of the cells.

The siRNA experiment did not show any significant reductions in *CIZ1* protein levels or proliferative rates. This could be due to the half-life of *CIZ1*, although there is no data available for the half-life of *CIZ1* in the literature, an increased half-life may explain the persistence of *CIZ1* protein after siRNA knockdown.

A single RNA construct was used to deplete *CIZ1* in this primary cell line, these gene knockout studies should be repeated using a range of siRNA constructs targeting *CIZ1* to see if the results produced are consistent with those in this study. The use of different siRNA constructs may result in a more robust depletion of *CIZ1* providing a more accurate representation of the role of *CIZ1* in this GBM cell line.

The results presented in this chapter highlight the need for an alternative approach to protein knockdown. The use of proteolysis-targeting chimeras (PROTACs), heterobifunctional molecules able to target proteins of interest for degradation, could be a more effective approach towards specific *CIZ1* degradation. PROTACs function by bringing an E3 ligase into close proximity with a target protein resulting in degradation of the target protein by the proteasome. Halo-PROTACs consist of a von Hippel–Lindau (VHL) ligand and a chloroalkane moiety joined by a chemical linker. The chloroalkane moiety is able to irreversibly bind HaloTags leading to the ubiquitination and degradation of overexpressed Halo-tagged proteins offering an alternative to protein knockout (Caine et al., 2020).

## Chapter 5: Evaluation of CIZ1 as a biomarker in GBM

There is an unmet need for the identification of new biomarkers for early brain tumour detection. Minimally invasive methods are required for diagnosis or monitoring effectiveness of treatment in CNS tumours (Jelski and Mroczko, 2021). MRI is the main imaging technique used in patients with a suspected brain tumour. Whilst MRI can help guide surgery, further analysis is required to distinguish between high-grade gliomas. For diagnosis of tumour type and grade, examination of a tissue biopsy or resected tumour is required, however biopsies are highly invasive and difficult to repeat (Müller Bark et al., 2020). Liquid biopsies are being investigated as an alternative to collecting tissue samples; analysis of blood and cerebrospinal fluid (CSF) can potentially be used to identify diagnostic and prognostic markers in brain tumours (Jelski and Mroczko, 2021).

Biomarkers of tumours can be nucleic acids, proteins and extracellular vesicles that accumulate in the blood or CSF. In GBM patients, circulating tumour cells (CTCs) have also been detected in the blood (Gao et al., 2016). Molecular biomarkers can be used to distinguish between different types of cancer, but the majority are unreliable as predictive markers of diagnosis and prognosis. Molecular biomarkers of GBM include *MGMT* (Cabrini et al., 2015), *EGFR* (Shinojima et al., 2003) and *IDH1/2* (Sanson et al., 2009). *MGMT* is an enzyme encoded for by a gene localised on chromosome 10q26 and plays an important role in DNA repair; reversing DNA alkylation by removing guanine-alkyl groups which prevents apoptosis (Patel et al., 2012). Expression of *MGMT* is regulated by the transcription factors specificity protein 1 (Sp1) and nuclear factor kappa B (NF-κB) which induce expression of *MGMT* via activation of the *MGMT* promoter (Cabrini et al., 2015). Methylation of the *MGMT* promoter is found in approximately 40% of GBM cases and is more commonly observed in secondary GBM due to its association with mutant *TP53*. Methylation of the *MGMT* promoter has shown to be a predictor of prognosis in GBM as patients with increased methylation showed better therapeutic responses to TMZ, the standard chemotherapy for GBM. Patients with *MGMT* promoter methylation had an OS of 18.2 months in comparison to 12.2 months in patients without promoter methylation (Hegi et al., 2005). *MGMT*

promoter methylation is most frequently detected by PCR using SYBR Green or in combination with mass spectrometry (MS) (Thon et al., 2013).

As GBM is a highly proliferative tumour, cell growth and proliferation is controlled by growth factors and their receptors such as EGFR. *EGFR* amplification and mutation were determined as prognostic markers in GBM. *EGFRvIII* overexpression in the presence of *EGFR* amplification is currently the most reliable marker of poor prognosis and overall survival in GBM (Jelski and Mroczko, 2021). Although, some studies suggest *EGFRvIII* to be an indicator of positive prognosis and longer survival in patients which have undergone the standard therapy of surgery, chemotherapy and radiotherapy (Montano et al., 2011). *EGFR* may also predict patient response to RTK inhibitors. Patients with *EGFR* amplification initially respond to RTK inhibition, however often acquire resistance to this treatment (Patel et al., 2012).

IDH can also be used as a molecular biomarker in GBM. IDH is an enzyme that catalyses decarboxylation in the Krebs cycle. IDH enzymes can be subdivided into the isoenzymes IDH1 and IDH2 which catalyse the reversible oxidation of isocitrate to produce  $\alpha$ -ketoglutarate ( $\alpha$ -KG) whilst simultaneously reducing NADP<sup>+</sup> to NADPH, a molecule involved in the protection of cells from oxidative stress (Lee et al., 2002). *IDH* mutations are found in up to 85% of secondary GBM cases but are rare in primary GBM. The most common *IDH1/2* mutation consists of the replacement of arginine with histidine via a single-residue change converting  $\alpha$ -KG to D-2-hydroxy-glutarate (D-2HG) which is an oncometabolite. The mechanism by which D-2HG promotes tumourigenesis is unclear but is possibly due to the effect on DNA methylases which promote DNA and histone demethylation (Balss et al., 2008). IDH serves as a prognostic marker for predicting patient survival in GBM as *IDH* mutant cells are more sensitive to radiotherapy than *IDH* wild-type cells; a secondary *IDH* mutation confers increased sensitivity to TMZ (SongTao et al., 2012). *IDH* mutation is typically detected by IHC or spectroscopy, pyrosequencing or droplet-type digital polymerase chain reaction (ddPCR) can also be used to detect mutations. One limitation of IDH as a biomarker is the incapability to determine the effect of *IDH* mutation on tumour progression (Turcan et al., 2012).

GFAP is an intermediate fibre protein produced by astrocytes and other cells of the CNS, its expression is often higher in GBM cells compared to normal brain tissue (Jung et al., 2007). However, GFAP is not used as a circulatory diagnostic marker in the blood due to some tumours having heterogenous or low expression of GFAP leading to undetectable amounts being released into the bloodstream, known as a “sensitivity gap”. Increased *GFAP* expression is linked to tumour volume, intratumoural *GFAP* expression and degree of necrosis (Tichy et al., 2016), serum GFAP levels are linked to *IDH* mutational status (Kiviniemi et al., 2015). GFAP is the main marker used to detect CTCs, its expression is often maintained in GBM despite its heterogeneity.

## 5.1 Aims

In order to successfully analyse the expression and localisation of CIZ1 in GBM, a robust antibody which specifically targets CIZ1 is required for IHC analysis (Figure 2.1). This chapter will demonstrate the optimisation of a specific anti-CIZ1 immunopurified antibody and the establishment of staining parameters for use in IHC analysis. A cohort of patient-derived FFPE tissue sections will be subject to immunostaining using an indirect method of antibody detection consisting of avidin-biotin complexes to determine differences in CIZ1 expression and localisation between healthy and tumour tissue.

## 5.2 Validation of the CIZ1-N471 antibody

The first step of the antibody validation process was to assess antibody specificity using western blotting. The antibody must be able to recognise the denatured antigen and this was demonstrated by visualization of a strong band at approximately 100kDa, the molecular weight of CIZ1. Although there are bands present further down the blot, these bands are less prominent and are likely to be splice variants of CIZ1.

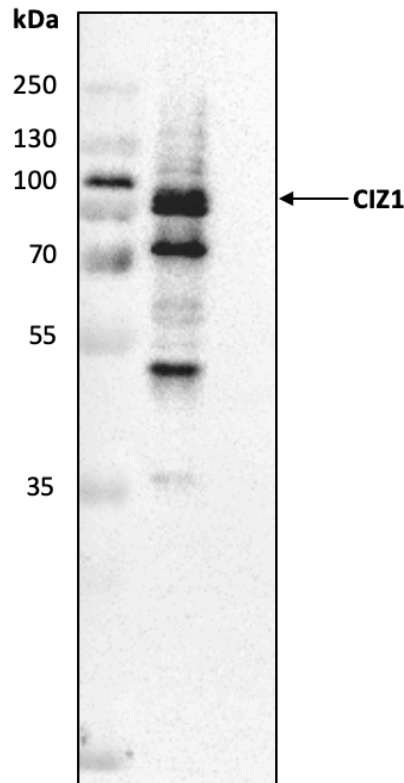


**Figure 5.1 Confirmation of antibody specificity using western blotting.** Western blot analysis of U87-MG cells, blots were probed with the immunopurified CIZ1-N471 antibody and show a strong band at approximately 100 kDa representing CIZ1. Molecular weight markers are shown to the left of the blot (kDa).

### 5.3 Optimisation of immunopurified anti-CIZ1 antibody concentration for IHC analysis of patient GBM tissue sections

Optimisation of antibody concentration was performed by titration of the anti-CIZ1 antibody to determine the optimal dilution that allowed for maximal visualisation of CIZ1 staining with minimal non-specific staining. Staining was performed using tissue sections from patient sample BTNW2760. Tissue sections were stained using antibody dilutions ranging from 1:50 to 1:3200 and images taken. As the antibody concentration decreases there is a reduction in brown DAB staining observed. The areas which retain the brown stain over decreasing antibody concentrations demonstrate the selectivity and specificity of CIZ1 staining. Based on this principle, an optimal antibody concentration of 1:800 was determined and used in all subsequent IHC analysis (Figure 5.2).

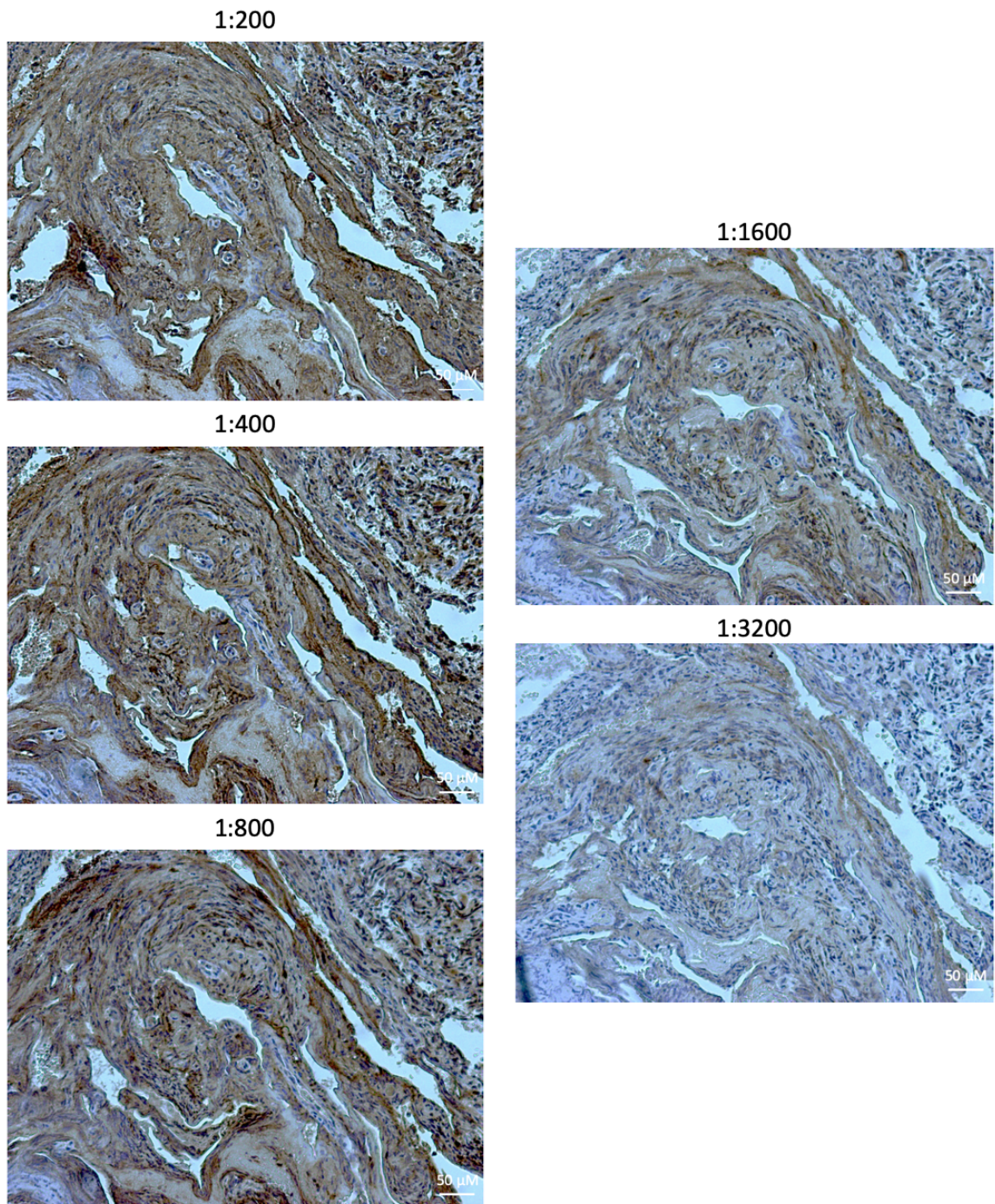


**Figure 5.2 Optimisation of immunopurified anti-CIZ1 antibody for IHC.** Sections were stained with antibody concentrations ranging from 1:50 to 1:3200. CIZ1 staining was visualised with DAB (brown) and sections were counterstained with haematoxylin (blue). Scale bars represented by black bars in bottom right of image (all images magnification 20x).

## 5.4 IHC analysis of patient-derived FFPE GBM tissue sections

The BTNW biobank at Preston Royal Hospital provided 20 FFPE patient tissue sections for IHC analysis, the use of these patient samples was ethically approved by the BTNW committee. All sections were derived from grade IV glioma (GBM) patients and were IDH 1/2 wild-type (Table 5.1). Sections were prepared to the point of paraffin removal and stained according to the procedure outlined in section 3.5. Each patient sample is associated with a 4-digit code which is referred to throughout.

**Table 5.1** List of tissue samples used in IHC analysis. Patient sample numbers, their diagnosis and IDH 1/2 mutational status are indicated.

BTNW no.	Diagnosis	IDH 1/2 status
2737	GBM	wt
2740	GBM	wt
2741	GBM	wt
2744	GBM	wt
2745	GBM	wt
2748	GBM	wt
2756	GBM	wt
2760	GBM	wt
2764	GBM	wt
2777	GBM	wt
2778	GBM	wt
2803	GBM	wt
2809	GBM	wt
2817	GBM	wt
2819	GBM	wt
2821	GBM	wt
2824	GBM	wt
2827	GBM	wt
2844	GBM	wt
2853	GBM	wt

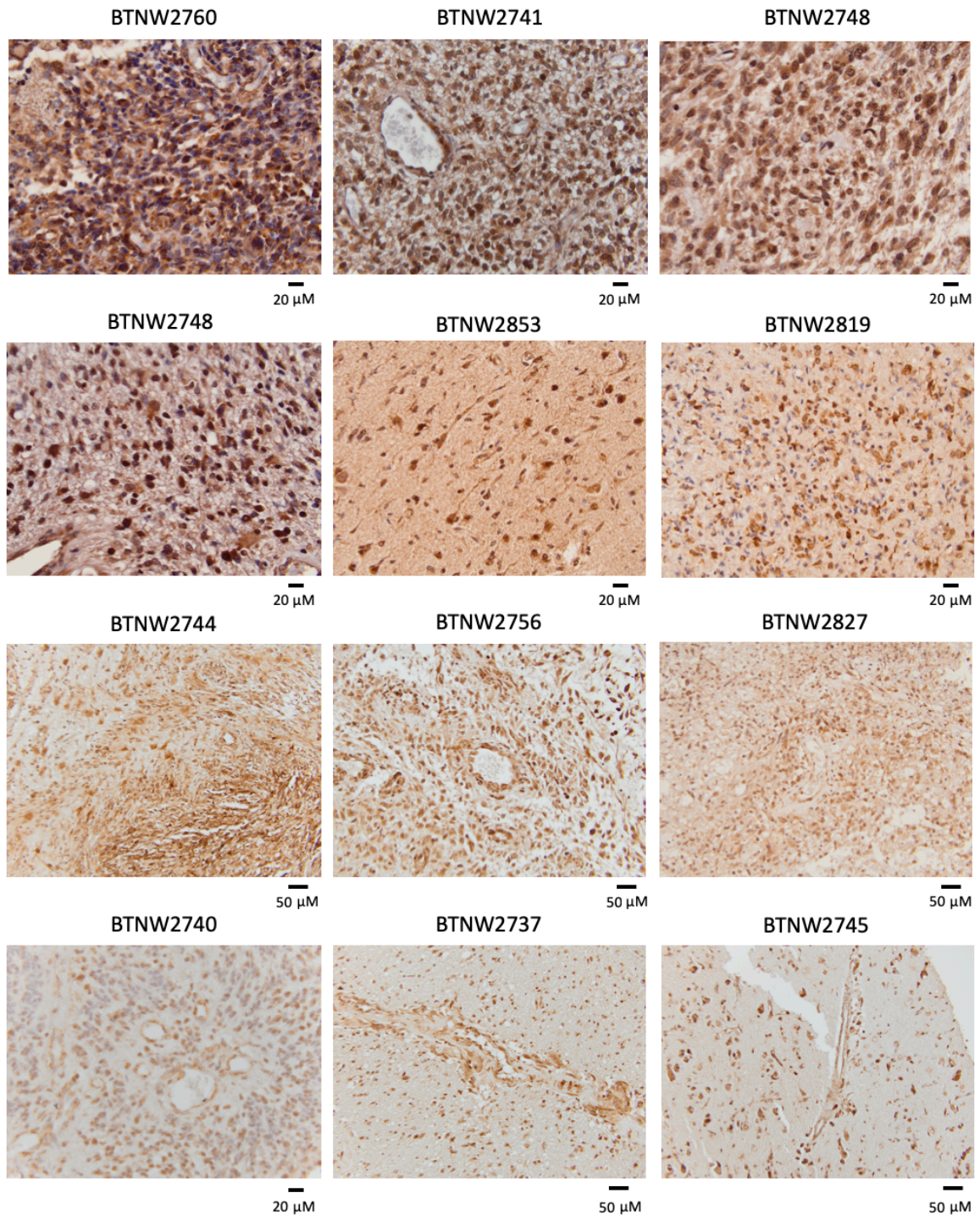


**Figure 5.3** IHC analysis of 12 patient-derived FFPE tissue sections from primary GBM patients. Sections were stained with DAB (brown) and nuclei counterstained with haematoxylin (blue). Scale bars represented by black bars in bottom right of image.

The panel of images captured in figure 5.3 demonstrates the range of CIZ1 staining across a number of patient samples, CIZ1 staining varies from high intensity to low intensity demonstrating the heterogeneity within these tumours. Although, common

features can be observed among the tumour samples such as consistent endothelial cell staining within blood vessels and mislocalisation of CIZ1 to the cytoplasm. This observation contrasts with studies which have used immunofluorescence or overexpression of GFP-CIZ1 to find CIZ1 to be a predominantly nuclear protein. This mislocalisation of CIZ1 may be an important feature for detection of dysregulated CIZ1 function in GBM, although the precise function, if any, has yet to be determined.

#### 5.4.1 Organisation of cells in the brain

Patient sample BTNW2853 portrays the organisation of cells within the brain and the weak staining of CIZ1 associated with neurons (Figure 5.4). Neurons in the cortex of the brain are organised vertically in columnar columns, a type of cellular patterning within the brain. These columns consist of pyramidal neurons running up towards the pial surface and the stacking of neurons within these columns aids in communication and processing of external information.

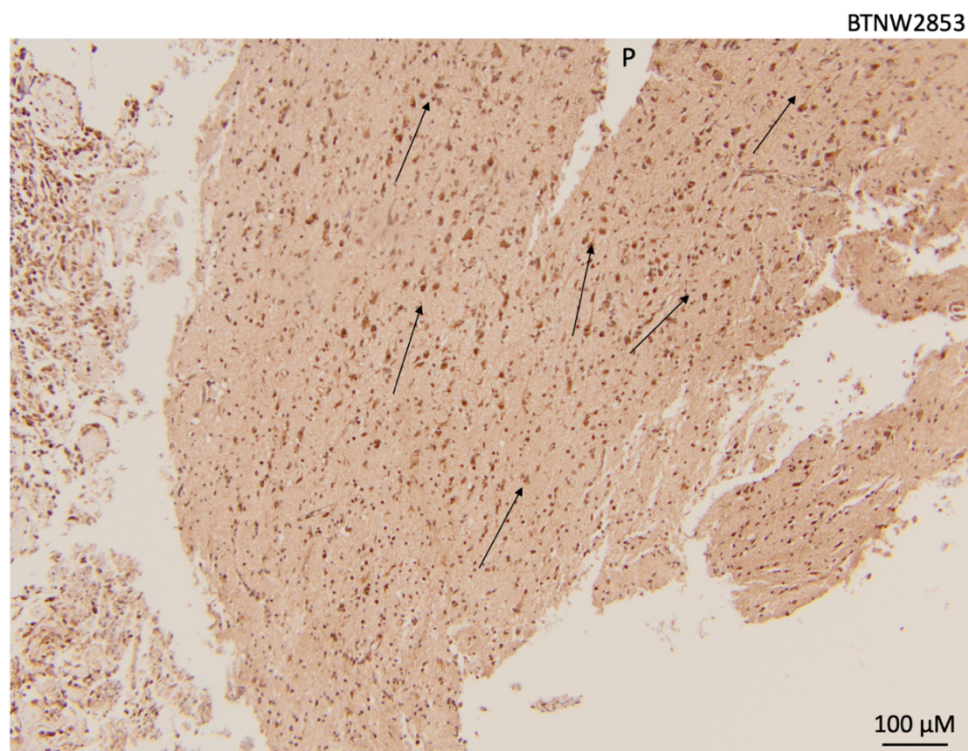


**Figure 5.4 Neuron structure within the brain cortex.** Neurons arranged in columns point up towards the pial surface (P) as indicated by the black arrows. Sections were stained with DAB (brown) and nuclei counterstained with haematoxylin (blue). Scale bars represented by black bars in bottom right of image (magnification 10x).

#### 5.4.2 Imaging of 'normal' regions identified CIZ1 staining in specific cell types

To allow for identification of abnormal staining patterns in tumour tissue, CIZ1 staining patterns of specific cell types in normal brain tissue were examined. Patient sample BTNW2745 demonstrates the staining patterns of CIZ1 in astrocytes and satellite oligodendrocytes, crucial cells for normal brain functioning. Astrocytes have many regulatory roles in brain functioning including providing a structural framework for neurons, regulating neuronal signalling, protecting neurons from oxidative damage and controlling the permeability of the BBB (Siracusa et al., 2019). Weak positive CIZ1 staining can be seen in the astrocytes indicated by the red arrows (Figure 5.5). Satellite oligodendrocytes associate with the cell bodies of pyramidal neurons in the neocortical layer, although their exact function is unknown, they are thought to be involved in the production and maintenance of myelin surrounding the processes of neurons within the CNS (Simons and Nave, 2015). Positive CIZ1 staining can be seen in the nucleus and nuclear periphery of the oligodendrocytes indicated by the black arrows (Figure 5.5).

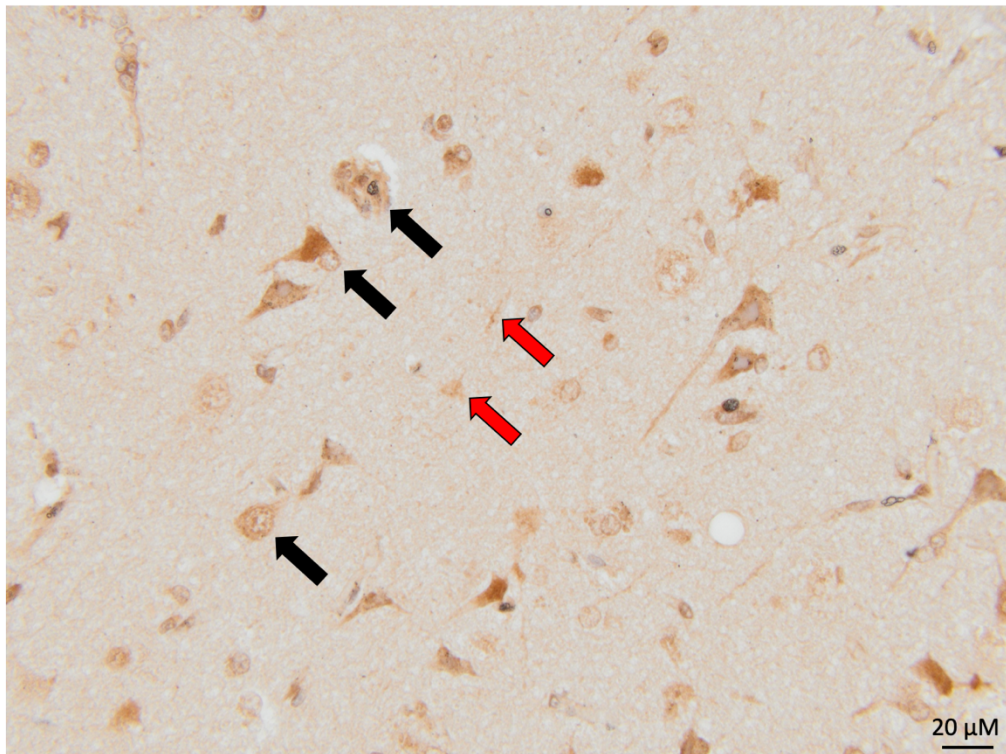


**Figure 5.5 CIZ1 staining patterns in specific cell types of normal brain tissue.** Astrocytes are indicated by the red arrows and satellite oligodendrocytes are indicated by the black arrows. Sections were stained with DAB (brown) and nuclei counterstained with haematoxylin (blue). Scale bars represented by black bars in bottom right of image (magnification 40x).

#### 5.4.3 CIZ1 staining patterns in normal tissue vs tumour tissue

Differential CIZ1 staining patterns were observed upon comparison of normal and tumour tissue. The lack of cells in patient samples BTNW2853 and BTNW2745 shows that this is relatively normal brain tissue, high levels of nuclear staining can be seen in the neurons indicated by the black arrows. Contrastingly, the cell density in tissue sections from BTNW2844 and BTNW2748 clearly indicates this is tumour tissue. Variable CIZ1 staining can be seen in both the nucleus and cytoplasm (Figure 5.6) demonstrating the mis-localisation of CIZ1 in tumour cells for reasons not yet established. However, some cytoplasmic staining is also visible in the relatively normal brain tissue, emphasising the need for further experiments to confirm these staining patterns. Alternatively, method optimisation may be required to increase the specificity of CIZ1 staining. These findings support previous *in vitro* data demonstrating

lower levels of CIZ1 in nuclear fractions compared to cytoplasmic fractions in the GBM cell lines BTNW914 and U87-MG (Falkingham, 2019).

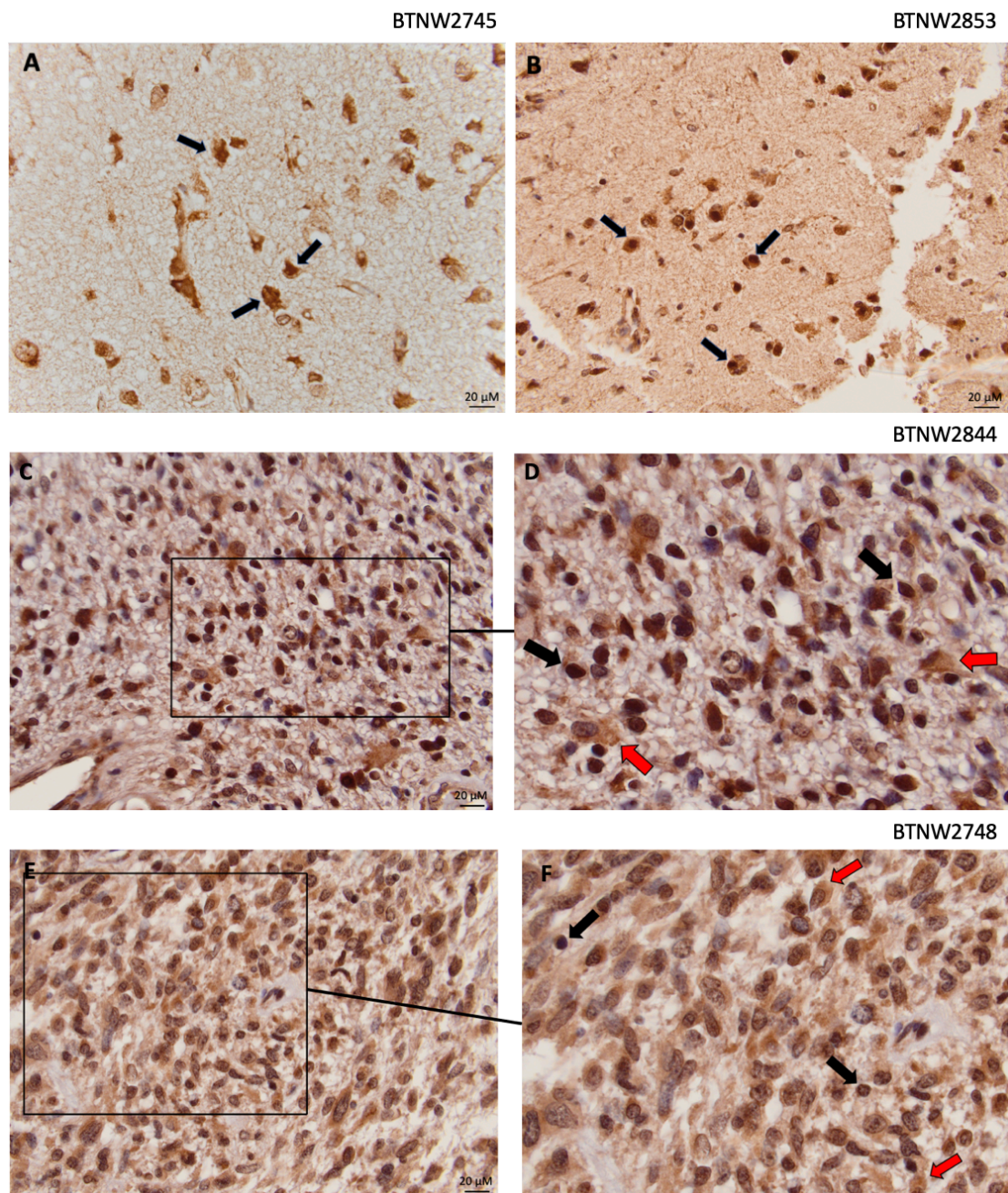


**Figure 5.6 Differential CIZ1 staining between healthy and tumour tissue. A and B)** Positive CIZ1 staining in the neurons indicated by the black arrows. **C, D, E and F)** Nuclear CIZ1 staining is indicated by the black arrows and cytoplasmic staining is indicated by the red arrows. Sections were stained with DAB (brown) and nuclei counterstained with haematoxylin (blue). Scale bars represented by black bars in bottom right of image (all images magnification 40x).

CIZ1 staining was observed in specific nuclear compartments of tumour cells. In patient sample BTNW2741, nuclear membrane and nucleolus staining can be seen in cells indicated by the black arrows. A fine stipple pattern of chromatin can also be seen running through the nucleus demonstrating the specificity of CIZ1 staining (Figure 5.7 A). Nuclear membrane and nuclear CIZ1 staining can also be seen in patient sample BTNW2748 indicated by the black arrows (Figure 5.7 B).

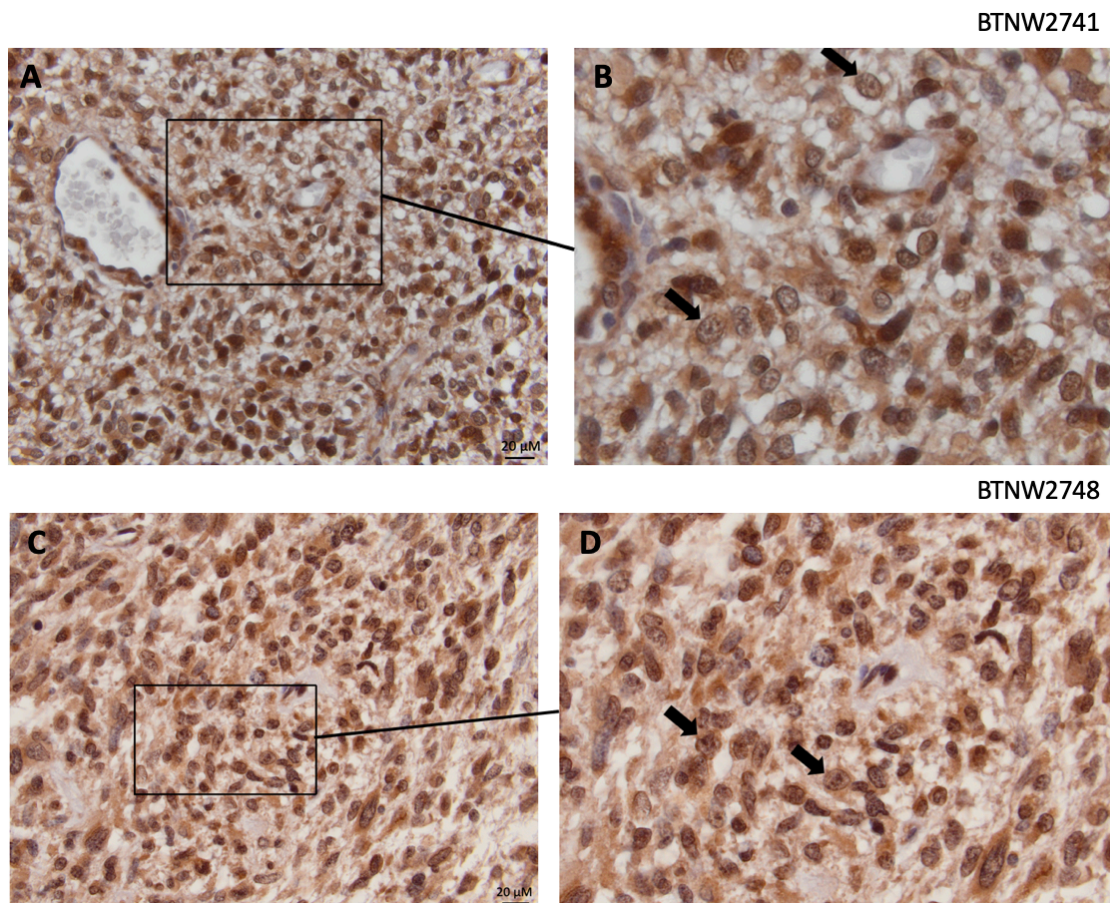


**Figure 5.7 CIZ1 staining in the nuclear compartments of tumour cells. A and B)** CIZ1 staining of chromatin within the nucleus of the cells indicated by the black arrows. **C and D)** CIZ1 staining of the nucleus and nuclear membrane in the cells indicated by the black arrows. Sections were stained with DAB (brown) and nuclei counterstained with haematoxylin (blue). Scale bars represented by black bars in bottom right of image (all images magnification 40x).

#### 5.4.4 Cancer morphology in GBM tissue

Tumour heterogeneity is a critical hallmark of GBM. Both intertumoural and intratumoural genetic, molecular and histopathological heterogeneity have been observed in GBM and are important in the development of prognostic and diagnostic

biomarkers, which in turn guide the development of personalised therapies. Intratumoural heterogeneity contributes to failure of targeted therapies and so there is an increasing need to further our understanding of the complex tumour microenvironment in GBM (Alves et al., 2011).

The region of patient sample BTNW2760 captured in figure 5.8 is highly cell dense indicating an aggressive tumour phenotype. Heterogeneity within the tumour microenvironment is demonstrated by the presence of actively dividing cells; a cell undergoing metaphase of mitosis can be seen (white arrow), together with cells which have undergone successive cell divisions and have subsequently dropped out of the growth fraction; a large post-mitotic cell can be seen which is likely to have undergone replicative or premature senescence (red arrow). Replicative senescence occurs when shortened telomeres prevent further successive cell division cycles as they would lead to chromosome erosion. Premature senescence occurs as a result of oxidative, genotoxic or replicative stresses. Senescent cells are morphologically characterised by an enlarged cytoplasm with increased granularity (Pawlowska et al., 2018). There is also differential CIZ1 staining in the nuclei of the cells within this region, some nuclei are stained blue whereas others appear darker suggesting heterogenous CIZ1 expression in tumour tissue.

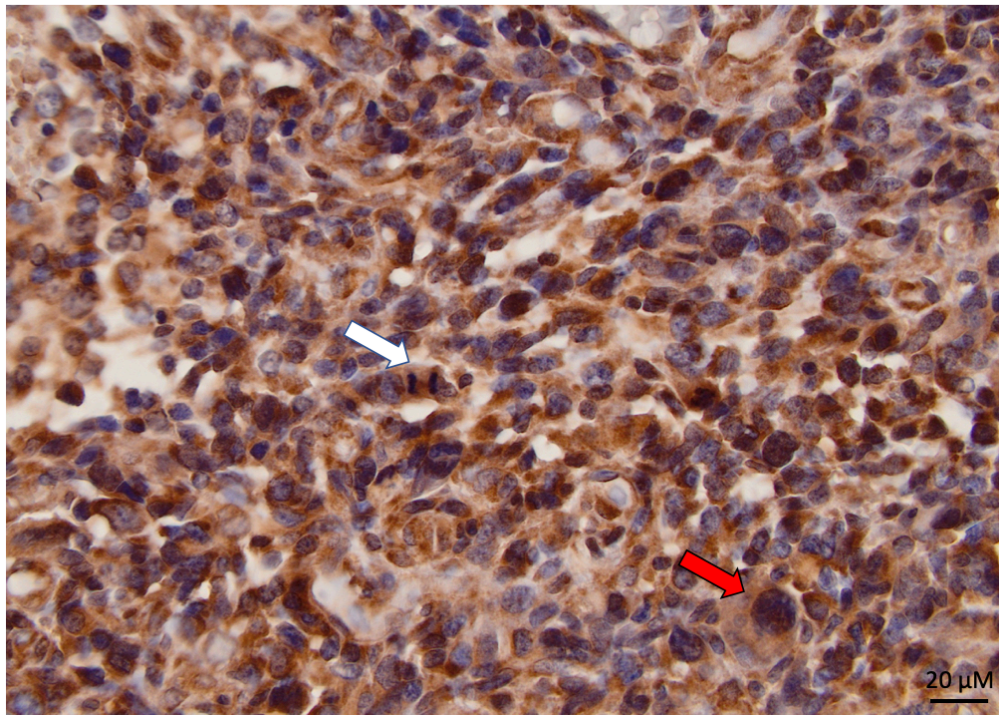


**Figure 5.8 Heterogeneity within the tumour microenvironment.** Actively dividing cells can be seen with a telophase cell indicated by the white arrow. A senescent cell is labelled with a red arrow. Sections were stained with DAB (brown) and nuclei counterstained with haematoxylin (blue). Scale bars represented by black bars in bottom right of image (magnification 40x).

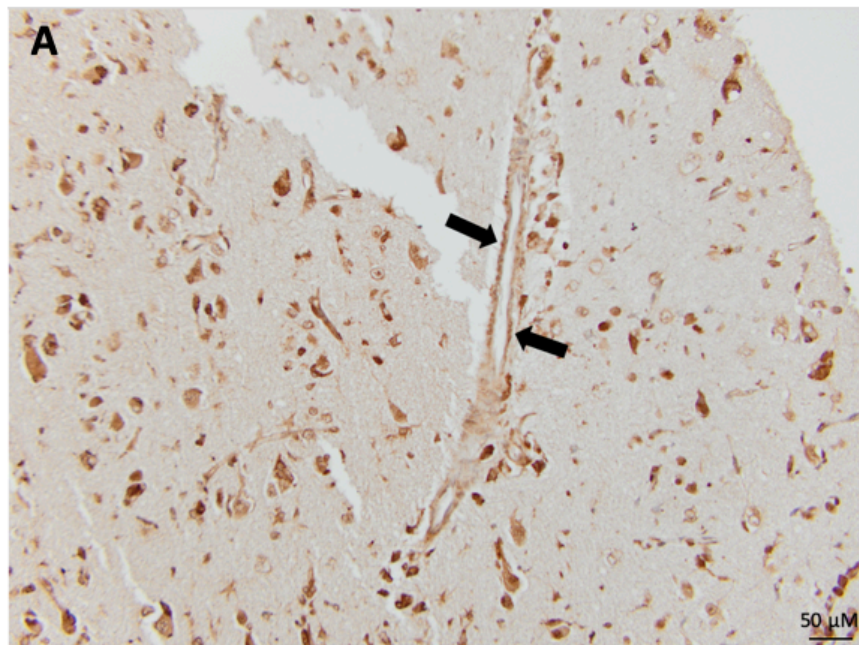
#### 5.4.5 Abnormalities in vasculature of tumour tissue

High degrees of vascularisation and vascular proliferation are key diagnostic indicators of GBM, characterised by enhanced expression of *VEGF* which promotes the growth of endothelial cells (Nicolas et al., 2019). In order to assess the staining patterns of endothelial cells in tumour tissue, the staining of blood vessels in relatively normal tissue within tissue sections and tumour tissue were compared.

Patient samples BTNW2745 and BTNW2737 show regions of tissue that are tumour proximal normal tissue based on the low cell density within these specific regions. In figure 5.9 A, a blood vessel can be seen with positive endothelial cell staining. The staining pattern of *CIZ1* in these cells appears to be localised to the nucleus as expected in normal tissue (Copeland et al., 2015). In figure 5.9 B, a blood vessel can be seen located in the leptomeninges, the innermost layers of tissue covering the surface

of the brain which consists of the arachnoid mater and pia mater. Again, the endothelial cells lining this blood vessel are stained positively for CIZ1 within the nucleus and their cellular structure is typical of the endothelial cells.

BTNW2745



BTNW2737

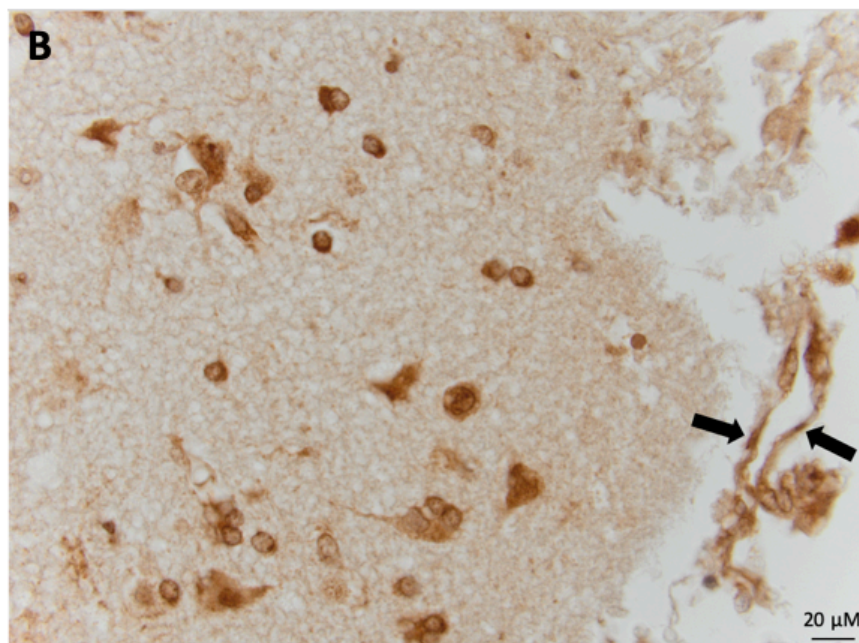


**Figure 5.9 Vasculature and endothelial cell staining in normal tissue.** Positive CIZ1 staining in endothelial cells is indicated by the black arrows. Sections were stained with DAB (brown) and nuclei counterstained with haematoxylin (blue). Scale bars represented by black bars in bottom right of image (A: magnification 20x, B: magnification 40x).

A number of tissue sections have been used to demonstrate the increased vascularisation in patient samples (Figure 5.10). In figure 5.10 A and B, large blood vessels can be seen with CIZ1 staining visible in the endothelial cells lining the vessels indicated by the black arrows. Smaller vessels can be seen in figure 5.10 C and D, again positive for nuclear CIZ1 staining in endothelial cells. As CIZ1 is thought to be involved in the initiation of DNA replication, this staining pattern may represent higher proliferative rates of endothelial cells. The red blood cells within the blood vessel lumen indicated by the red arrows are not stained demonstrating the specificity of CIZ1 staining.

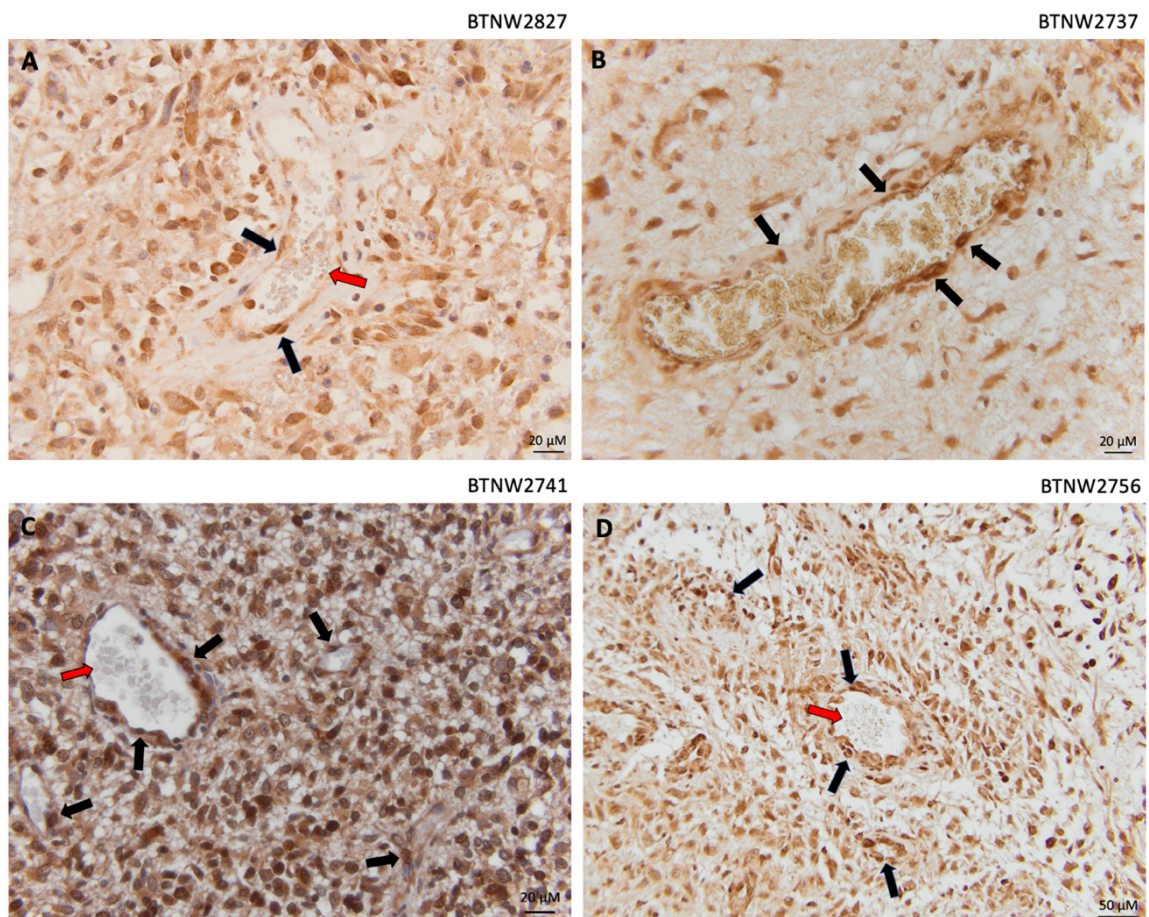
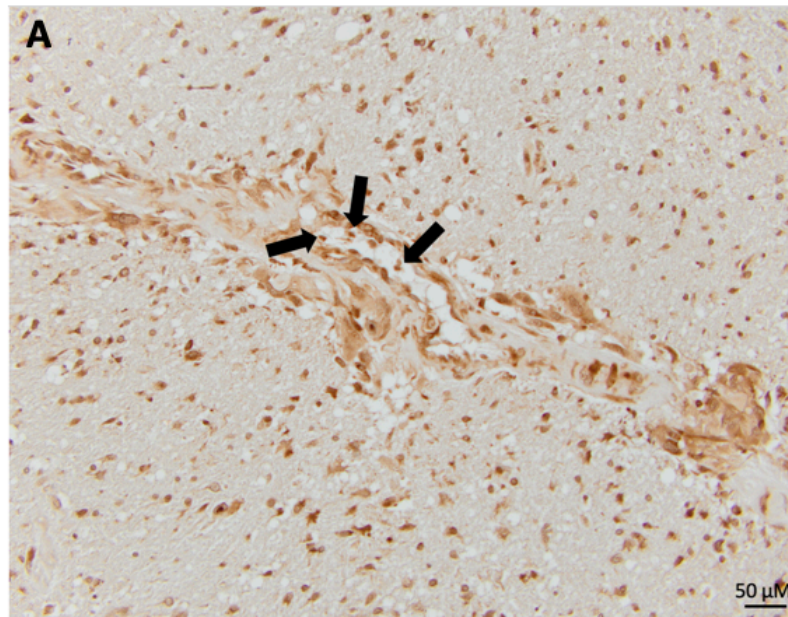


**Figure 5.10 Vascularisation and staining of endothelial cells.** Nuclear CIZ1 staining of endothelial cells indicated by the black arrows and unstained red blood cells indicated by the red arrows. Sections were stained with DAB (brown) and nuclei counterstained with haematoxylin (blue). Scale bars represented by black bars in bottom right of image (A,B and C: magnification 40x, D: magnification 20x).

An adequate blood supply is essential for normal brain functioning. To support tumour growth in GBM, the brain requires an increased supply of blood in ways such that the existing vascular morphology is compromised. Patient sample BTNW2737 (Figure 5.11 A) demonstrates the abnormality of endothelial cells within blood vessels of tumour tissue. The endothelial cells indicated by the black arrows can be seen protruding into the lumen of the blood vessel generating turbulent blood flow, an abnormal behavior of endothelial cells.

BTNW2737



BTNW2740

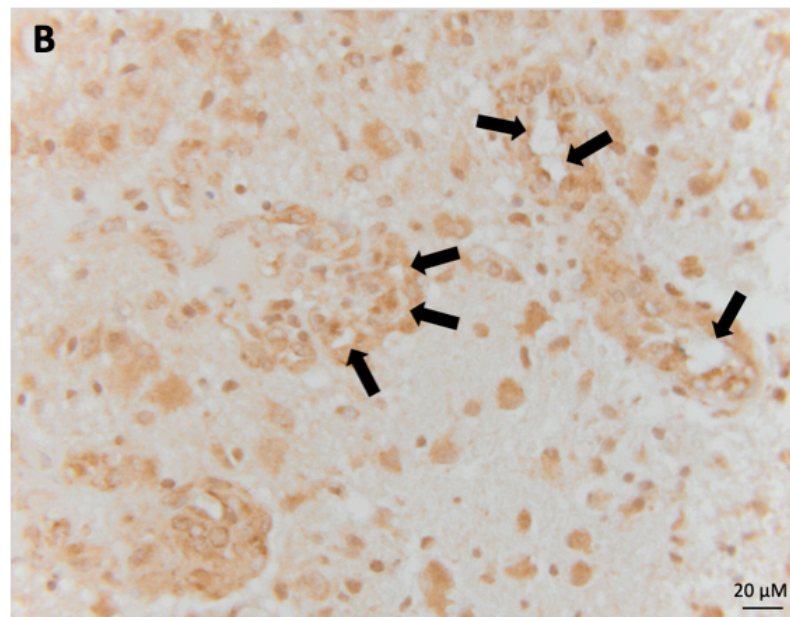


**Figure 5.11 Morphology of vasculature in tumour tissue. A and B)** Nuclear CI21 staining can be seen in the endothelial cells indicated by the black arrows. Sections were stained with DAB (brown) and nuclei counterstained with haematoxylin (blue). Scale bars represented by black bars in bottom right of image (A: magnification 20x, B: magnification 40x).

In tissue section BTNW2740 (Figure 5.11 B) multiple regions of neovascularisation are present, a key hallmark of GBM. Neovascularisation is associated with the formation of glomeruloid bodies, tufts of blood vessels with multiple vessel lumens (black arrows) which resemble a renal glomerulus. These blood vessels are comprised of a

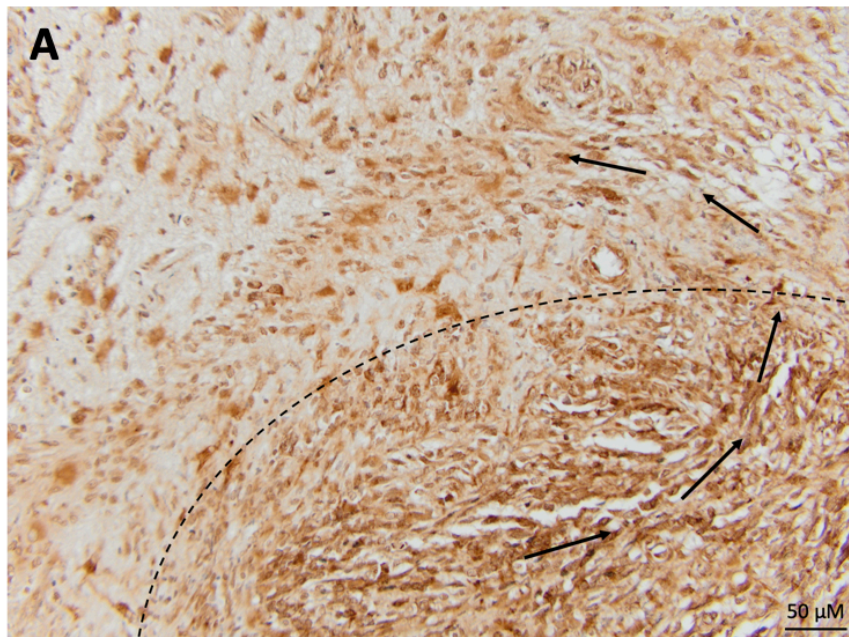
proliferative mass of hyperplastic endothelial cells surrounded by a basal laminar and layer of pericytes. Although increased vascularisation is a characteristic associated with tumour progression, the efficiency of blood vessels can often be poor forming blind ends and loop circuits.

#### 5.4.6 Migration and invasion

Diffuse gliomas are characterised by the diffuse infiltrative growth of tumour cells in the neuropil, a network of neuronal and glial cell processes. GBM is the most aggressive of the gliomas and its topographic diffuse nature means tumour cells often detach from the tumour mass and migrate into adjacent normal tissue, rendering surgical resection ineffective at removing the whole tumour mass without disturbing surrounding normal tissue. The arrangement of infiltrative tumour cells along the pre-existent parenchyma is useful in the diagnosis of diffuse glioma (Wesseling et al., 2011). Patient sample BTNW2744 demonstrates an invasive front of tumour where a tumour cell gradient can be seen in the infiltrative region. Tumour cells can be observed migrating towards and invading surrounding tissue either as single cells or in clusters (Figure 5.12 A). Importantly, the intensity of CIZ1 staining is increased in the tumour tissue compared to the adjacent normal tissue suggesting CIZ1 is overexpressed in GBM cells, however further analysis of the tumour intersection using an expanded cohort of patient samples is required.

Patient sample BTNW2853 provides an example of a tumour infiltrative edge at an increased magnification to show the migration of tumour cells towards normal tissue structures (black arrows), satellite oligodendrocytes in the pre-existing parenchyma can also be seen within this infiltrated region (red arrows) (Figure 5.12 B)

BTNW2744



BTNW2853

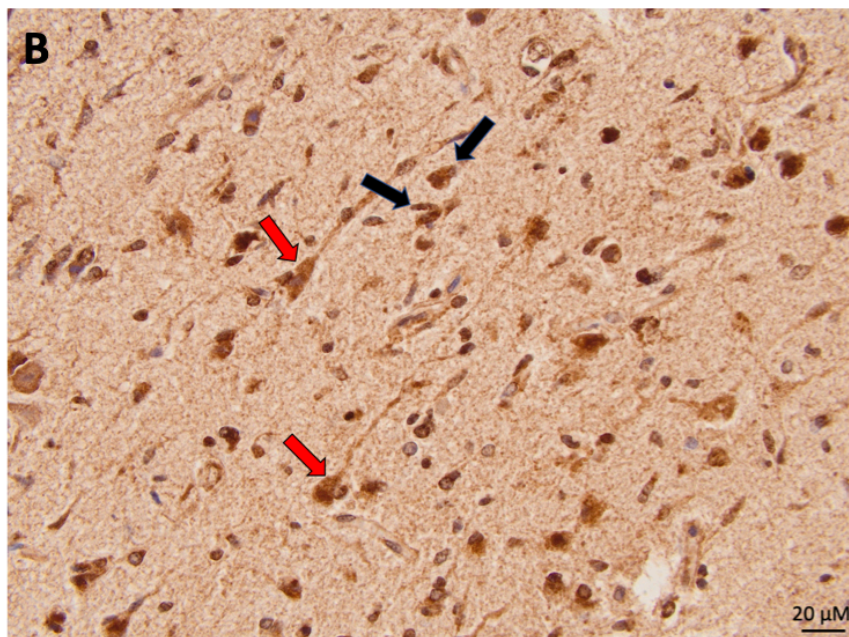


**Figure 5.12 Infiltrating edge of tumour.** **A)** Advancing front of tumour. The tumour margin is indicated by the black line and the direction of travel by tumour cell clusters indicated by the black arrows. **B)** Diffuse infiltrating tumour cells observed migrating towards normal tissue (black arrows). Satellite oligodendrocytes can also be seen (red arrows). Sections were stained with DAB (brown) and nuclei counterstained with haematoxylin (blue). Scale bars represented by black bars in bottom right of image (A: magnification 20x, B: magnification 40x).

Patient sample BTNW2756 is an example of leptomeningeal metastasis, whereby the tumour has migrated along the brain surface and invaded the leptomeninges. This metastatic spread is confirmed by the abnormality of blood vessels within the leptomeninges, the nuclei of endothelial cells can be seen protruding into the lumen of the vessel (Figure 5.13 A). Tumour cells can also be seen migrating along the pia mater, the innermost layer of the brain surface (Figure 5.13 A, B). A pial vessel can be seen infiltrating the pia mater and protruding into the tumour (Figure 5.13 C).

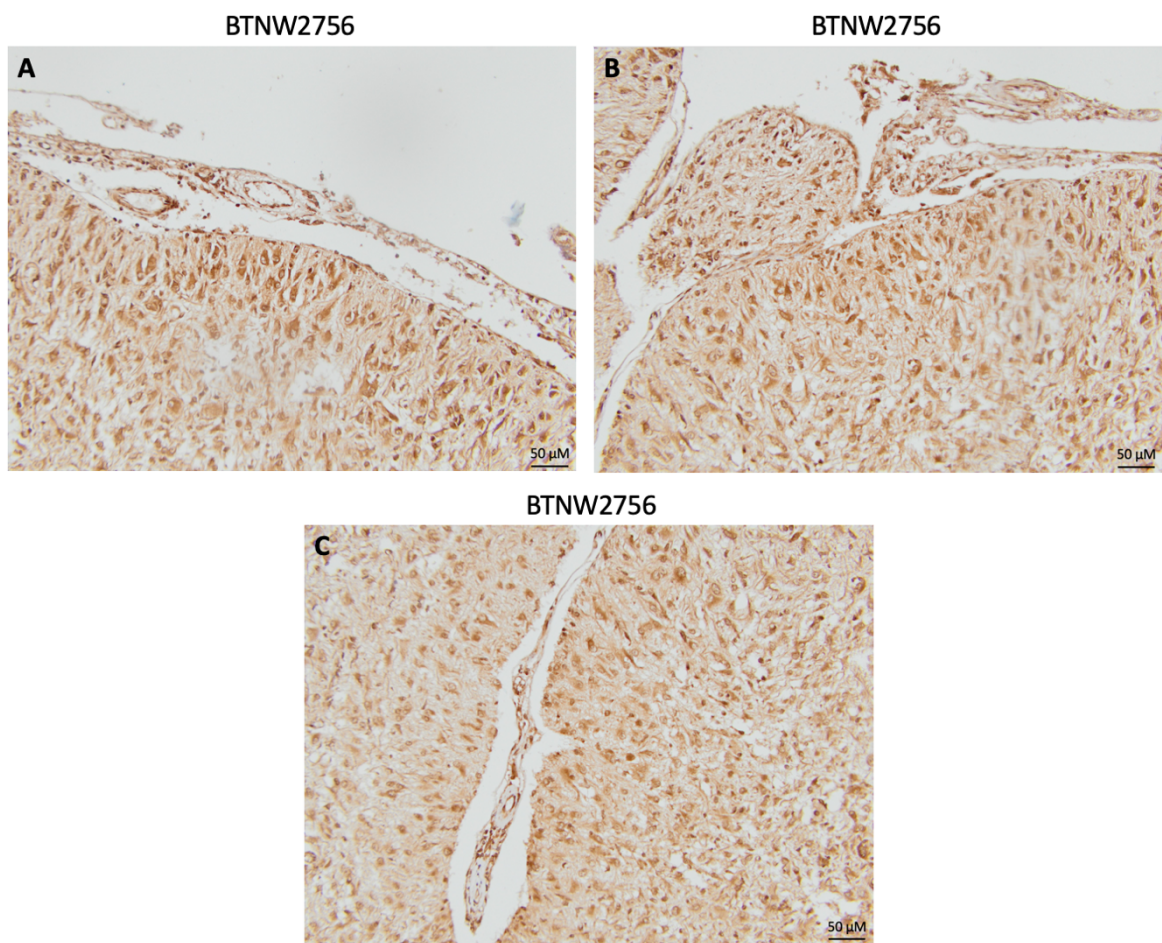


**Figure 5.13 Migration and invasion of tumour cells along the brain surface.** Sections were stained with DAB (brown) and nuclei counterstained with haematoxylin (blue). Scale bars represented by black bars in bottom right of image (all images magnification 20x).

## 5.5 Chapter discussion

### 5.5.1 Validity of CIZ1 as a biomarker in GBM

The discovery of a marker to provide diagnostic and prognostic information in GBM is of increased importance. CIZ1 is currently used as a diagnostic biomarker in lung cancer, the overexpression of the CIZ1 b-variant is specific to tumour cells and can be detected in the circulation of SCLC and NSCLC patients (Higgins et al., 2012), validating CIZ1 as a circulating biomarker in these tumours. The use of CIZ1 as a biomarker in GBM shows potential as it can be used to distinguish between healthy and tumour tissue. However, IHC can only be performed via histopathological examination of resected tumour tissue, which is highly invasive and will not be performed without confirmed presence of a tumour.

The results demonstrate that the CIZ1-N471 antibody stains with the highest intensity in tumour regions allowing us to distinguish between normal and tumour tissue. The panel of tissue sections in figure 5.3 shows clear variation in the intensity of CIZ1 staining across the different patient samples indicating heterogenous expression of CIZ1 within GBM tumours. There is also consistent nuclear staining of normal cells such as endothelial cells where blood vessels are visible, possibly due to the upregulation of *VEGF* expression promoting increased proliferation of the endothelial cells.

The mislocalisation of CIZ1 from the nuclear matrix to the cytoplasm was a common feature observed across all of the patient samples and could be important in the diagnosis and pathogenesis of GBM. CIZ1 predominantly resides in nuclear foci confirmed by *in vitro* studies in both murine and human cell lines, CIZ1 localisation also remains nuclear when expressed ectopically (Ainscough et al., 2007; Copeland et al., 2010; Copeland et al., 2015; Coverley et al., 2005). The genomic instability in cancer cells can lead to the subcellular mislocalisation of proteins which can in turn develop into one of the hallmarks of cancer. The mislocalisation of tumour suppressor proteins, oncoproteins and other cancer-associated proteins can promote tumour development and metastasis or increase resistance to drugs. Therefore the mechanisms underlying

aberrant subcellular localisation of CIZ1 and how this affects protein function could be of relevance in the development of novel diagnostic and therapeutic approaches (Wang and Li, 2014). The tumour suppressor Rb is often mislocalised from the nucleus to the cytoplasm in cancer due to CDK phosphorylation-dependant nuclear export resulting in the loss of Rb's tumour suppressor function (Jiao et al., 2008). Therefore, if CIZ1 possesses both oncogenic and tumour suppressor functions, it should be considered whether the mislocalisation of CIZ1 observed in GBM is associated with tumour growth. Furthermore, if the mislocalisation of CIZ1 to the cytoplasm is specific to cancer cells, there is potential for use of CIZ1 as a diagnostic indicator and for the development of targeted therapies.

There is some evidence to suggest that p21<sup>Cip1/Waf1</sup> is responsible for the mislocalisation of CIZ1 to the cytoplasm. Co-expression of CIZ1 and p21<sup>Cip1/Waf1</sup> resulted in cytoplasmic distribution of p21<sup>Cip1/Waf1</sup> although the precise mechanism behind this co-localisation is yet to be determined (Mitsui et al., 1999). P21<sup>Cip1/Waf1</sup> does not solely act as a tumour suppressor but also as an oncogene. When p21<sup>Cip1/Waf1</sup> is localised in the cytoplasm, it is able to regulate migration, apoptosis, and proliferation which correlates with a poor prognosis in a number of tumours including breast, prostate and brain (Romanov et al., 2012). Although there is little evidence to suggest a common overexpression of p21<sup>Cip1/Waf1</sup> in GBM, one study demonstrated that p21<sup>Cip1/Waf1</sup> knockout considerably decreased PDGF-induced formation of gliomas identifying a potential role of p21<sup>Cip1/Waf1</sup> and CIZ1 in the pathogenesis of these tumours (Liu et al., 2007).

CIZ1 staining allowed for identification of migration and invasion, possibly implying more aggressive tumour phenotypes. CIZ1 staining patterns were able to enhance the visualisation of advancing fronts and infiltrating edges demonstrating tumour progression in certain patient samples (Figure 5.12, Figure 5.13). GBM is characterised by diffuse infiltrative growth, while CIZ1 is capable of identifying this invasive nature, other tools are already in practice to identify these features including simple haematoxylin and eosin (H&E) staining.

CIZ1 staining was also able to identify leptomeningeal spread (LMS) in one of the patient samples. Leptomeningeal metastasis of GBM was first described in 1931 and is the spread of tumour cells from pre-existing brain parenchyma to the leptomeninges and CSF (Alatakis et al., 2001). Leptomeningeal spread is associated with tumour aggressiveness and poses severe complications in terms of diagnosis and treatment. Upon diagnosis of LMS, survival rates vary from 2 to 5 months. However, the low sensitivity of MRI technology and cytological analysis of CSF obtained from a lumbar puncture often fails to detect LMS. One study estimated the incidence rate of symptomatic LMS at 2% (Vertosick Jr and Selker, 1990) however this is likely to be underestimated due to undiagnosed and asymptomatic cases. Autopsy studies estimated an LMS rate of 25% in high-grade glioma patients emphasising the need for more reliable diagnostic tools. There is currently no standard of care treatment for LMS and diagnosis is considered as an untreatable end stage complication. Intrathecal chemotherapeutics and radiotherapy have been shown to improve median survival from 4-6 weeks to 3-6 months however further investigation is needed (Birzu et al., 2020).

The pathogenesis of LMS remains poorly understood. GBM cells migrate from the tumour site along blood vessels and into the subpial, subarachnoid and subependymal spaces. Invasion of the subpial space is an intermediate step during leptomeningeal metastasis. During this migration, tumour cells secrete proteases to degrade the ECM including MMP-1, MMP-2 and MMP-9 and adhesion-migration proteins such as fibronectin, integrins and glycosylated chondroitin sulfate proteoglycans. These proteins work closely with the cytoskeleton to guide the migration of cells towards the CSF and leptomeninges (Birzu et al., 2020). In a mouse model of GBM, prolonged inhibition of VEGF with bevacizumab resulted in conversion of tumour cell phenotype to invasive/mesenchymal and subsequent invasion via perivascular and subpial spaces (de Groot et al., 2010).

## Chapter 6: General discussion

The use of small molecule kinase inhibitors in cancer therapy has shown to be effective in a number of tumour types (Cao et al., 2020; Haas-Kogan et al., 2005; Jo et al., 2012). This approach was extended to assess the effectiveness of these small molecule inhibitors in GBM. The use of CDK and DDK inhibitors in the GBM cell lines U87-MG and BTNW914 showed some efficacy in the reduction of CIZ1 protein levels and proliferation *in vitro*, although no significant effects were found demonstrating the resistance of these cell lines to kinase inhibition. Furthermore, the effects of CDK and DDK inhibition may be enhanced when used in combination with chemotherapeutic agents and warrants further investigation. The use of CDK and DDK inhibitors to investigate the role of CIZ1 within the cell cycle has limitations due to the off-target activity of kinase inhibitors. This means any findings cannot solely be attributed to the activity of CIZ1 and alternative pathways are likely to contribute to any observed effects. Due to the ambiguous specificity and selectivity of CDKs and DDKs, further work is needed into the mechanisms by which these kinase inhibitors suppress the growth of tumour cells in order to identify the most relevant CDKs in particular tumour types.

Gene knockout studies didn't appear to effect CIZ1 levels despite downstream effects on proliferation and cell cycle progression demonstrating the need for a more robust and accurate method of gene knockout, possibly implementing a CRISPR-Cas9 system. The model implying CIZ1 regulation by opposing activities of CDK and DDKs and the UPS is supported in the data presented. With previous work identifying the three putative E3 ligases involved in CIZ1 degradation, future work should investigate the manipulation of these UPS components to disrupt CIZ1 regulation and determine the downstream effects on cell growth in this tumour type.

With *in vitro* work supporting the use of kinase inhibitors in GBM, this approach should be extended to more representative *in vitro* models such as 3D spheroids; co-cultures containing microglial, endothelial and GBM cells. These models provide a better

understanding of drug behaviour within the complex tumour microenvironment and provide the opportunity to perform chronic dosing studies allowing for long-term monitoring of drug treatments. Future work should also include migration and invasion studies to determine the effects of kinase inhibition on the invasive potential of GBM cells, a key hallmark of progression in these tumours.

Despite the effects of CDK and DDK inhibition not previously being investigated in the NSCLC cell line A549, this was the only cell line to show significant reductions in CIZ1 levels and proliferative rates across all of the kinase inhibitors, showing promising potential for the use of these inhibitors as anti-cancer agents, prompting the need for further research into this cancer type.

The expression profile of CIZ1 in high-grade gliomas is yet to be investigated. This work provides insight into the expression of CIZ1 in the grade IV glioma GBM, the most aggressive and malignant of the gliomas. The poor prognosis of GBM tumours encourages the need for further research into the discovery and development of a robust biomarker for early detection to ultimately improve patient outcome.

Similarly to some types of lung cancer, CIZ1 could potentially be used as a circulating biomarker in GBM. The use of CIZ1 as a circulating biomarker presents difficulties due to the BBB, although the aggressive nature of GBM can in some cases cause disruption to the BBB releasing tumour cells into the circulation (Dubois et al., 2014). Detection of CTCs would be beneficial as they can potentially provide information on the tumour prior to clinical progression. Very few studies have detected brain tumour-derived CTCs in GBM due to the technical difficulties associated with isolating CTCs and the rarity of these cells within the circulation. Detection rates spanned from 20-77% dependant on the method of isolation used. In 2014, MacArthur et al. were the first group to detect CTCs in the peripheral blood of GBM patients. Using an adenoviral detection system, a telomerase promoter-based assay was able to detect CTCs based on the elevated expression of telomerase in nearly all tumour cells but not in normal cells (MacArthur et al., 2014). Prospective larger studies are required to assess the reproducibility of these findings. In conclusion, there is an increasing need for more

robust methods of sampling and detection of tumour activity for effective and reliable information on disease prognosis and to monitor patient response to treatment.

The validity of CIZ1 as a biomarker in GBM remains unclear and requires further investigation. Histopathological analysis clearly demonstrates the overexpression and aberrant subcellular localisation of CIZ1 in tumour tissue. As GBM is a highly proliferative tumour, does the increased expression of CIZ1 simply reflect increased proliferative rates due to its role in the initiation of DNA replication or are there other contributing factors. Although no quantitative analysis of CIZ1 expression was performed, IHC analysis has provided a basis for further work into the expression profile of CIZ1 in GBM at the transcriptional level and methodologies to reduce CIZ1 levels and determine the effects on tumour growth. Furthermore, the expression profile of CIZ1 in GBM and lower-grade gliomas should be compared to determine whether overexpression of CIZ1 is specific to GBM or is widespread across the gliomas.

## 6.1 Future perspectives

In order to gain a deeper understanding of the expression profile of CIZ1 in GBM, there is a need for information on the clinical history of tissue donors, we are aware that the patient samples are derived from primary GBM patients and are IDH1/2 wild-type. However, comparison with other tumour subtypes and prognosis would allow us to draw correlations between CIZ1 expression and patient survival. Data surrounding patient prognosis, including the age and sex of each patient, would also be useful to assess the value of CIZ1 as a prognostic marker. Tissue microarray analysis of patient-derived tissue sections confirmed CIZ1 was significantly overexpressed in colorectal cancer patients and this was associated with poor OS (Wang et al., 2014). We could adopt this approach in attempt to correlate CIZ1 overexpression with patient survival in GBM.

The data presented implies CIZ1 is overexpressed in tumour tissue compared to adjacent normal tissue although only a limited number of patient samples demonstrated this. An expanded cohort of patient samples where the tumour

intersection is visible are required to confirm the overexpression of CIZ1 in tumour tissue. Furthermore, this data should be accompanied by RNA sequencing analysis to confirm increased CIZ1 expression at the transcript level and determine any statistical significance.

Intratumoural heterogeneity is a key hallmark of GBM and was observed across the majority of patient samples. Interestingly, CIZ1 staining patterns varied amongst tumour cells within the same regions of tumour tissue. One of the heterogenous features of GBM is the presence of multiple subtype signatures being expressed across individual cells within a tumour (Patel et al., 2014) and therefore GBM classification could be linked to CIZ1 expression; using a panel of representative tumour samples for each of the 4 classifications and repeating the analysis for IDH1/2 WT patients as performed here would allow for insight into the expression profile of CIZ1 across the different GBM subtypes.

## Chapter 7: References

- Ahmadipour, Y., Gembruch, O., Pierscianek, D., Sure, U. & Jabbarli, R. (2020) Does the expression of glial fibrillary acid protein (GFAP) stain in glioblastoma tissue have a prognostic impact on survival? *Neurochirurgie*, 66(3), 150-154.
- Ainscough, J. F. X., Rahman, F. A., Sercombe, H., Sedo, A., Gerlach, B. & Coverley, D. (2007) C-terminal domains deliver the DNA replication factor Ciz1 to the nuclear matrix. *Journal of Cell Science*, 120(1), 115.
- Alatakis, S., Malham, G. M. & Thien, C. (2001) Spinal leptomeningeal metastasis from cerebral glioblastoma multiforme presenting with radicular pain: Case report and literature review. *Surgical Neurology*, 56(1), 33-37.
- Alcantara Llaguno, S., Chen, J., Kwon, C.-H., Jackson, E. L., Li, Y., Burns, D. K., Alvarez-Buylla, A. & Parada, L. F. (2009) Malignant astrocytomas originate from neural stem/progenitor cells in a somatic tumor suppressor mouse model. *Cancer cell*, 15(1), 45-56.
- Aldape, K., Zadeh, G., Mansouri, S., Reifenberger, G. & Von Deimling, A. (2015) Glioblastoma: pathology, molecular mechanisms and markers. *Acta Neuropathologica*, 129(6), 829-848.
- Alifieris, C. & Trafalis, D. T. (2015) Glioblastoma multiforme: Pathogenesis and treatment. *Pharmacology & Therapeutics*, 152, 63-82.
- Alver, R. C., Chadha, G. S., Gillespie, P. J. & Blow, J. J. (2017) Reversal of DDK-mediated MCM phosphorylation by Rif1-PP1 regulates replication initiation and replisome stability independently of ATR/Chk1. *Cell reports*, 18(10), 2508-2520.
- Alves, T. R., Lima, F. R. S., Kahn, S. A., Lobo, D., Dubois, L. G. F., Soletti, R., Borges, H. & Neto, V. M. (2011) Glioblastoma cells: A heterogeneous and fatal tumor interacting with the parenchyma. *Life Sciences*, 89(15), 532-539.
- Arnedos, M., Bayar, M. A., Cheaib, B., Scott, V., Bouakka, I., Valent, A., Adam, J., Leroux-Kozal, V., Marty, V., Rapinat, A., Mazouni, C., Sarfati, B., Bieche, I., Balleyguier, C., Gentien, D., Delalogue, S., Lacroix-Triki, M., Michiels, S. & Andre, F. (2018) Modulation of Rb phosphorylation and antiproliferative response to palbociclib: the preoperative-palbociclib (POP) randomized clinical trial. *Annals of Oncology*, 29(8), 1755-1762.
- Arnoult, N., Schluth-Bolard, C., Letessier, A., Drascovic, I., Bouarich-Bourimi, R., Campisi, J., Kim, S.-H., Boussouar, A., Ottaviani, A., Magdinier, F., Gilson, E. & Londoño-Vallejo, A. (2010) Replication timing of human telomeres is chromosome arm-specific, influenced by subtelomeric structures and connected to nuclear localization. *PLoS genetics*, 6(4), e1000920-e1000920.
- Balss, J., Meyer, J., Mueller, W., Korshunov, A., Hartmann, C. & Von Deimling, A. (2008) Analysis of the IDH1 codon 132 mutation in brain tumors. *Acta Neuropathologica*, 116(6), 597-602.
- Banerjee, S., Crouse, N. R., Emnett, R. J., Gianino, S. M. & Gutmann, D. H. (2011) Neurofibromatosis-1 regulates mTOR-mediated astrocyte growth and glioma formation in a TSC/Rheb-independent manner. *Proceedings of the National Academy of Sciences*, 108(38), 15996.
- Baris, Y., Taylor, M. R. G., Aria, V. and Yeeles, J. T. P. (2022) 'Fast and efficient DNA replication with purified human proteins', *Nature*, 606(7912), 204-210.

- Barton, K. L., Misuraca, K., Cordero, F., Dobrikova, E., Min, H. D., Gromeier, M., Kirsch, D. G. & Becher, O. J. (2013) PD-0332991, a CDK4/6 inhibitor, significantly prolongs survival in a genetically engineered mouse model of brainstem glioma. *PLoS one*, 8(10), e77639-e77639.
- Bassermann, F., Eichner, R. & Pagano, M. (2014) The ubiquitin proteasome system — Implications for cell cycle control and the targeted treatment of cancer. *Biochimica et Biophysica Acta (BBA) - Molecular Cell Research*, 1843(1), 150-162.
- Bhagavan, N. V. & Ha, C.-E. (2015) Chapter 22 - DNA Replication, Repair, and Mutagenesis. In: Bhagavan, N. V. & Ha, C.-E. (eds.) *Essentials of Medical Biochemistry (Second Edition)*. San Diego: Academic Press.
- Birzu, C., Tran, S., Bielle, F., Touat, M., Mokhtari, K., Younan, N., Psimaras, D., Hoang-Xuan, K., Sanson, M., Delattre, J.-Y. & Idhahbi, A. (2020) Leptomeningeal Spread in Glioblastoma: Diagnostic and Therapeutic Challenges. *The oncologist*, 25(11), e1763-e1776.
- Bleichert, F., Botchan, M. R. & Berger, J. M. (2015) Crystal structure of the eukaryotic origin recognition complex. *Nature*, 519(7543), 321-326.
- Breen, M. E. & Soellner, M. B. (2015) Small molecule substrate phosphorylation site inhibitors of protein kinases: approaches and challenges. *ACS chemical biology*, 10(1), 175-189.
- Brooks, E. E., Gray, N. S., Joly, A., Kerwar, S. S., Lum, R., Mackman, R. L., Norman, T. C., Rosete, J., Rowe, M., Schow, S. R., Schultz, P. G., Wang, X., Wick, M. M. & Shiffman, D. (1997) CVT-313, a Specific and Potent Inhibitor of CDK2 That Prevents Neointimal Proliferation \*. *Journal of Biological Chemistry*, 272(46), 29207-29211.
- Brown, N. R., Korolchuk, S., Martin, M. P., Stanley, W. A., Moukhametzianov, R., Noble, M. E. M. & Endicott, J. A. (2015) CDK1 structures reveal conserved and unique features of the essential cell cycle CDK. *Nature Communications*, 6(1), 6769.
- Burgers, P. M. J. & Kunkel, T. A. (2017) Eukaryotic DNA Replication Fork. *Annual Review of Biochemistry*, 86(1), 417-438.
- Cabrini, G., Fabbri, E., Lo Nigro, C., Dechecchi, M. C. & Gambari, R. (2015) Regulation of expression of O6-methylguanine-DNA methyltransferase and the treatment of glioblastoma (Review). *International journal of oncology*, 47(2), 417-428.
- Caine, E. A., Mahan, S. D., Johnson, R. L., Nieman, A. N., Lam, N., Warren, C. R., Riching, K. M., Urh, M. and Daniels, D. L. (2020) Targeted protein degradation phenotypic studies using HaloTag CRISPR/Cas9 endogenous tagging coupled with HaloPROTAC3. *Current Protocols in Pharmacology*, 91(1), e81.
- Cancer Genome Atlas Research, N. (2008) Comprehensive genomic characterization defines human glioblastoma genes and core pathways. *Nature*, 455(7216), 1061-1068.
- Cantanhede, I. G. & De Oliveira, J. R. M. (2017) PDGF Family Expression in Glioblastoma Multiforme: Data Compilation from Ivy Glioblastoma Atlas Project Database. *Scientific Reports*, 7(1), 15271.
- Cao, Y., Li, X., Kong, S., Shang, S. & Qi, Y. (2020) CDK4/6 inhibition suppresses tumour growth and enhances the effect of temozolomide in glioma cells. *Journal of Cellular and Molecular Medicine*, 24(9), 5135-5145.

- Carrano, A., Juarez, J. J., Incontri, D., Ibarra, A. & Guerrero Cazares, H. (2021) Sex-Specific Differences in Glioblastoma. *Cells*, 10(7), 1783.
- Cen, L., Carlson, B. L., Schroeder, M. A., Ostrem, J. L., Kitange, G. J., Mladek, A. C., Fink, S. R., Decker, P. A., Wu, W., Kim, J.-S., Waldman, T., Jenkins, R. B. & Sarkaria, J. N. (2012) p16-Cdk4-Rb axis controls sensitivity to a cyclin-dependent kinase inhibitor PD0332991 in glioblastoma xenograft cells. *Neuro-oncology*, 14(7), 870-881.
- Chandrika, G., Natesh, K., Ranade, D., Chugh, A. & Shastry, P. (2016) Suppression of the invasive potential of Glioblastoma cells by mTOR inhibitors involves modulation of NFκB and PKC-α signaling. *Scientific Reports*, 6(1), 22455.
- Chen, F., Liu, C., Zhang, J., Xu, W. & Zhang, Y. (2018) Progress of CDK4/6 inhibitor palbociclib in the treatment of cancer. *Anti-Cancer Agents in Medicinal Chemistry (Formerly Current Medicinal Chemistry-Anti-Cancer Agents)*, 18(9), 1241-1251.
- Chinot, O. L., Wick, W., Mason, W., Henriksson, R., Saran, F., Nishikawa, R., Carpentier, A. F., Hoang-Xuan, K., Kavan, P., Cernea, D., Brandes, A. A., Hilton, M., Abrey, L. & Cloughesy, T. (2014) Bevacizumab plus Radiotherapy–Temozolomide for Newly Diagnosed Glioblastoma. *New England Journal of Medicine*, 370(8), 709-722.
- Clark, D. P., Pazdernik, N. J. & McGehee, M. R. (2019) Chapter 10 - Cell Division and DNA Replication. In: Clark, D. P., Pazdernik, N. J. & McGehee, M. R. (eds.) *Molecular Biology (Third Edition)*. Academic Cell.
- Cloughesy, T. F., Cavenee, W. K. & Mischel, P. S. (2014) Glioblastoma: From Molecular Pathology to Targeted Treatment. *Annual Review of Pathology: Mechanisms of Disease*, 9(1), 1-25.
- Copeland, N. A., Sercombe, H. E., Ainscough, J. F. X. & Coverley, D. (2010) Ciz1 cooperates with cyclin-A–CDK2 to activate mammalian DNA replication in vitro. *Journal of Cell Science*, 123(7), 1108.
- Copeland, N. A., Sercombe, H. E., Wilson, R. H. C. & Coverley, D. (2015) Cyclin-A–CDK2-mediated phosphorylation of CIZ1 blocks replisome formation and initiation of mammalian DNA replication. *Journal of Cell Science*, 128(8), 1518.
- Coverley, D., Marr, J. & Ainscough, J. (2005) Ciz1 promotes mammalian DNA replication. *Journal of Cell Science*, 118(1), 101.
- Davis, M. E. (2016) Glioblastoma: Overview of Disease and Treatment. *Clinical journal of oncology nursing*, 20(5 Suppl), S2-S8.
- De Groot, J. F., Fuller, G., Kumar, A. J., Piao, Y., Eterovic, K., Ji, Y. & Conrad, C. A. (2010) Tumor invasion after treatment of glioblastoma with bevacizumab: radiographic and pathologic correlation in humans and mice. *Neuro-oncology*, 12(3), 233-242.
- Dubois, L. G., Campanati, L., Righy, C., D'andrea-Meira, I., Spohr, T. C. L. D. S. E., Porto-Carreiro, I., Pereira, C. M., Balça-Silva, J., Kahn, S. A., Dossantos, M. F., Oliveira, M. D. A. R., Ximenes-Da-Silva, A., Lopes, M. C., Faveret, E., Gasparetto, E. L. & Moura-Neto, V. (2014) Gliomas and the vascular fragility of the blood brain barrier. *Frontiers in cellular neuroscience*, 8, 418-418.
- Duong-Ly, K. C. & Peterson, J. R. (2013) The human kinome and kinase inhibition. *Current protocols in pharmacology*, Chapter 2.

- Eng, L. F., Vanderhaeghen, J. J., Bignami, A. & Gerstl, B. (1971) An acidic protein isolated from fibrous astrocytes. *Brain Research*, 28(2), 351-354.
- Erbayraktar, Z., Alural, B., Erbayraktar, R. S. & Erkan, E. P. (2016) Cell division cycle 7-kinase inhibitor PHA-767491 hydrochloride suppresses glioblastoma growth and invasiveness. *Cancer cell international*, 16, 88-88.
- Esemen, Y., Awan, M., Parwez, R., Baig, A., Rahman, S., Masala, I., Franchini, S. and Giakoumettis, D. (2022a) 'Molecular Pathogenesis of Glioblastoma in Adults and Future Perspectives: A Systematic Review', *International journal of molecular sciences*, 23(5), 2607.
- Evrin, C., Clarke, P., Zech, J., Lurz, R., Sun, J., Uhle, S., Li, H., Stillman, B. & Speck, C. (2009) A double-hexameric MCM2-7 complex is loaded onto origin DNA during licensing of eukaryotic DNA replication. *Proceedings of the National Academy of Sciences of the United States of America*, 106(48), 20240-20245.
- Fomchenko, E. I., Dougherty, J. D., Helmy, K. Y., Katz, A. M., Pietras, A., Brennan, C., Huse, J. T., Milosevic, A. & Holland, E. C. (2011) Recruited cells can become transformed and overtake PDGF-induced murine gliomas in vivo during tumor progression. *PloS one*, 6(7), e20605-e20605.
- Fragkos, M., Ganier, O., Coulombe, P. & Méchali, M. (2015) DNA replication origin activation in space and time. *Nature Reviews Molecular Cell Biology*, 16(6), 360-374.
- Fu, P., He, Y.-S., Huang, Q., Ding, T., Cen, Y.-C., Zhao, H.-Y. & Wei, X. (2016) Bevacizumab treatment for newly diagnosed glioblastoma: Systematic review and meta-analysis of clinical trials. *Molecular and clinical oncology*, 4(5), 833-838.
- Gao, F., Cui, Y., Jiang, H., Sui, D., Wang, Y., Jiang, Z., Zhao, J. & Lin, S. (2016) Circulating tumor cell is a common property of brain glioma and promotes the monitoring system. *Oncotarget*, 7(44), 71330-71340.
- Garcia, J., Hurwitz, H. I., Sandler, A. B., Miles, D., Coleman, R. L., Deurloo, R. & Chinot, O. L. (2020) Bevacizumab (Avastin®) in cancer treatment: A review of 15 years of clinical experience and future outlook. *Cancer Treatment Reviews*, 86, 102017.
- Giacinti, C. & Giordano, A. (2006) RB and cell cycle progression. *Oncogene*, 25(38), 5220-5227.
- Goel, S., Decristo, M. J., Mcallister, S. S. & Zhao, J. J. (2018) CDK4/6 Inhibition in Cancer: Beyond Cell Cycle Arrest. *Trends in cell biology*, 28(11), 911-925.
- Gopalan, P. K., Villegas, A. G., Cao, C., Pinder-Schenck, M., Chiappori, A., Hou, W., Zajac-Kaye, M., Ivey, A. M. & Kaye, F. J. (2018) CDK4/6 inhibition stabilizes disease in patients with p16-null non-small cell lung cancer and is synergistic with mTOR inhibition. *Oncotarget*, 9(100), 37352-37366.
- Haas-Kogan, D. A., Prados, M. D., Lamborn, K. R., Tihan, T., Berger, M. S. & Stokoe, D. (2005) Biomarkers to predict response to epidermal growth factor receptor inhibitors. *Cell Cycle*, 4(10), 1369-1372.
- Hashizume, R., Zhang, A., Mueller, S., Prados, M. D., Lulla, R. R., Goldman, S., Saratsis, A. M., Mazar, A. P., Stegh, A. H., Cheng, S.-Y., Horbinski, C., Haas-Kogan, D. A., Sarkaria, J. N., Waldman, T. & James, C. D. (2016) Inhibition of DNA damage repair by the CDK4/6 inhibitor palbociclib delays irradiated intracranial atypical

- teratoid rhabdoid tumor and glioblastoma xenograft regrowth. *Neuro-oncology*, 18(11), 1519-1528.
- Hegi, M. E., Diserens, A.-C., Gorlia, T., Hamou, M.-F., De Tribolet, N., Weller, M., Kros, J. M., Hainfellner, J. A., Mason, W., Mariani, L., Bromberg, J. E. C., Hau, P., Mirimanoff, R. O., Cairncross, J. G., Janzer, R. C. & Stupp, R. (2005) MGMT Gene Silencing and Benefit from Temozolomide in Glioblastoma. *New England Journal of Medicine*, 352(10), 997-1003.
- Higgins, G., Roper, K. M., Watson, I. J., Blackhall, F. H., Rom, W. N., Pass, H. I., Ainscough, J. F. X. & Coverley, D. (2012) Variant Ciz1 is a circulating biomarker for early-stage lung cancer. *Proceedings of the National Academy of Sciences of the United States of America*, 109(45), E3128-E3135.
- Huse, J. T., Brennan, C., Hambardzumyan, D., Wee, B., Pena, J., Rouhanifard, S. H., Sohn-Lee, C., Le Sage, C., Agami, R., Tuschl, T. & Holland, E. C. (2009) The PTEN-regulating microRNA miR-26a is amplified in high-grade glioma and facilitates gliomagenesis in vivo. *Genes & development*, 23(11), 1327-1337.
- Inda, M.-D.-M., Bonavia, R., Mukasa, A., Narita, Y., Sah, D. W. Y., Vandenberg, S., Brennan, C., Johns, T. G., Bachoo, R., Hadwiger, P., Tan, P., Depinho, R. A., Cavenee, W. & Furnari, F. (2010) Tumor heterogeneity is an active process maintained by a mutant EGFR-induced cytokine circuit in glioblastoma. *Genes & development*, 24(16), 1731-1745.
- Jelski, W. & Mroczko, B. (2021) Molecular and Circulating Biomarkers of Brain Tumors. *International journal of molecular sciences*, 22(13), 7039.
- Jiao, W., Lin, H. M., Datta, J., Braunschweig, T., Chung, J. Y., Hewitt, S. M. & Rane, S. G. (2008) Aberrant nucleocytoplasmic localization of the retinoblastoma tumor suppressor protein in human cancer correlates with moderate/poor tumor differentiation. *Oncogene*, 27(22), 3156-3164.
- Jin, S., Ma, H., Yang, W., Ju, H., Wang, L. & Zhang, Z. (2018) Cell division cycle 7 is a potential therapeutic target in oral squamous cell carcinoma and is regulated by E2F1. *Journal of Molecular Medicine*, 96(6), 513-525.
- Jo, M.-Y., Kim, Y. G., Kim, Y., Lee, S. J., Kim, M. H., Joo, K. M., Kim, H. H. & Nam, D.-H. (2012) Combined therapy of temozolomide and ZD6474 (vandetanib) effectively reduces glioblastoma tumor volume through anti-angiogenic and anti-proliferative mechanisms. *Mol Med Rep*, 6(1), 88-92.
- Jung, C. S., Foerch, C., Schänzer, A., Heck, A., Plate, K. H., Seifert, V., Steinmetz, H., Raabe, A. & Sitzer, M. (2007) Serum GFAP is a diagnostic marker for glioblastoma multiforme. *Brain*, 130(12), 3336-3341.
- Juric, V. & Murphy, B. (2020) Cyclin-dependent kinase inhibitors in brain cancer: current state and future directions. *Cancer Drug Resistance*, 3(1), 48-62.
- Kanke, M., Kodama, Y., Takahashi, T. S., Nakagawa, T. & Masukata, H. (2012) Mcm10 plays an essential role in origin DNA unwinding after loading of the CMG components. *The EMBO Journal*, 31(9), 2182-2194.
- Keller, S. & Schmidt, M. H. H. (2017) EGFR and EGFRvIII Promote Angiogenesis and Cell Invasion in Glioblastoma: Combination Therapies for an Effective Treatment. *International Journal of Molecular Sciences*, 18(6).
- Khosla, D. (2016) Concurrent therapy to enhance radiotherapeutic outcomes in glioblastoma. *Annals of translational medicine*, 4(3), 54-54.

- Kim, M. M., Umemura, Y. & Leung, D. (2018) Bevacizumab and Glioblastoma: Past, Present, and Future Directions. *The Cancer Journal*, 24(4).
- Kiviniemi, A., Gardberg, M., Frantzén, J., Parkkola, R., Vuorinen, V., Pesola, M. & Minn, H. (2015) Serum levels of GFAP and EGFR in primary and recurrent high-grade gliomas: correlation to tumor volume, molecular markers, and progression-free survival. *Journal of Neuro-Oncology*, 124(2), 237-245.
- Kojima, K., Shimanuki, M., Shikami, M., Andreeff, M. & Nakakuma, H. (2009) Cyclin-dependent kinase 1 inhibitor RO-3306 enhances p53-mediated Bax activation and mitochondrial apoptosis in AML. *Cancer science*, 100(6), 1128-1136.
- Koltun, E. S., Tshako, A. L., Brown, D. S., Aay, N., Arcalas, A., Chan, V., Du, H., Engst, S., Ferguson, K., Franzini, M., Galan, A., Holst, C. R., Huang, P., Kane, B., Kim, M. H., Li, J., Markby, D., Mohan, M., Noson, K., Plonowski, A., Richards, S. J., Robertson, S., Shaw, K., Stott, G., Stout, T. J., Young, J., Yu, P., Zaharia, C. A., Zhang, W., Zhou, P., Nuss, J. M., Xu, W. & Kearney, P. C. (2012) Discovery of XL413, a potent and selective CDC7 inhibitor. *Bioorganic & Medicinal Chemistry Letters*, 22(11), 3727-3731.
- Kousholt, A. N., Menzel, T. & Sørensen, C. S. (2012) Pathways for genome integrity in G2 phase of the cell cycle. *Biomolecules*, 2(4), 579-607.
- Kreisl, T. N., Kim, L., Moore, K., Duic, P., Royce, C., Stroud, I., Garren, N., Mackey, M., Butman, J. A., Camphausen, K., Park, J., Albert, P. S. & Fine, H. A. (2009) Phase II trial of single-agent bevacizumab followed by bevacizumab plus irinotecan at tumor progression in recurrent glioblastoma. *Journal of clinical oncology : official journal of the American Society of Clinical Oncology*, 27(5), 740-745.
- Kreisl, T. N., McNeill, K. A., Sul, J., Iwamoto, F. M., Shih, J. & Fine, H. A. (2012) A phase I/II trial of vandetanib for patients with recurrent malignant glioma. *Neuro-Oncology*, 14(12), 1519-1526.
- Kwon, C.-H., Zhao, D., Chen, J., Alcantara, S., Li, Y., Burns, D. K., Mason, R. P., Lee, E. Y. H. P., Wu, H. & Parada, L. F. (2008) Pten haploinsufficiency accelerates formation of high-grade astrocytomas. *Cancer research*, 68(9), 3286-3294.
- Lee, S. M., Koh, H.-J., Park, D.-C., Song, B. J., Huh, T.-L. & Park, J.-W. (2002) Cytosolic NADP+-dependent isocitrate dehydrogenase status modulates oxidative damage to cells. *Free Radical Biology and Medicine*, 32(11), 1185-1196.
- Lee, S. Y. (2016) Temozolomide resistance in glioblastoma multiforme. *Genes & Diseases*, 3(3), 198-210.
- Lei, L., Wu, J., Gu, D., Liu, H. & Wang, S. (2016) CIZ1 interacts with YAP and activates its transcriptional activity in hepatocellular carcinoma cells. *Tumor Biology*, 37(8), 11073-11079.
- Li, W., Zhao, X.-L., Shang, S.-Q., Shen, H.-Q. & Chen, X. (2015) Dual inhibition of Cdc7 and Cdk9 by PHA-767491 suppresses hepatocarcinoma synergistically with 5-fluorouracil. *Current cancer drug targets*, 15(3), 196-204.
- Liu, Q., Niu, N., Wada, Y. & Liu, J. (2016) The Role of Cdkn1A-Interacting Zinc Finger Protein 1 (CIZ1) in DNA Replication and Pathophysiology. *International journal of molecular sciences*, 17(2), 212-212.
- Liu, T., Ren, X., Li, L., Yin, L., Liang, K., Yu, H., Ren, H., Zhou, W., Jing, H. & Kong, C. (2015) Ciz1 promotes tumorigenicity of prostate carcinoma cells. *Front Biosci (Landmark Ed)*, 20, 705-15.

- Liu, Y., Yeh, N., Zhu, X. H., Leversha, M., Cordon-Cardo, C., Ghossein, R., Singh, B., Holland, E. and Koff, A. (2007) Somatic cell type specific gene transfer reveals a tumor-promoting function for p21Waf1/Cip1. *The EMBO journal*, 26(22), 4683-4693.
- Louis, D. N. (2006) Molecular Pathology Of Malignant Gliomas. *Annual Review of Pathology: Mechanisms of Disease*, 1(1), 97-117.
- Macarthur, K. M., Kao, G. D., Chandrasekaran, S., Alonso-Basanta, M., Chapman, C., Lustig, R. A., Wileyto, E. P., Hahn, S. M. & Dorsey, J. F. (2014) Detection of Brain Tumor Cells in the Peripheral Blood by a Telomerase Promoter-Based Assay. *Cancer Research*, 74(8), 2152.
- Malkki, H. (2016) Glioblastoma vaccine therapy disappointment in Phase III trial. *Nature Reviews Neurology*, 12(4), 190-190.
- Michaud, K., Solomon, D. A., Oermann, E., Kim, J.-S., Zhong, W.-Z., Prados, M. D., Ozawa, T., James, C. D. & Waldman, T. (2010) Pharmacologic inhibition of cyclin-dependent kinases 4 and 6 arrests the growth of glioblastoma multiforme intracranial xenografts. *Cancer research*, 70(8), 3228-3238.
- Mitsui, K., Matsumoto, A., Ohtsuka, S., Ohtsubo, M. & Yoshimura, A. (1999) Cloning and Characterization of a Novel p21Cip1/Waf1-Interacting Zinc Finger Protein, Ciz1. *Biochemical and Biophysical Research Communications*, 264(2), 457-464.
- Mohanty, B. K., Bairwa, N. K. & Bastia, D. (2006) The Tof1p-Csm3p protein complex counteracts the Rrm3p helicase to control replication termination of *Saccharomyces cerevisiae*. *Proceedings of the National Academy of Sciences of the United States of America*, 103(4), 897-902.
- Montano, N., Cenci, T., Martini, M., D'alessandris, Q. G., Pelacchi, F., Ricci-Vitiani, L., Maira, G., De Maria, R., Larocca, L. M. & Pallini, R. (2011) Expression of EGFRvIII in glioblastoma: prognostic significance revisited. *Neoplasia (New York, N.Y.)*, 13(12), 1113-1121.
- Müller Bark, J., Kulasinghe, A., Chua, B., Day, B. W. & Punyadeera, C. (2020) Circulating biomarkers in patients with glioblastoma. *British journal of cancer*, 122(3), 295-305.
- Natoni, A., Coyne, M. R. E., Jacobsen, A., Rainey, M. D., Brien, G., Healy, S., Montagnoli, A., Moll, J., Dwyer, M. & Santocanale, C. (2013) Characterization of a Dual CDC7/CDK9 Inhibitor in Multiple Myeloma Cellular Models. *Cancers*, 5(3).
- Nicolas, S., Abdellatef, S., Haddad, M. A., Fakhoury, I. & El-Sibai, M. (2019) Hypoxia and EGF Stimulation Regulate VEGF Expression in Human Glioblastoma Multiforme (GBM) Cells by Differential Regulation of the PI3K/Rho-GTPase and MAPK Pathways. *Cells*, 8(11).
- Nishibe, R., Watanabe, W., Ueda, T., Yamasaki, N., Koller, R., Wolff, L., Honda, Z.-I., Ohtsubo, M. & Honda, H. (2013) CIZ1, a p21Cip1/Waf1-interacting protein, functions as a tumor suppressor in vivo. *FEBS Letters*, 587(10), 1529-1535.
- Nishikawa, R., Sugiyama, T., Narita, Y., Furnari, F., Cavenee, W. K. & Matsutani, M. (2004) Immunohistochemical analysis of the mutant epidermal growth factor, ΔEGFR, in glioblastoma. *Brain Tumor Pathology*, 21(2), 53-56.
- Ohno, M., Miyakita, Y., Takahashi, M., Igaki, H., Matsushita, Y., Ichimura, K. & Narita, Y. (2019) Survival benefits of hypofractionated radiotherapy combined with temozolomide or temozolomide plus bevacizumab in elderly patients with

- glioblastoma aged  $\geq 75$  years. *Radiation oncology (London, England)*, 14(1), 200-200.
- Olmez, I., Brennenman, B., Xiao, A., Serbulea, V., Benamar, M., Zhang, Y., Manigat, L., Abbas, T., Lee, J., Nakano, I., Godlewski, J., Bronisz, A., Abounader, R., Leitinger, N. & Purow, B. (2017) Combined CDK4/6 and mTOR Inhibition Is Synergistic against Glioblastoma via Multiple Mechanisms. *Clinical cancer research : an official journal of the American Association for Cancer Research*, 23(22), 6958-6968.
- Ostrom, Q. T., Gittleman, H., Fulop, J., Liu, M., Blanda, R., Kromer, C., Wolinsky, Y., Kruchko, C. & Barnholtz-Sloan, J. S. (2015) CBTRUS Statistical Report: Primary Brain and Central Nervous System Tumors Diagnosed in the United States in 2008-2012. *Neuro-oncology*, 17 Suppl 4(Suppl 4), iv1-iv62.
- Parker, M. W., Botchan, M. R. & Berger, J. M. (2017) Mechanisms and regulation of DNA replication initiation in eukaryotes. *Critical Reviews in Biochemistry and Molecular Biology*, 52(2), 107-144.
- Patel, A. P., Tirosh, I., Trombetta, J. J., Shalek, A. K., Gillespie, S. M., Wakimoto, H., Cahill, D. P., Nahed, B. V., Curry, W. T., Martuza, R. L., Louis, D. N., Rozenblatt-Rosen, O., Suvà, M. L., Regev, A. & Bernstein, B. E. (2014) Single-cell RNA-seq highlights intratumoral heterogeneity in primary glioblastoma. *Science (New York, N.Y.)*, 344(6190), 1396-1401.
- Patel, M., Vogelbaum, M. A., Barnett, G. H., Jalali, R. & Ahluwalia, M. S. (2012) Molecular targeted therapy in recurrent glioblastoma: current challenges and future directions. *Expert Opinion on Investigational Drugs*, 21(9), 1247-1266.
- Pauzaite, T., Thacker, U., Tollitt, J. & Copeland, N. A. (2016) Emerging Roles for Ciz1 in Cell Cycle Regulation and as a Driver of Tumorigenesis. *Biomolecules*, 7(1), 1.
- Pawlowska, E., Szczepanska, J., Szatkowska, M. & Blasiak, J. (2018) An Interplay between Senescence, Apoptosis and Autophagy in Glioblastoma Multiforme—Role in Pathogenesis and Therapeutic Perspective. *International Journal of Molecular Sciences*, 19(3).
- Phillips, H. S., Kharbanda, S., Chen, R., Forrest, W. F., Soriano, R. H., Wu, T. D., Misra, A., Nigro, J. M., Colman, H., Soroceanu, L., Williams, P. M., Modrusan, Z., Feuerstein, B. G. & Aldape, K. (2006) Molecular subclasses of high-grade glioma predict prognosis, delineate a pattern of disease progression, and resemble stages in neurogenesis. *Cancer Cell*, 9(3), 157-173.
- Phillips, J. J., Aranda, D., Ellison, D. W., Judkins, A. R., Croul, S. E., Brat, D. J., Ligon, K. L., Horbinski, C., Venneti, S., Zadeh, G., Santi, M., Zhou, S., Appin, C. L., Sioletic, S., Sullivan, L. M., Martinez-Lage, M., Robinson, A. E., Yong, W. H., Cloughesy, T., Lai, A., Phillips, H. S., Marshall, R., Mueller, S., Haas-Kogan, D. A., Molinaro, A. M. & Perry, A. (2013) PDGFRA Amplification is Common in Pediatric and Adult High-Grade Astrocytomas and Identifies a Poor Prognostic Group in IDH1 Mutant Glioblastoma. *Brain Pathology*, 23(5), 565-573.
- Rhind, N. & Gilbert, D. M. (2013) DNA replication timing. *Cold Spring Harbor perspectives in biology*, 5(8), a010132-a010132.
- Rich, J. N., Reardon, D. A., Peery, T., Dowell, J. M., Quinn, J. A., Penne, K. L., Wikstrand, C. J., Van Duyn, L. B., Dancey, J. E. & Mclendon, R. E. (2004) Phase II trial of gefitinib in recurrent glioblastoma. *Journal of Clinical Oncology*, 22(1), 133-142.

- Ridings-Figueroa, R., Stewart, E. R., Nesterova, T. B., Coker, H., Pintacuda, G., Godwin, J., Wilson, R., Haslam, A., Lilley, F., Ruigrok, R., Bageghni, S. A., Albadrani, G., Mansfield, W., Roulson, J.-A., Brockdorff, N., Ainscough, J. F. X. & Coverley, D. (2017) The nuclear matrix protein CIZ1 facilitates localization of Xist RNA to the inactive X-chromosome territory. *Genes & development*, 31(9), 876-888.
- Romanov, V. S., Pospelov, V. A. and Pospelova, T. V. (2012) Cyclin-dependent kinase inhibitor p21Waf1: Contemporary view on its role in senescence and oncogenesis. *Biochemistry (Moscow)*, 77(6), 575-584.
- Rominyi, O., Vanderlinden, A., Clenton, S. J., Bridgewater, C., Al-Tamimi, Y. & Collis, S. J. (2021) Tumour treating fields therapy for glioblastoma: current advances and future directions. *British Journal of Cancer*, 124(4), 697-709.
- Sakurikar, N. & Eastman, A. (2016) Critical reanalysis of the methods that discriminate the activity of CDK2 from CDK1. *Cell cycle (Georgetown, Tex.)*, 15(9), 1184-1188.
- Sanson, M., Marie, Y., Paris, S., Idbaih, A., Laffaire, J., Ducray, F., El Hallani, S., Boisselier, B., Mokhtari, K., Hoang-Xuan, K. & Delattre, J.-Y. (2009) Isocitrate Dehydrogenase 1 Codon 132 Mutation Is an Important Prognostic Biomarker in Gliomas. *Journal of Clinical Oncology*, 27(25), 4150-4154.
- Schultz, S., Pinsky, G. S., Wu, N. C., Chamberlain, M. C., Rodrigo, A. S. & Martin, S. E. (2005) Fine needle aspiration diagnosis of extracranial glioblastoma multiforme: Case report and review of the literature. *CytoJournal*, 2, 19-19.
- Schuster, J., Lai, R. K., Recht, L. D., Reardon, D. A., Paleologos, N. A., Groves, M. D., Mrugala, M. M., Jensen, R., Baehring, J. M., Sloan, A., Archer, G. E., Bigner, D. D., Cruickshank, S., Green, J. A., Keler, T., Davis, T. A., Heimberger, A. B. & Sampson, J. H. (2015) A phase II, multicenter trial of rindopepimut (CDX-110) in newly diagnosed glioblastoma: the ACT III study. *Neuro-oncology*, 17(6), 854-861.
- Schwartzbaum, J. A., Fisher, J. L., Aldape, K. D. & Wrensch, M. (2006) Epidemiology and molecular pathology of glioma. *Nature Clinical Practice Neurology*, 2(9), 494-503.
- Sclafani, R. A. & Holzen, T. M. (2007) Cell cycle regulation of DNA replication. *Annual review of genetics*, 41, 237-280.
- Serra, F., Lapidari, P., Quaquarini, E., Tagliaferri, B., Sottotetti, F. & Palumbo, R. (2019) Palbociclib in metastatic breast cancer: current evidence and real-life data. *Drugs in context*, 8, 212579-212579.
- Shinojima, N., Tada, K., Shiraishi, S., Kamiryō, T., Kochi, M., Nakamura, H., Makino, K., Saya, H., Hirano, H., Kuratsu, J.-I., Oka, K., Ishimaru, Y. & Ushio, Y. (2003) Prognostic Value of Epidermal Growth Factor Receptor in Patients with Glioblastoma Multiforme. *Cancer Research*, 63(20), 6962.
- Simons, M. & Nave, K.-A. (2015) Oligodendrocytes: Myelination and Axonal Support. *Cold Spring Harbor perspectives in biology*, 8(1), a020479-a020479.
- Siracusa, R., Fusco, R. & Cuzzocrea, S. (2019) Astrocytes: Role and Functions in Brain Pathologies. *Frontiers in pharmacology*, 10, 1114-1114.
- Songtao, Q., Lei, Y., Si, G., Yanqing, D., Huixia, H., Xuelin, Z., Lanxiao, W. & Fei, Y. (2012) IDH mutations predict longer survival and response to temozolomide in secondary glioblastoma. *Cancer Science*, 103(2), 269-273.

- Spring, L., Bardia, A. & Modi, S. (2016) Targeting the cyclin D-cyclin-dependent kinase (CDK) 4/6-retinoblastoma pathway with selective CDK 4/6 inhibitors in hormone receptor-positive breast cancer: rationale, current status, and future directions. *Discovery medicine*, 21(113), 65-74.
- Stewart, E. R., Turner, R. M. L., Newling, K., Ridings-Figueroa, R., Scott, V., Ashton, P. D., Ainscough, J. F. X. & Coverley, D. (2019) Maintenance of epigenetic landscape requires CIZ1 and is corrupted in differentiated fibroblasts in long-term culture. *Nature Communications*, 10(1), 460.
- Stupp, R., Taillibert, S., Kanner, A. A., Kesari, S., Steinberg, D. M., Toms, S. A., Taylor, L. P., Lieberman, F., Silvani, A., Fink, K. L., Barnett, G. H., Zhu, J.-J., Henson, J. W., Engelhard, H. H., Chen, T. C., Tran, D. D., Sroubek, J., Tran, N. D., Hottinger, A. F., Landolfi, J., Desai, R., Caroli, M., Kew, Y., Honnorat, J., Idbaih, A., Kirson, E. D., Weinberg, U., Palti, Y., Hegi, M. E. & Ram, Z. (2015) Maintenance Therapy With Tumor-Treating Fields Plus Temozolomide vs Temozolomide Alone for Glioblastoma: A Randomized Clinical Trial. *JAMA*, 314(23), 2535-2543.
- Stupp, R., Wong, E. T., Kanner, A. A., Steinberg, D., Engelhard, H., Heidecke, V., Kirson, E. D., Taillibert, S., Liebermann, F., Dbalý, V., Ram, Z., Villano, J. L., Rainov, N., Weinberg, U., Schiff, D., Kunschner, L., Raizer, J., Honnorat, J., Sloan, A., Malkin, M., Landolfi, J. C., Payer, F., Mehdorn, M., Weil, R. J., Pannullo, S. C., Westphal, M., Smrcka, M., Chin, L., Kostron, H., Hofer, S., Bruce, J., Cosgrove, R., Paleologous, N., Palti, Y. & Gutin, P. H. (2012) NovoTTF-100A versus physician's choice chemotherapy in recurrent glioblastoma: A randomised phase III trial of a novel treatment modality. *European Journal of Cancer*, 48(14), 2192-2202.
- Sunwoo, H., Colognori, D., Froberg, J. E., Jeon, Y. & Lee, J. T. (2017) Repeat E anchors Xist RNA to the inactive X chromosomal compartment through CDKN1A-interacting protein (CIZ1). *Proceedings of the National Academy of Sciences of the United States of America*, 114(40), 10654-10659.
- Talapati, S. R., Nataraj, V., Pothuganti, M., Gore, S., Ramachandra, M., Antony, T., More, S. S. & Krishnamurthy, N. R. (2020) Structure of cyclin-dependent kinase 2 (CDK2) in complex with the specific and potent inhibitor CVT-313. *Acta Crystallographica Section F*, 76(8), 350-356.
- Tamura, R., Tanaka, T., Miyake, K., Tabei, Y., Ohara, K., Sampetean, O., Kono, M., Mizutani, K., Yamamoto, Y., Murayama, Y., Tamiya, T., Yoshida, K. & Sasaki, H. (2016) Histopathological investigation of glioblastomas resected under bevacizumab treatment. *Oncotarget*, 7(32), 52423-52435.
- Taylor, J. W., Parikh, M., Phillips, J. J., James, C. D., Molinaro, A. M., Butowski, N. A., Clarke, J. L., Oberheim-Bush, N. A., Chang, S. M., Berger, M. S. & Prados, M. (2018) Phase-2 trial of palbociclib in adult patients with recurrent RB1-positive glioblastoma. *Journal of neuro-oncology*, 140(2), 477-483.
- Thon, N., Kreth, S. & Kreth, F.-W. (2013) Personalized treatment strategies in glioblastoma: MGMT promoter methylation status. *OncoTargets and therapy*, 6, 1363-1372.
- Tichy, J., Spechtmeyer, S., Mittelbronn, M., Hattingen, E., Rieger, J., Senft, C. & Foerch, C. (2016) Prospective evaluation of serum glial fibrillary acidic protein (GFAP) as a diagnostic marker for glioblastoma. *Journal of Neuro-Oncology*, 126(2), 361-369.

- Turcan, S., Rohle, D., Goenka, A., Walsh, L. A., Fang, F., Yilmaz, E., Campos, C., Fabius, A. W. M., Lu, C., Ward, P. S., Thompson, C. B., Kaufman, A., Guryanova, O., Levine, R., Heguy, A., Viale, A., Morris, L. G. T., Huse, J. T., Mellingshoff, I. K. & Chan, T. A. (2012) IDH1 mutation is sufficient to establish the glioma hypermethylator phenotype. *Nature*, 483(7390), 479-483.
- Urbańska, K., Sokołowska, J., Szmiedt, M. & Sysa, P. (2014) Glioblastoma multiforme - an overview. *Contemporary oncology (Poznan, Poland)*, 18(5), 307-312.
- Verhaak, R. G. W., Hoadley, K. A., Purdom, E., Wang, V., Qi, Y., Wilkerson, M. D., Miller, C. R., Ding, L., Golub, T., Mesirov, J. P., Alexe, G., Lawrence, M., O'Kelly, M., Tamayo, P., Weir, B. A., Gabriel, S., Winckler, W., Gupta, S., Jakkula, L., Feiler, H. S., Hodgson, J. G., James, C. D., Sarkaria, J. N., Brennan, C., Kahn, A., Spellman, P. T., Wilson, R. K., Speed, T. P., Gray, J. W., Meyerson, M., Getz, G., Perou, C. M. & Hayes, D. N. (2010) Integrated Genomic Analysis Identifies Clinically Relevant Subtypes of Glioblastoma Characterized by Abnormalities in PDGFRA, IDH1, EGFR, and NF1. *Cancer Cell*, 17(1), 98-110.
- Vertosick Jr, F. T. & Selker, R. G. (1990) Brain stem and spinal metastases of supratentorial glioblastoma multiforme: a clinical series. *Neurosurgery*, 27(4), 516-522.
- Vijayaraghavan, S., Moulder, S., Keyomarsi, K. & Layman, R. M. (2018) Inhibiting CDK in Cancer Therapy: Current Evidence and Future Directions. *Targeted Oncology*, 13(1), 21-38.
- Walter, F. M., Penfold, C., Joannides, A., Saji, S., Johnson, M., Watts, C., Brodbelt, A., Jenkinson, M. D., Price, S. J., Hamilton, W. & Scott, S. E. (2019) Missed opportunities for diagnosing brain tumours in primary care: a qualitative study of patient experiences. *The British journal of general practice : the journal of the Royal College of General Practitioners*, 69(681), e224-e235.
- Wang, D.-Q., Wang, K., Yan, D.-W., Liu, J., Wang, B., Li, M.-X., Wang, X.-W., Liu, J., Peng, Z.-H., Li, G.-X. & Yu, Z.-H. (2014) Ciz1 is a novel predictor of survival in human colon cancer. *Experimental Biology and Medicine*, 239(7), 862-870.
- Wang, H., Xu, T., Jiang, Y., Xu, H., Yan, Y., Fu, D. & Chen, J. (2015) The challenges and the promise of molecular targeted therapy in malignant gliomas. *Neoplasia (New York, N.Y.)*, 17(3), 239-255.
- Wang, X. & Li, S. (2014) Protein mislocalization: mechanisms, functions and clinical applications in cancer. *Biochimica et biophysica acta*, 1846(1), 13-25.
- Warder, D. E. & Keherly, M. J. (2003) Ciz1, Cip1 interacting zinc finger protein 1 binds the consensus DNA sequence ARYSR(0-2)YYAC. *Journal of Biomedical Science*, 10(4), 406-417.
- Wei, Q., Clarke, L., Scheidenhelm, D. K., Qian, B., Tong, A., Sabha, N., Karim, Z., Bock, N. A., Reti, R., Swoboda, R., Purev, E., Lavoie, J.-F., Bajenaru, M. L., Shannon, P., Herlyn, D., Kaplan, D., Henkelman, R. M., Gutmann, D. H. & Guha, A. (2006) High-Grade Glioma Formation Results from Postnatal Pten Loss or Mutant Epidermal Growth Factor Receptor Expression in a Transgenic Mouse Glioma Model. *Cancer Research*, 66(15), 7429.
- Wesseling, P., Kros, J. M. & Jeuken, J. W. M. (2011) The pathological diagnosis of diffuse gliomas: towards a smart synthesis of microscopic and molecular information in a multidisciplinary context. *Diagnostic Histopathology*, 17(11), 486-494.

- Wilhelmsson, U., Eliasson, C., Bjerkvig, R. & Pekny, M. (2003) Loss of GFAP expression in high-grade astrocytomas does not contribute to tumor development or progression. *Oncogene*, 22(22), 3407-3411.
- Wu, J., Lei, L., Gu, D., Liu, H. & Wang, S. (2016) CIZ1 is upregulated in hepatocellular carcinoma and promotes the growth and migration of the cancer cells. *Tumor Biology*, 37(4), 4735-4742.
- Zhang, D., Wang, Y., Dai, Y., Wang, J., Suo, T., Pan, H., Liu, H., Shen, S. & Liu, H. (2015) CIZ1 promoted the growth and migration of gallbladder cancer cells. *Tumor Biology*, 36(4), 2583-2591.
- Zhang, M., Zhang, L., Hei, R., Li, X., Cai, H., Wu, X., Zheng, Q. & Cai, C. (2021) CDK inhibitors in cancer therapy, an overview of recent development. *American journal of cancer research*, 11(5), 1913-1935.
- Zhu, Y., Guignard, F., Zhao, D., Liu, L., Burns, D. K., Mason, R. P., Messing, A. & Parada, L. F. (2005) Early inactivation of p53 tumor suppressor gene cooperating with NF1 loss induces malignant astrocytoma. *Cancer cell*, 8(2), 119-130.